IMPLEMENTATION OF ^{153}Sm IN DUAL PHOTON ABSORPTIOMETRY FOR THE DETECTION OF BMC

IMPLEMENTATION OF ^{153}Sm IN DUAL PHOTON ABSORPTIOMETRY FOR THE DETECTION OF BMC

by

ROBERT R. ROWNTREE, B.Eng.

A Thesis

Submitted to the School of Graduate Studies

in Partial Fulfilment of the Requirements

for the Degree

Master of Engineering

McMaster University

August 1985

MASTER OF ENGINEERING (1985) McMASTER UNIVERSITY

(Engineering Physics) Hamilton, Ontario

Canada

TITLE: Implementation of ^{153}Sm in Dual Photon Absorptiometry for the Detection of BMC.

AUTHOR: Robert R. Rowntree, B.Eng. (McMaster University)

SUPERVISOR: Dr. T. J. Kennett (Professor Engineering Physics)

ADVISOR: Dr. Colin Webber (Professor Radiology)

NUMBER OF PAGES: xxi,202

RIDE THE WAVE

OR

DRIFT OUT TO SEA

R.R.R.

...IN MEMORY OF MY FATHER...

Acknowledgements

Thanks for help in the completion of this manuscript go to my supervisors, the health physics staff, the reactor staff, the machine shop staff, family and friends. Firstly, I would like to express my sincere gratitude to the "head honcho", Dr. T. J. Kennett for taking me on and adding another hoser to his overcrowded table. In addition, thanks for his invaluable suggestions that always seemed to provide the missing link in the evolution of a new species, namely "Kennettites". To Dr. Colin Webber thanks for providing one gigantic beacon to a near-sighted sailor on a rough dark sea. His door was always open for the reviewing of this manuscript and he made numerous proposals that helped produce the quality of the experimental work. Thanks to Dr. William "Bill" Prestwich for several clues that lead me to the right information at the right time. Honourable mention goes to the health physics group, especially Dr. John "Mr. Baseball" Harvey, for putting up with numerous TLD measurements. For help with the electronics involved in this project, my thanks go to Kenrick Chin - without him the Novas would all "die", the research group would cease to function and most likely all the Nova computers would be sold to a technological museum as antiques. Special thanks go to (Dr. Pepper) Gary and Ed "The Beave" Beaver for their suggestions and morale-boosting humour. I extend my appreciation to John and Dave for expedient delivery of piping hot coffees from senior

science and for adding humour to sometimes dull days.

Throughout this project numerous interactions with the reactor staff required diplomacy and tact. I would like to first mention the man in the sinecure position, Mr. Mike "the butler" Butler for his unyielding kindness and in-depth knowledge of the MNR. Secondly, to the man behind the bureaucratic facade, Chris Lopresti, who helped verify some of the calculations in this thesis and provided that jolly old Saint Nick laugh which is useful on those "hum drum" days(Ho! Ho!). To George "The Globe" Hanas and Nick "The Star" Vander Vliet thanks for those fun midnight "suds" and "pool" parties. For expert workmanship, numerous suggestions (i.e., where to go) and service with a smile, my hat goes off to the boys in the senior science machine shop, especially Gino and Bill.

To those in my family who had to endure through my absence, I am eternally indebted (parole in 5 years). I would like to thank my mother "Mrs. Clean" for kindness and understanding in my undergraduate years. And to my wife Veronica, I would like to thank for critical proofreading of this manuscript for grammatical and spelling errors, bringing dinner and late night snacks to the research building, and for understanding the commitment required to complete this rather large task. Lastly, to the memory of my father, Robert Patterson Rowntree, I would like to express my gratitude. For it is the two of us who are largely

responsible for my character and stamina that is required to obtain my present and future accomplishments. Thanks to all!

Robert R. Rowntree

ABSTRACT

A ^{153}Sm source was used with a dual photon absorptiometry technique *in vitro* to determine the feasiblity of using this isotope as an alternative source to ^{153}Gd for further *in vivo* studies. The source activity was typically .4 Ci (i.e., at the source collimator exit) with a half life of 46.8 hours and photon energies of "103" keV and ^{153}Eu X-rays at "42.5" keV.

The system was evaluted using phantom measurements of water, aluminum and polyethylene to simulate soft tissue, bone and fat respectively. During stationary measurements, a total absorber thickness between 15 and 22.5 cm. was used in conjunction with an aluminum thickness range of .314 to 1.91 cm. (.848-5.16 g/cm^2). The coefficient of variation and the accuracy at most total absorber thicknesses was less than 2%. This showed that ^{153}Sm could produce precision and accuracy comparable to ^{153}Gd. When polyethylene (fat) was present, as the amount of polyethylene in the RST measurement increased, the error due to a difference in the amount of polyethylene between the RST and the BMC measurements increased. For a percent difference in polyethylene thickness between the RST and BMC measurement of less than 50% at 16.3% RST polyethylene content, measurements of aluminum (bone) above 1.8 g/cm^2 (.662 cm. of aluminum) produced results accurate to within 10% of the true aluminum (BMC) value for this

experimental geometry.

Motional studies were performed using a modified OHIO NUCLEAR rectilinear scanner. The optimal scan speed was shown to be in the range of 4-6 mm./sec. with a sample space of between .5 to .7 cm.. The worst-case dose using the optimal scan parameters was determined as 6.2 and 1.4 mRad per scan of approximately 24 minutes for bone and soft tissue respectively. The combination of stationary and motional in vitro studies indicated that ^{153}Sm could be an economical and effective alternative to ^{153}Gd for clinical studies.

A Monte Carlo simulation was implemented to determine the optimal detector collimator entrance size. Simulation of the experimental geometry indicated that the .6 cm. detector collimation used experimentally was near the optimal size to produce efficient results in terms of accuracy and precision. A brief summary of Monte Carlo methods and radiation theory is also included.

TABLE OF CONTENTS

APPENDICES

TABLE of FIGURES

TABLE OF TABLES

Nomenclature

D	Dose to tissue (mRad)
E	Photon energy in keV
I'	Attenuated intensity of the lower energy photons (counts/second)
I_o'	Unattenuated intensity of the lower energy photons (counts/second)
I	Attenuated intensity of the higher energy photons (counts/second)
I_o	Unattenuated intensity of the higher energy photons (counts/second)
M_a	Mass of absorber a (g/cm^2)
M_b	Mass of absorber b (g/cm^2)
N_o	Observed count rate (counts per second)
N_i	True count rate (counts per second)
N_z	Number of atoms of material z
OX	Cross-over correction
R	The rotation matrix
u_a'	Mass attenuation coefficient of absorber a at the lower energy (cm^2/g)
u_b'	Mass attenuation coefficient of absorber b at the lower energy (cm^2/g)
u_a	Mass attenuation coefficient of absorber a at the higher energy (cm^2/g)

u_b Mass attenuation coefficient of absorber b at the higher energy (cm^2/g)

$\frac{u_{en}}{\rho}$ Mass-energy absorption coefficient (cm^2/g)

X Exposure in roentgens

τ Dead-time constant (seconds)

λ_z Decay constant for Material z (1/hours)

$\sigma_{c,z}$ Capture cross-section of neutrons for material z (cm^2)

$\sigma_{a,z}$ Absorption cross-section of neutrons for material z (cm^2)

ϕ Neutron flux (neutrons/cm^2-sec)

α Activity in disintegrations/second

Γ Gamma-ray constant

Chapter 1

Introduction

The measurement of bone mineral content (BMC) is of vital importance for three major reasons: (1) The detection and monitoring of bone loss in metabolic bone disease (Wahner[1]); (2) The assessment of drug effects on bone mineral content (Hansson[2], Lagrelius[3]); and (3) The recognition of age-related BMC loss and associated fracture risk at specific bone sites such as the spine or femoral neck (Wahner[1], Bartley[4], Mather[5]). For in vivo measurements, "BMC" is measured in lieu of "bone mineral density" because assessment of bone density to the same precision and accuracy as the associated mass is difficult. This is due to the fact that there is a large error in determining the volume of bone through which the photon beam has passed. Bones consist primarily of a mineral compound, hydroxyapatite, laid down on an organic matrix of collagen. The organic components of bone cannot be distinguished easily from soft tissue surrounding the bone by attenuation methods whereas inorganic mineral is quite distinct from soft tissue. Resultingly, mineral in a bone can be measured with a high degree of accuracy and precision by photon transmission techniques. Henceforth, BMC will be used to mean the mass of mineral in a particular section of the skeleton.

One method that shows promise in the monitoring of changes in BMC is dual photon absorptiometry (DPA). BMC

measurements using DPA have been well established by many researchers (Roos[6], Wilson[7], Krolner and Neilsen[8], Mazess[9], Dunn[10]). DPA was developed by Reed[11] in 1966, and is an extension of the single photon absorptiometry (SPA) pioneered by Cameron and Sorenson[12] in 1963. The difference between SPA and DPA can be understood by considering the body as a three-component tissue model of bone, soft tissue and fat as shown in figure 1-1. For SPA, the assumption is made that soft tissue and fat can be classified as one component. In addition, the combined thickness of bone, soft tissue and fat must be constant over the entire scan area. If these criteria are met than valid information about the bone can be produced. However, this restricts measurement to areas where soft tissue thickness is constant (e.g., forearm) or to experiments in which the total thickness is artificially kept constant (e.g., water tanks). Due to non-uniform fat and soft tissue content in many skeletal areas of clinical interest, SPA proved to be limited in both precision and applicability. This prompted reseachers to develop the second generation of photon absorptiometry known as DPA, in which the thickness of the tissue and bone does not have to remain constant.

Dual photon absorptiometry utilizes two different photon energies to differentiate between two substances. Precise results can be obtained only if the two substances differ in attenuation ability with respect to the two

energies employed. For photon energies below 30 keV, the difference in attenuation between bone and tissue is large. However, the attenuation of either of the two components is so large, that, for a source strength of reasonable activity (e.g., .5 Ci), the count rate for photons transmitted through a human thorax would be comparable with background radiation and there would be a serious deterioration in the counting statistics. At an energy of 100 keV, attenuation is less dependent on atomic number due to decreasing influence of photoelectric interactions. This results in mass attenuation coefficients (cm^2/g) of bone and soft tissue that approach the same value. Consequently, the higher energy photons interact with soft tissue and bone as though they were the same component, while the low energy photons recognize bone and soft tissue as two distinct elements. Intuitively, the technique subtracts the soft tissue from the combined soft tissue and bone leaving only the information about the bone. The most demanding and crucial element of DPA is the choice of optimal energies to provide adequate precision and accuracy such that the acquired information can be used to monitor or detect changes in BMC.

Generally, the optimal choice for the low energy photon beam will be a compromise between statistical counting criteria and a sufficient difference in attenuation coefficients of bone and soft tissue. The high energy photon level will depend, as stated above, on the energy at which

photoelectric interactions are insignificant and Compton scattering predominates. Judy[13] concluded that the optimal lower energy for DPA is between 30 to 40 keV for a total sample thickness of 5 g/cm^2**. In addition, this optimal thickness was independent of the tissue to fat ratio. Watt[14], in an attempt to determine the optimal energy levels, deduced that the lower energy should be 40 keV while the upper energy should be approximately 400 keV for sample thicknesses of 15 g/cm^2 at bone mineral content of 10% (1.5 g/cm^2). However, Smith[15] believes that Watt and Judy cited total sample thicknesses that are on the order of half that found in human subjects at the lumbar spine.

** All radiation attenuation methods measure the mass of material within the photon beam. The units for such measurement are usually "g/cm^2" which refers to the equivalent bone mineral mass per unit area in a cylinder of bone of the same dimension as the photon beam and the same attenuation as the sample. No information about the distribution of that mineral within the beam is revealed. To obtain the density of material in "g/cm^3", the volume of distribution of the mineral within the beam would have to be known. This would lower the precision in the density determination to less than that which can be achieved by measuring the mass.

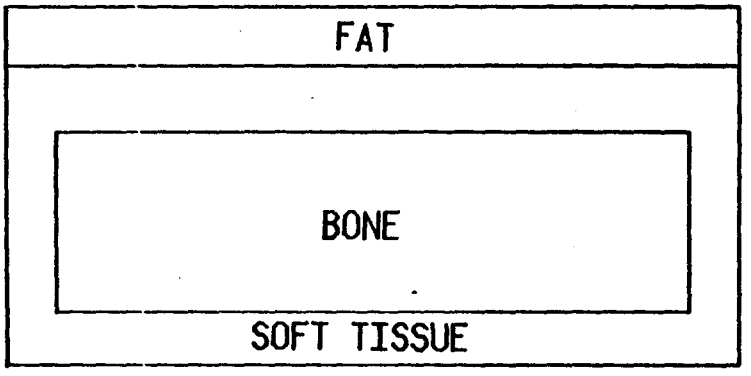

Figure 1-1 Tissue component model for dual photon absorptiometry.

In 180 normal subjects, Smith found that the mean supine anterior to posterior thickness is 22 cm. (15-29 cm.) in men and 19.8 cm. (15-29 cm.) in women. If the density of soft tissue is taken as that of water (1 g/cm^3), this would give a minimum thickness in g/cm^2 of 15 and a maximum of 29. Using this as a guideline, he tested a BMC of 1 g/cm^2 and a soft tissue thickness of 20 g/cm^2 and found optimal energies of 43 and 180 keV. Finally, he showed that while the lower energy level is critical to precision, variation in the upper energy level to 50% created precision losses of less than 1% and confirmed that 153-Gadolinium possesses the ideal lower energy for spinal BMC measurement even though the higher energy is less than optimal.

Past research involving DPA for assessing BMC has been limited to one well-established and relatively costly radioactive source, ^{153}Gd (Wilson[7], Krolner[8], Mazess[9]). For the last decade researchers have been seeking viable alternatives that are more economical and readily available. Smith[15] concluded that the combination of ^{241}Am and ^{137}Cs is an effective alternative to ^{153}Gd considering cost and availablity. However, ^{153}Gd still produced 1.5 times higher precision than the ^{241}Am amd ^{137}Cs combination. Prior to Smith's work, Davis and Webber[16] showed that 153-Samarium, an isobar of ^{153}Gd, could prove considerably more cost-effective than ^{153}Gd, even though the former would have to be produced weekly instead of yearly. Table 1-1[16] shows

a comparison of ^{153}Gd and ^{153}Sm. Technically, the two isobars have the same daughter, 153-Europium. ^{153}Sm decays by electron capture producing 103.2(28.2%) keV photons whereas ^{153}Gd decays by beta emission and produces 69(2.6%), 97.5(36.2%), and 103(26.6%) keV photons. The ^{153}Eu isotope emits x-rays at 41(55.4%), 44(100%), 47(30.5%) and 48.3(8.7%) keV. The 97.5 and 103 keV photopeaks of ^{153}Gd are considered as "100" keV while the ^{153}Eu x-rays are grouped as one "42.5" keV peak since sodium iodide detectors have an insufficient ability to resolve each individual energy. The major difference between the two isotopes is that the half life of ^{153}Gd is approximately 242 days while that of ^{153}Sm is 46.8 hours. In addition, ^{153}Sm can be produced for hundreds of times less than the cost of ^{153}Gd, although the availability of ^{153}Sm is limited due to the need for a local reactor. Table 1-2[17] shows a summary of the absorption coefficients and relative intensities of the two photon groups for each isotope. Although ^{153}Gd has an advantage over ^{153}Sm due to a greater intensity at 42.5 keV, this is partially offset by its greater self-absorption. For source mass greater than .7 g/cm^2 the 42.5 and 103 keV photon intensities are greater for ^{153}Sm than for ^{153}Gd(appendix 2).

There is only one isotope that is widely used for DPA studies at present, ^{153}Gd. ^{153}Sm is almost identical in decay structure to ^{153}Gd, yet has a greater natural abundance and a much lower relative cost. If the technical difficulty

of a short half life can be overcome, ^{153}Sm could become a viable alternative to ^{153}Gd.

1.1 Measurement of BMC

For completeness, the various methods which are available for measurement of mineral mass should be described. Several factors such as precision, accuracy, convenience, cost, and radiation dose are important when considering the most viable method.

1.1.1 Methods

There are several methods presently used to measure mineral mass in normal as well as abnormal conditions. These methods include radioscopy, radiographic photodensitometry, radiogrammetry, quantitative computed tomography, neutron activation analysis and single and dual photon absorptiometry. Since at appendicular and spinal measurement sites the geometries are very different, effective use of the above-mentioned methods is restricted to either central or peripheral bones. Methods such as SPA, radiogrammetry and computed tomography provide reliable measures of appendicular bone mass with a typical precision error of about 3% (Mazess[9]). Radiographic photodensitometry provides larger errors of 5 to 10% (Mazess[9]). Wahner[1] feels that SPA is still the most practical method to measure bone mineral content at appendicular sites. For spinal BMC measurement

	^{153}Gd	^{153}Sm
Predominant gamma ray energy(keV) and intensity(%)	97.5(36.2%) 103.2(26.6%)	103.2(28.2%)
Available abundance of target nucleus(%)	45-55	>95
Relative cost per mg. of enriched target	320	1
Relative cost of enriched target to produce equal activity in 1 day irradiation	64000	1
Half life	242(days)	46.8(hrs)

Table 1-1 Comparison of ^{153}Sm and ^{153}Gd.

	$^{153}Sm_2O_3$		$^{153}Gd_2O_3$	
E(keV)	U cm^2/g	I %	U cm^2/g	I %
42.5	4.582	60.8	5.725	121.6
103	2.221	28.3	2.748	21.1

Table 1-2 Mass attenuation coefficients and emission intensities of $^{153}Gd_2O_3$ and $^{153}Sm_2O_3$.

there are three techniques that are considered suitable: computed tomography; neutron activation; and DPA. These techniques provide precisions of 10, 5, and 3% respectively (Mazess[9]). In addition, Krolner[18] has shown that spinal radiography and DPA must be regarded as complimentary rather than alternative diagnostic procedures. Lastly, the dose delivered by these three methods is quite different. Computed tomograghy imparts a dose typically in the several rem range; spinal activation in the range of hundreds of mrem and DPA with the lowest dose of approximately 2 mrem (Mazess[9]).

Overall, SPA is best suited for the measurement of BMC in appendicular bone. For measurement in the spinal region, DPA provides a lower dose and greater precision than the other methods mentioned. However, there is considerable controversy over the relationship between the loss of mineral in appendicular sites and the spinal region. If there is a relationship between loss at the two sites, perhaps only the techniques that investigate the spinal region best will survive. Conversely, if there is no relationship, appendicular and spinal techniques will both have continued use. Presently, there is no conclusive evidence about whether measurements to detect abnormal conditions should be performed in one or both of these regions (Atkinson[19], Schaadt and Bohr[20]).

1.1.2 BMC Measurement Sites

For clinical monitoring and diagnosis of loss of BMC, the spine is advocated as the preferred location for investigation (Roos[6], Wilson[7], Krolner[8], Mazess[9]). Foremost, the spine is frequently the most susceptible site to spontaneous fractures due to loss of BMC. This clinical finding is in agreement with the facts that vertebrae contain almost entirely trabecular bone, and that, due to a disease such as osteoporosis, there is a greater and much faster loss of trabecular than cortical bone (Russell[21], Gallagher[22], Schaaht[23][24], Krolner[25], Riggs[26]). Table 1-3[1] shows the percentage of cortical and trabecular bone at different sites in the body. Riggs[26] found that BMC measurements in the distal forearm and in the total skeleton tend to underestimate trabecular bone mineral loss since only about 20 to 25% of either the total body or distal radius mineral is trabecular. He also compared the hip and spine for BMC measurements and found that BMC was lower in patients with osteoporosis than in age and sex matched normal subjects. The important findings were that the spinal measurements best discriminated the two patient groups and that there were greater losses of mineral from the axial skeleton compared to appendicular bone. In another study by Riggs[27], no discernable bone loss occurred in the lumbar spine for hip fracture cases. This may be due to the fact that spinal osteoporosis and senile(age-related) hip fractures may be two

different osteoporotic syndromes.

1.2 BMC and Disease

The primary affliction by which bone mass may change is through a group of diseases collectively termed metabolic bone disease, and may result in either a bone loss or gain. Reifenstein[28] devised a method of categorizing physiological and chemical changes of bone due to diseases. His classification is shown in table 1-4. Decreases in bone density are associated with lack of bone matrix, decreased mineralization, or increased destruction. Increases in bone density imply the converse. Although bone metabolic disease can cause an increase or decrease in BMC, more grave consequences arise through decreases. This is due to a loss of bone strength and an increased incidence of bone fractures. Therefore, our discussion will be limited to diseases causing bone density decreases. Osteomalacia results from insufficient mineralization of bone matrix whereas osteoporosis acts indirectly through a deficiency of bone matrix which precludes subsequent mineralization. These two diseases are the focus of DPA investigations.

1.3 Summary

There are many different methods and measurement sites for the determination of BMC. The method that provides the highest precision and lowest dose to the spine of the

previously mentioned techniques is DPA. The uniqueness of DPA lies in the fact that BMC can be determined even though there is overlying non-uniform soft tissue. The most drastic loss of BMC occurs in trabecular bone. Since the spine is composed predominantly of trabecular bone, it appears to be the best site for the detection of osteoporosis. Lastly, ^{153}Gd is practically the only source in widespread use for DPA studies. However, ^{153}Gd is very expensive whereas ^{153}Sm is relatively cheap. Therefore, there is a large economic gain possible if ^{153}Sm can be shown to be practical with the same precision and accuracy as ^{153}Gd.

Bone	Site	Cortical %	Trabecular %
Radius	midshaft	>90	<10
	distal	75	25
Femur	neck	75	25
	trochanter	50	50
Spine	lumbar	50	50
Skeleton		80	20

Table 1-3 Comparison of bone sites and proportion of cortical and trabecular bone.

I. Too little calcified bone

A. Too little bone formation

1. Osteoporosis - Too little formation of matrix

2. Osteomalacia - Too little calcification of matrix

B. Too much bone resorption

1. Hyperparathyroidism - Excess resorption of matrix

2. Pagets disease

II. Too much calcified bone

A. Too much bone formation

1. Hyperosteogenesis - Too much formation of matrix

2. Too much calcification of matrix (apparently non-existent)

B. Too little bone resorption

1. Osteosclerosis - Too little resorption of matrix and calcium

Table 1-4 Metabolic bone diseases classification.

Chapter 2

Theory of DPA

The DPA technique requires the understanding of the fundamentals of radiation theory and the relationship between the physical and mathematical interpretation. Inherent in the above is the comprehension of phenomena that may adversely affect the agreement between theoretical and experimental results.

2.1 Exponential Attenuation of Radiation

For the measurement of gamma rays and X-rays that follow exponential attenuation laws, the apparatus in figure 2-1 is required. A beam of photons is defined by the source and detector collimators so that the detection of multiple scattering is prevented. Figure 2-2 shows the detector response with and without multiple scattering. The intensity of the detected radiation is described mathematically by equation 2-1 assuming narrow beam geometry and that the source emits a monoenergetic beam of photons.

$$I=I_o\exp(-um) \qquad (2\text{-}1)$$

where

I = attenuated intensity of the photon beam

I_o = initial intensity of the photon beam

u = mass attenuation coefficient(cm^2/g)

m = mass of material (g/cm^2) traversed by the beam of photons

Narrow beam refers to the situation where the detector is responsive only to those gamma-ray photons that escape interaction within a homogeneous medium. Therefore the medium can be characterized by a single-valued narrow beam attenuation coefficient. A homogeneous medium from a macroscopic point of view entails two criteria: (1) That the density is the same throughout; and (2) That atomic composition in a small volume (of dimensions << 1/u) of the medium at any point is constant.

Experimentally, it is difficult to reduce the multiple scattering to zero. Multiple scattering can be introduced mathematically through a build-up factor B as a function of u and m. Equation 2-1 becomes:

$$I = I_o B(um) \exp(-um) \qquad (2\text{-}2)$$

Because of the complexity of the DPA method, the build-up factor is determined empirically by counting the number of higher energy photons that are scattered into the lower photon energy window. This process is known as cross-over

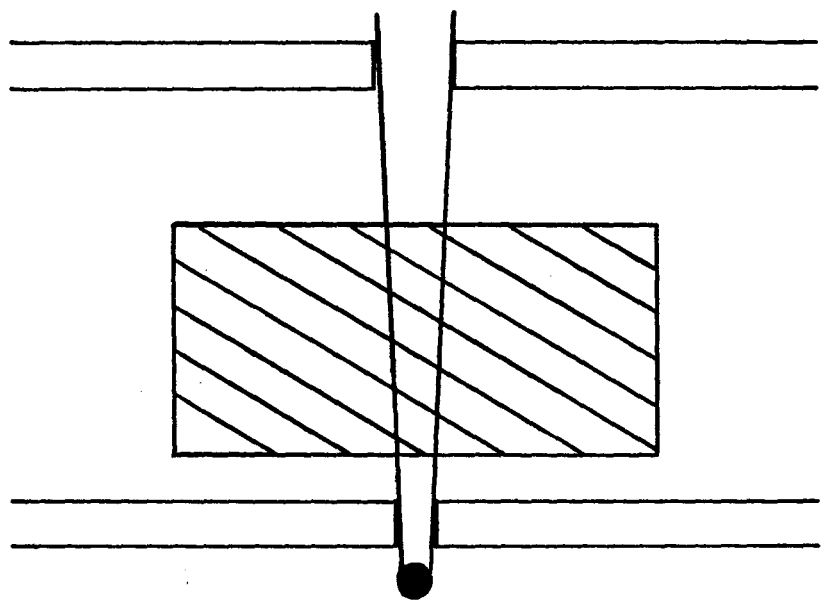

Figure 2-1 Experimental collimation for narrow beam geometry.

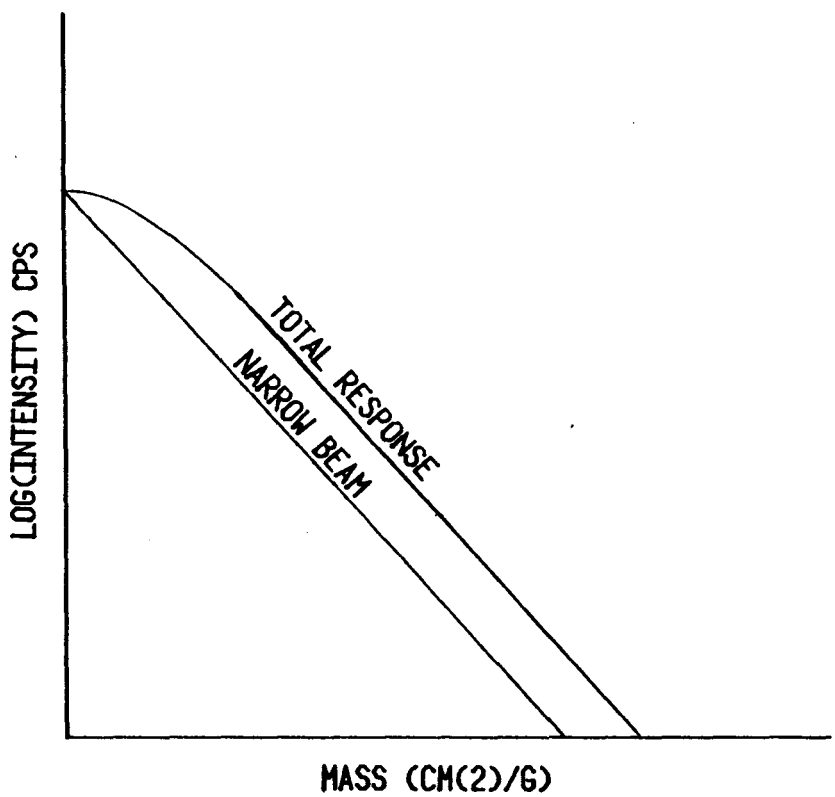

Figure 2-2 Detector response to photons with and without multiple scattering.

correction and will be discussed in detail in the following chapter.

Equation 2-1 is valid for one photon energy and one attenuating material. For multiple energies and attenuating media, equation 2-1 becomes:

$$I_n = I_{o,n} \exp\left(-\sum_{j=1}^{k} u_{j,n} m_j\right) \qquad (2\text{-}3)$$

where

I_n = the attenuated intensity of the nth photon energy

$I_{o,n}$ = the unattenuated intensity of the nth photon energy

$u_{j,n}$ = the mass attenuation coefficient of the jth attenuating material at the nth photon energy

m_j = mass of the jth substance

k = number of substances

Intuitively, to analyze a discrete number of media there must be an equivalent number of photon energies. That is to say, to obtain a unique solution in a system of linear equations there must be as many independent equations as there are unknowns. To analyze a dual media system with components A and B, two energies must be used to produce two linearly independent equations. Solving equation 2-3 for m_b in a dual media system gives:

$$m_b = \frac{\ln\left(\frac{I_o'}{I'}\right) - \left(\frac{u_a'}{u_a}\right)\ln\left(\frac{I_o}{I}\right)}{u_b' - \left(\frac{u_a'}{u_a}\right)u_b} \qquad (2\text{-}4)$$

where

I_o = initial counts of the high energy photons.

I = attenuated counts of the high energy photons.

I_o' = initial counts of the low energy photons.

I' = attenuated counts of the low energy photons.

u_a = mass attenuation coefficient of medium a.

u_b = mass attenuation coefficient of medium b.

2.2 Mathematical Model for DPA

If the body can be categorized into three distinct components and two discrete photons energies are present in the incident beam, the attenuated photon beam intensities are described by:

$$I = I_o \exp[-(u_s m_s + u_f(m_f - m_{fo}) + u_b m_b)] \qquad (2\text{-}5)$$

$$I' = I_o' \exp[-(u_s' m_s + u_f'(m_f - m_{fo}) + u_b' m_b)] \qquad (2\text{-}6)$$

where s, b, and f represent soft tissue, bone and fat respectively. The factor m_{fo} is a constant included to indicate that if the mass of fat m_f during BMC measurement is kept constant, the effect of fat mathematically is

eliminated. Solving these two simultaneous equations for mass of bone gives:

$$m_b = \frac{\ln\left(\frac{I_o'}{I'}\right) - \left(\frac{u_s'}{u_s}\right)\ln\left(\frac{I_o}{I}\right)}{u_b' - \left(\frac{u_s'}{u_s}\right)u_b} + \frac{\left[\left(\frac{u_s'}{u_s}\right)u_f - u_f'\right](m_f - m_{fo})}{\left(\frac{u_s'}{u_s}\right)u_b - u_b'} \qquad (2\text{-}7)$$

To produce a more concise solution let

$$G_{sf} = \left(\frac{u_s'}{u_s}\right)u_f - u_f' \qquad (2\text{-}8)$$

$$G_{sb} = u_b' - \left(\frac{u_s'}{u_s}\right)u_b \qquad (2\text{-}9)$$

and

$$P = \ln\left(\frac{I_o'}{I}\right) - \left(\frac{u_s'}{u_s}\right)\ln\left(\frac{I_o}{I}\right) \qquad (2\text{-}10)$$

So that

$$m_b = \frac{P - G_{sf}(m_f - m_{fo})}{G_{sb}} \qquad (2\text{-}11)$$

Ultimately, the possibility of using equation 2-7 to calculate BMC in an object comprised of bone, soft tissue and fat depends upon a knowledge of the attenuation coefficients of the three components at the two energies, measurement of

the incident and transmitted intensities for the two energies and the variability in the amount of adipose tissue m_f in the object. The following factors are of prime importance: (1) Highly active and more energetic sources produce better statistical results; (2) Attenuation coefficients that are relatively the same make discrimination of substances difficult; (3) Thicker absorbers cause greater build-up; and (4) Three unknowns with two equations create a need for either a third energy or the determination of the exact path-length of the radiation through the absorber (i.e., keep the fat thickness constant). If the mass of fat ($m_f - m_{fo}$) is set to zero, equation 2-11 will be in the same form as equation 2-4:

$$m_b = \frac{P}{G_{sb}} \tag{2-12}$$

From equation 2-4, if $m_b = 0$ then

$$\frac{u_s}{u_s'} = \frac{\ln\left(\frac{I_o}{I}\right)}{\ln\left(\frac{I_o'}{I}\right)} \tag{2-13}$$

This ratio is typically given the name "relative soft tissue" (RST). The assumption is made that only a single component is present (i.e., no fat). Equation 2-12 presents the theoretical approach and the assumption is made that fat

thickness is constant throughout the scanned region. Experimentally, it is difficult to measure the initial photon intensity with count rates typically in the order of 10^5 counts/second without experiencing excessive dead-time errors. Hence, the initial intensities are measured indirectly using a known "standard" to attenuate the beam to a count rate such that dead-time losses are negligible.

2.3 Data Distortion and Losses

The accuracy and precision of results obtained by DPA are dependent on many factors of which the most pronounced are:

1/ Beam hardening
2/ Dead-time losses
3/ Compton crosstalk
4/ Scanning geometry

2.3.1 Beam Hardening

The probability that a photon will interact with matter is a function of photon energy. As a polyenergetic beam of photons traverses matter, the photons with high interaction probabilities (low energy) will be "stripped" away from the beam preferentially over the photons with lower interaction probabilities (high energy). This process is known as beam hardening. Beam hardening causes an apparent decrease in the attenuation coefficient of a given material as the distance from the source increases. Other factors as well as beam hardening that can apparently decrease the

attenuation coefficient of a material include multiple Compton scattering and a change in geometry at increasing absorber thickness. The lower energy photopeak for ^{153}Sm represents ^{153}Eu X-rays and is comprised of a range of photons with energies between 40-48 keV. This will cause deviations from the experimental attenuation model due to beam hardening.

2.3.2 Dead-time Losses

When a detector such as a NaI crystal receives a photon, a photomultiplier tube is required to convert an extremely weak light signal into an electrical pulse. This pulse is subsequently sent to nuclear electronics for signal processing. However, all electronic instruments require a certain finite time to process a signal. During this time no other input pulses can be serviced and the electronics are essentially considered "dead". The time interval during which the electronics are "dead" is known as dead-time.

There are two fundamental types of dead-time; paralyzable and non-paralyzable. Mathematically, paralyzable and non-paralyzable dead-times are described by equations 2-14 and 2-15:

$$N_o = N_i e^{-N_i \tau} \qquad (2\text{-}14)$$

$$N_i = \frac{N_o}{1 - N_o \tau} \qquad (2\text{-}15)$$

A paralyzable system exists when a second pulse is detected within the dead-time period of the first pulse; the second pulse is not counted and the dead-time period is restarted at the time of the arrival of the second pulse. Conversely, non-paralyzable systems cause all pulses arriving during the dead-time period to be simply ignored and a new dead-time cycle cannot start until the previous period has ended. Therefore, the non-paralyzable system can recognize a maximum of one pulse for every dead-time interval while the paralyzable system could conceivably produce only one pulse in every, say, hour. This means that the non-paralyzable system approaches asymptotically a value of $1/\tau$ for the observed count rate, while paralyzable behaviour will cause observed count rates to increase to a maximum and then decrease as count rate increases. Since the non-paralyzable model for dead-time has one observed value for each true value whereas the paralyzable systems may have two observed values for each true value, the non-paralyzable model is the preferred system.

2.3.3 Compton Crosstalk

Compton crosstalk or simply "cross-over" is the phenomenon resulting when photons deposit only a fraction of their original energies in the crystal and are detected as lower energy photons. This is primarily due to Compton events within the crystal and attenuator. The extent of

these two effects depends on: (1) The rejection of scattered photons by the detector and source collimation; (2) Crystal size and thickness; and (3) The SCA window settings affecting detector resolution.

Experimentally, cross-over is equivalent to the inclusion of the build-up factor in equation 2-2. For DPA, the build-up factor cannot be incorporated analytically but must be determined empirically from experiments prior to DPA calculations. The reason for this is two-fold. Firstly, by introducing even a linear model for build-up, the solution for the mass of either of the two components can only be arrived at by iterative techniques. Secondly, granting that the above can be performed, there are no tables of build-up factors for photon energies less than 200 keV. A cross-over correction is implemented simply by subtracting a percentage of the higher energy total counts from the lower energy total counts.

For wide beam geometry the build-up factor is no longer unity in equation 2-2. Figure 2-3 shows the relationship between absorber thickness, cross-over correction and beam geometry as determined by Smith and Tothill[29]. The difficulty with a wider beam is non-linear correction which can lower inherent accuracy. However, with a wider beam the statistical error can be reduced per unit sample time due to a higher count rate. Since the cross-over correction must be determined prior to DPA measurement,

correct estimation of total thickness is crucial for accurate results when the cross-over is non-constant (i.e., wide beam geometry). This essentially leads to a compromise between error due to incorrect total thickness estimate prior to DPA measurements at wide beam geometries and lower count rates at narrow beam geometries.

There is disagreement among researchers over the best detector and source collimator dimensions. Table 2-1 displays a summary of experimental variables used by several researchers. Those listed either mention that the cross-over correction is independent of absorber thickness or don't consider the dependence at all. An exception are Peppler and Mazess[30] who state that their cross-over correction varies with depth ; 1.8% at 14 cm. and 3.4% at 25 cm. Smith and Tothill[29] verified that the amount of cross-over depends on the size of the beam and the thickness of the patient. They concluded that, with small collimation similar to those used by Wilson[7], Witt[31], Dunn[10], and Riggs[26], the variation in cross-over due to changing absorber thickness is small. Consequently, the cross-over correction can essentially be considered constant. In addition, Smith and Tothill showed that, for a 13mm (diameter) source and 20mm (diameter) detector collimator using ^{153}Gd, the cross-over correction varied from 2.5% at 0 cm of soft tissue to 4.2% at 25 cm of soft tissue.

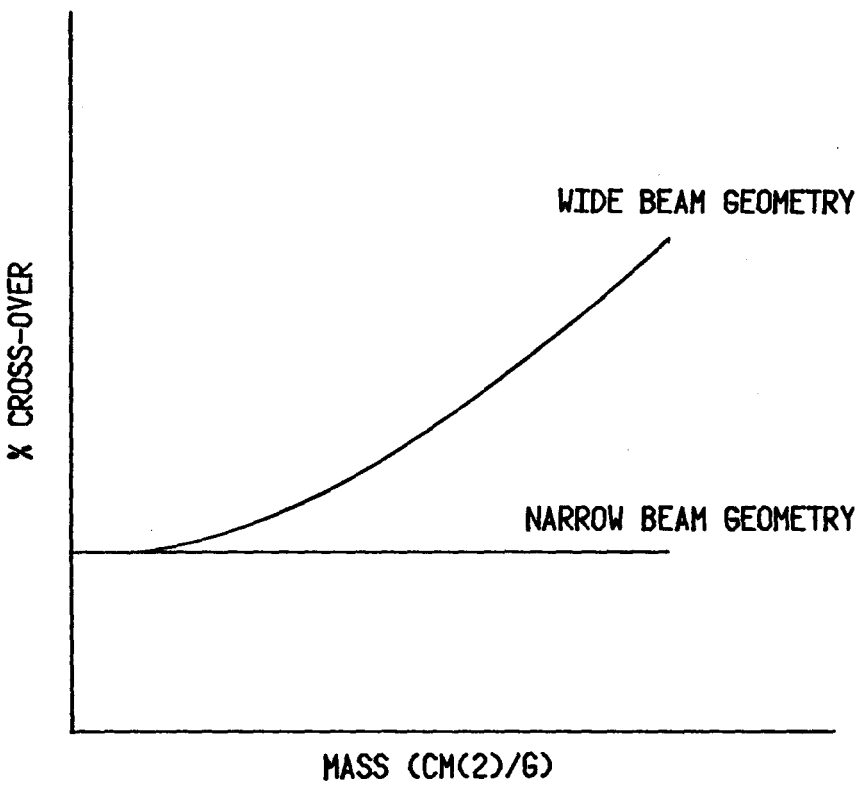

Figure 2-3 The relationship between cross-over correction, absorber thickness and beam geometry.

Researcher	Source Strength (Curies)	Detector size (dia.xthick.) mm.	Collimator		Distance Source/Det. cm.	OX %
			Source mm.	Detector mm.		
Wilson/Madsen [7] (1977)	1.5	12.5x37.5	4	-	55	3
Witt/Mazess [31] (1978)	<.1	10.0x3.0	3	6	-	-
Dunn/Wahner [10] (1980)	1.5	25.0x1.0	4	6	40	5
Krolner [8] (1980)	1.0	25.0x30.0	4	13	30	1
Riggs [26] (1981)	-	-	-	6	-	4-6
Peppler/Mazess [30] (1981)	.5-1.5	50.0x7.0	-	8x25	60	1.8-3.4

Table 2-1 Comparison of DPA experimental geometry.

-= information not available.

2.3.4 Scanning Geometry

The scanning geometry is the physical orientation in which the photon beam interacts with the attenuating material. Since it is the bone or bone substituting material that is being measured, this is the interaction of most concern. One phenomenon of major importance occurs at the interface parallel to the photon beam between the soft tissue and bone, and is known as "edge effects". At the edge of the bone there is a finite beam profile with non-uniformity of energy across the total beam at the bone exit point. This can cause an under-estimate of the BMC if the photon beam is only partially filled. Judy[13] and Watt[32] investigated this phenomenon and Watt termed it "partial volume effects".

Watt also investigated the accuracy and precision of the intermittent and continuous scanning methods. The intermittent scan method requires that stationary data be collected at several positions. Conversely, in the continuous mode, data are collected for a fixed time interval while the source and detector are in uniform motion across the sample. He found that intermittent scanning provided the greatest accuracy and precision because it does not involve finding the average BMC in a sample space. However, this argument represents the ideal situation and does not consider the effects of the mechanical system. Errors in positioning will result due to the limited ability of the motor brakes to compensate for the inertia of the transverse block.

Therefore, the choice of scan mode will depend not only on the mathematically optimal method but also on the scanner design.

CHAPTER 3

Experimental Apparatus and Material

Once the theoretical framework has been produced, the proper introduction of such theory to experimental scrutiny is highly contingent on the correct selection of experimental apparatus. For clarity, the materials selected as photon absorbers are differentiated from experimental apparatus.

3.1 Experimental Apparatus

To extract and analyze information obtained by the DPA method correctly and efficiently, the following equipment was required: (1) source and detector hardware; (2) signal processing hardware; (3) computer and interface hardware; and (4) a rectilinear scanner.

3.1.1 Source and Detector Hardware

The source and detector hardware included the brackets and collimators. The diagrams of all mechanical components are contained in appendix 7. The detector mounting bracket was designed such that the source-detector distance could be set between 15 and 50 cm. The detector collimator consisted of a lead cylinder 6 cm. long and 4.5 cm. in diameter with a single cylindrical hole 6mm. in diameter. The source holder was made of lead with an adjustable base for axial alignment with the detector. There was a circular photon beam port for

the source which was 2 mm. in diameter and 6.5 cm. in depth.

3.1.2 Signal Processing Hardware

The detector was a NaI(Tl) scintillation crystal (4.1 cm. diameter, .3175 cm. thick, with an aluminum shield .1 mm thick) supplied by a Harshaw NV-26 high voltage unit. The photomultiplier tube was optically coupled to the NaI crystal. The signal from the photomultiplier tube was shaped by a double delay line to provide a double pseudo-rectangular pulse such that the two timing single channel analyzers (SCA) can use cross-over detection of the incoming signal. The low energy channel utilized an SCA (Canberra 1436) while the high energy pulses were discriminated by a combined SCA (Canberra 1437) and delay module (Canberra 2055). The delay module was required because the Canberra 1437 had a maximum delay of 1.0 us while a 1.2 us delay was required. Each SCA was connected to the interface circuitry of a Nova™ (Data General) computer.

3.1.3 Computer and Interface Hardware

The block diagram of the computer interface for the rectilinear scanner and nuclear instrumentation is shown in figure 3-1. The schematic diagrams are contained in appendix 8. Each SCA was connected to a 64 kbit counter. Software could instruct the computer to transmit signals that would start, stop, and clear the counters. In addition, the

computer could receive longitudinal and transverse pulses from the scanner that indicated the probe's direction, location and speed. The longitudinal and transverse counters had a maximum count of 16 and 256 respectively before overflow occurred. While receiving data concerning the probe's motion, the computer could transmit signals to the motor relays to produce motion in either the forward, backward, left or right direction.

3.1.4 The Rectilinear Scanner

To allow stationary as well as motional studies, an OHIO Nuclear (now Technicare) rectilinear scanner (Model-84) was modified. Rectilinear is emphasized because the electronics that control the motion allow movement in either the x-axis or y-axis direction at one particular time but not both. Each directional counter located at the computer has two input signals; one to indicate the displacement and the other to indicate the direction of the transverse block. The signals are taken from the translator circuit boards located within the "C" frame of the scanner. The longitudinal signal provides 32 pulses/inch while the tranverse signal has 200 pulses/inch. There is a higher resolution in the transverse direction because the machine was designed such that data acquisition would predominate in this direction.

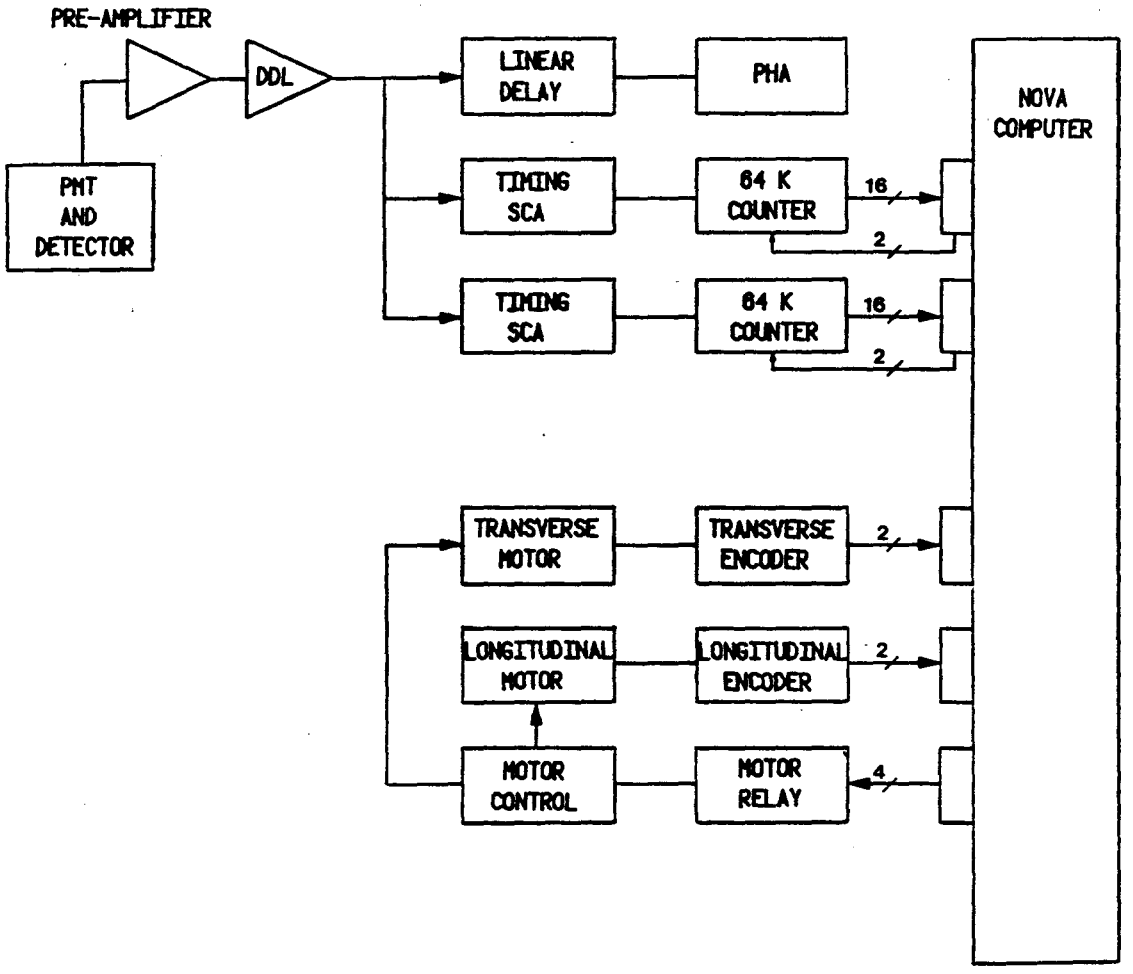

Figure 3-1 Block diagram of the signal processing and interface hardware.

3.2 Material Selection

Two areas that required optimal selection of materials were: (1) The standard used for reducing dead-time errors during measurement of the initial counts in air; and (2) The phantom materials used for body tissue substitutes.

3.2.1 Material for Standard

The initial counts could not be obtained directly through air because the electronics had a finite resolving time that would cause count rates above 5000 counts/second to result in dead-time errors above 1% (appendix 1). Therefore, an attenuating material or "standard" had to be used to lower the count rate. The major requirement that the standard had to fulfill was that the attenuation of the 42.5 and 103 kev photons resulted in observed count rates such that:

$$I^{42.5}_{observed} \doteq I^{103}_{observed} \qquad (3\text{-}1)$$

so that the precision of the low and high counts would be similar.

To determine the material z suitable as a standard, the ratio

$$\frac{u_z^{42.5}}{u_z^{103}} \qquad (3\text{-}2)$$

had to be optimized. Using equation 2-1 the attenuation

coefficient ratio in equation 3-2 was obtained from:

$$\frac{I^{42.5}_{observed}}{I^{103}_{observed}} = \frac{I^{42.5}_{o}\exp(-u^{42.5}_{z}m)}{I^{103}_{o}\exp(-u^{103}_{z}m)} \qquad (3\text{-}3)$$

From experimental results for ^{153}Sm and the associated geometry, the photopeak ratio at the source was approximately:

$$\frac{I^{42.5}_{o}}{I^{103}_{o}} = 1.1 \approx 1.0 \qquad (3\text{-}4)$$

The closer the attenuation coefficient ratio is to unity, the better the estimate of the initial counts will be. Consequently, the coefficients at the two energies should be similar. The attenuation coefficient ratios for aluminum, water and polyethylene are 1.98, 1.51 and 1.27 respectively. Based on the above argument, polyethylene should provide the best statistical results for the determination of initial counts.

3.2.2 Selection of Body Tissue Substitutes

For the initial experiments, body component substitutes of known physical and chemical constitution were used. The criteria for choosing a body tissue substitute are: (1) economy; (2) easy availability; and (3) close simulation of the tissue attenuating and scattering properties. Table 3-1 shows body tissue substitutes

previously used in DPA studies. Those researchers listed in table 3-1 gave no explanation or rationale to justify their choice of phantom material. In an extensive review of tissue substitutes by White[33] in 1977, four criteria were identified to assess the suitability of body tissue substitutes. These were the mass attenuation and energy absorption coefficients for photons and the electron mass stopping and angular scattering powers for an energy range of .01 to 100 MeV. If a material is to be considered as an adequate substitute of a body tissue for photon interaction, the scattering and radiation absorption characteristics for a particular thickness of the substitute must be the same for the same thickness of tissue. White found that the most popular muscle substitutes are water, wax, Mix D, polystyrene, TEMEX sheets, plexiglass and presswood. For fat and bone, polyethylene and aluminum are respectively the most frequently quoted substitutes. In the energy range of 10 to 100 keV, water proved to be the best soft tissue substitute considering the above criteria. White also concluded that if the fat substitute must be solid and readily available then polyethylene is a good choice. Aluminum is far from the best bone substitute. However, when the ease of use and availability are considered, aluminum is adequate for anthropomorphic studies. Therefore, the soft tissue, bone, and fat substitutes that were used in this study were water, aluminum, and polyethylene respectively.

Researcher	Body Tissue Substitute		
	Soft Tissue	Fat	Bone
Judy (1971) [13]	water	-	$Ca_{10}(PO_4)_6(OH)_2$ Hydroxyapatite
Wilson (1977) [7]	water	polystyrene	aluminum
Witt (1978) [31]	polymethyl-methacrylate	-	aluminum, saturated solution of K_2PO_4
Krolner(1980) [8]	water	triglyceride-3-oleic acid triglyceride-3-palmitic acid	aqueous solution KOH, KH_2PO_4

Table 3-1 Comparison of body tissue substitutes.

CHAPTER 4

Data Acquisition and Analysis

The DPA project goal was to produce a clinically viable instrument that could measure BMC with a reproducible precision within 3%. This process was sectioned into the three following phases:

1/ Stationary measurements with a two-component model.
2/ Stationary measurements with a three-component model.
3/ Motional measurements with a two-component model.

Phase 1 of the project attempted to demonstrate that DPA, using ^{153}Sm and the associated beam geometry, yields a precise and reproducible measurement of mass of bone-simulating material (i.e., phantoms) under limited conditions (i.e., no fat). Phase 2 introduced the effects of fat on the results obtained in phase 1. Once confidence in one-dimensional measurements was assured, phase 3 of the study instituted a two-dimensional measurement consisting of mass with the added dimension of width.

4.1 Phase 1: Stationary Measurements - Two-Component Model

Phase 1 provided a basis for the subsequent experiments. Although the major objective was to show that ^{153}Sm could produce precision greater than 3%, there were

other minor objectives that had to be satisfied. These minor objectives included determination of: (1) the cross-over correction; (2) the standard for initial counts; (3) dead-time; (4) effects of background and source decay correction; (5) the influence of detector collimator entrance diameter and depth; and (6) SCA window settings.

4.1.1 Experimental Description

The experimental configuration is shown in figure 4-1. The tank was made from .25 inch thick plexiglass and contained the aluminum plates submerged in water that were used to simulate bone and soft tissue respectively. The aluminum plate thickness used ranged from .314 to 1.91 cm. Because of impurities, the tabulated attenuation coefficients in Hubble[34] for aluminum could not be used uncorrected. Compensation was made for copper and iron concentrations that were different for each plate thickness (appendix 4). The distance between the faces of the source and detector collimators was 30 cm.. While the detector collimator was set at 6 mm., the source collimator was 2 mm. in diameter. The SCA windows were 13 and 30% for the low and high energy channels respectively. In addition, the source activity ranged from .8 to 2.8 curies for each experimental session over a period of 72 hours (appendix 5). The above factors were constant throughout the duration of phase 1.

The experimental method consisted of observing the effect of a non-constant water level (soft tissue), on the precision and accuracy of measured aluminum thicknesses (bone) between 0 and 1.91 cm. Water thicknesses ranging from 15 to 22.5 cm. were used since Smith[29] found that the mean supine anterior to posterior thickness at the lumbar region in 180 normal subjects is 22 cm (15-29) in men and 19.8 cm. (15-29) in women. If for each aluminum thickness the precision and accuracy was within 3% then confidence in the technique would be realized.

4.1.2 Cross-over Correction

The cross-over correction is dependent on measurement geometry, detector size, and the amount of absorber in the photon beam. Since the same detector was used for both high and low energy counts and only the ratios of high to low energy photons were considered, detector effects could be considered negligible. Once the measurement geometry was set, it remained the same throughout the experiment. As previously discussed, the wider the beam geometry the greater the absorber thickness effect on the cross-over correction. This results in a varying cross-over correction which is difficult to incorporate experimentally.

To determine the cross-over correction, researchers normally use various copper or aluminum plate filters (Smith[29], Peppler[30]). However, there seems to be limited

agreement on the best technique to use (Smith[29]). For this project the cross-over correction was determined by iterating the correction until the maximum accuracy was obtained. Narrow beam geometry can be determined by testing the cross-over correction through a range of absorber thicknesses. If the accuracy is constant within limits, then the correction is constant. However, if the accuracy decreases with increasing absorber thickness, the correction is not constant and must be determined at each thickness (i.e., wide beam geometry). To determine whether the iterative technique can unconditionally provide greater accuracy than the filter technique, further study is required.

A cross-over correction of 5.5% was determined empirically for the previously stated geometry. Figure 4-2 shows the relationship between the cross-over correction and the source-to-detector distance for the experimental geometry. The correction increases as the distance from the source increases. This is due to the increased detection of multiply scattered photons. The corrections were tested through a range of absorber thicknesses and the limit on the accuracy was found to be constant. This indicated that the geometry was essentially narrow beam allowing a constant cross-over correction to be used.

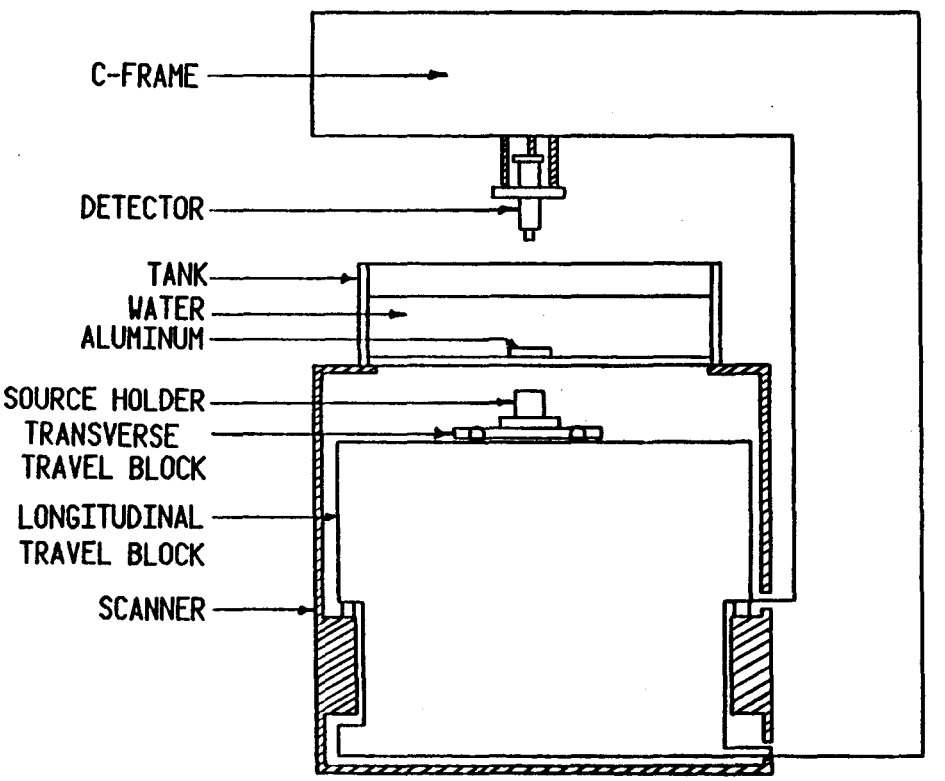

Figure 4-1 Pictorial of the experimental apparatus for phase 1.

4.1.3 Dead-time Correction

The dead-time for the experimental system was determined by two methods outlined in appendix 1. Method A incorporated the use of a double pulse circuit, in which both pulse width and delay between the two pulses were variable. Method B utilized the high count rate and short half life ($T_{1/2}$=24.99 min.) of ^{128}I to indicate the dead-time. Both methods produced a dead-time of approximately 2.0 us.. To keep the error due to dead-time to less than .5%, the count rate had to be less than 2500 c/s. In addition, Method B showed that the system was representative of a non-paralyzable model since the observed count rate was constant above $5x10^5$ c/s. This is the desired model because of the one to one relationship between observed and true counts. Experimentally, it was not practical to keep the count rate below 2500 c/s, so the non-paralyzable model was used to correct for dead-time losses. This is given by:

$$N_i = \frac{N_o}{1 - N_o\tau} \qquad (4\text{-}1)$$

Therefore, the true counts approach $1/\tau$ asymptotically as the observed counts approach infinity.

4.1.4 The Standard for Initial Counts

Because of the dead-time errors that would arise if the initial counts were measured through air, an attenuating medium had to used to lower the count rate at the detector. The attenuating medium is known as a "standard". As discussed previously, the best material for the standard is polyethylene. However, for phase 1 all data were acquired using a water standard because polyethylene was not available. For all subsequent experiments polyethylene was the standard.

The standard thickness was typically 22.9 cm., but was adjusted in some cases when the count rate was above 2500 counts/sec (.5% dead-time). To calculate the initial counts the density of the attenuating material had to be known. Since the manufacturer of the polyethylene gave an error of $\pm$ 3%, the density was determined by measuring the water displacement and mass of the polyethylene. The density was found to be .930 $\pm$ .005 g/cm^3. During the initial counts an effort was made to keep the count rate of both peaks between 1000 and 2000 c/s. This was done so that statistical considerations were balanced by the fact that at high count rates the dead-time correction was large and the model for non-paralyzable dead-time correction might not have accurately compensated for lost counts.

4.1.5 The Detector Collimator

The original detector collimator designed by Bhaskar[17] and the improvements subsequently incorporated are described in appendix 7. To determine the optimal detector collimation, a series of collimators with entrance diameters between 2 and 12 mm. were tested. The criteria for judgement of the most suitable collimator dimensions required a compromise between counting statistics and the build-up that was indicative of wide beam geometry. The resultant collimator entrance diameter was determined to be 6 mm. At smaller collimator entrance diameters there was a decrease in precision and accuracy while at wider diameters the accuracy decreased while precision increased.

4.1.6 Effects of Background and Source Decay

At high count rates (>1000 c/s) the background was essentially negligible. However, when the count rate decreased to approximately 100 c/s with an absorber in the beam of photons, the background constituted approximately 2% of the counts. Figure 4-3 shows the 42.5 keV energy photon count rate corrected for background and cross-over. At low count rates the curve deviates from linearity. When corrected for both cross-over and background the curve is linear.

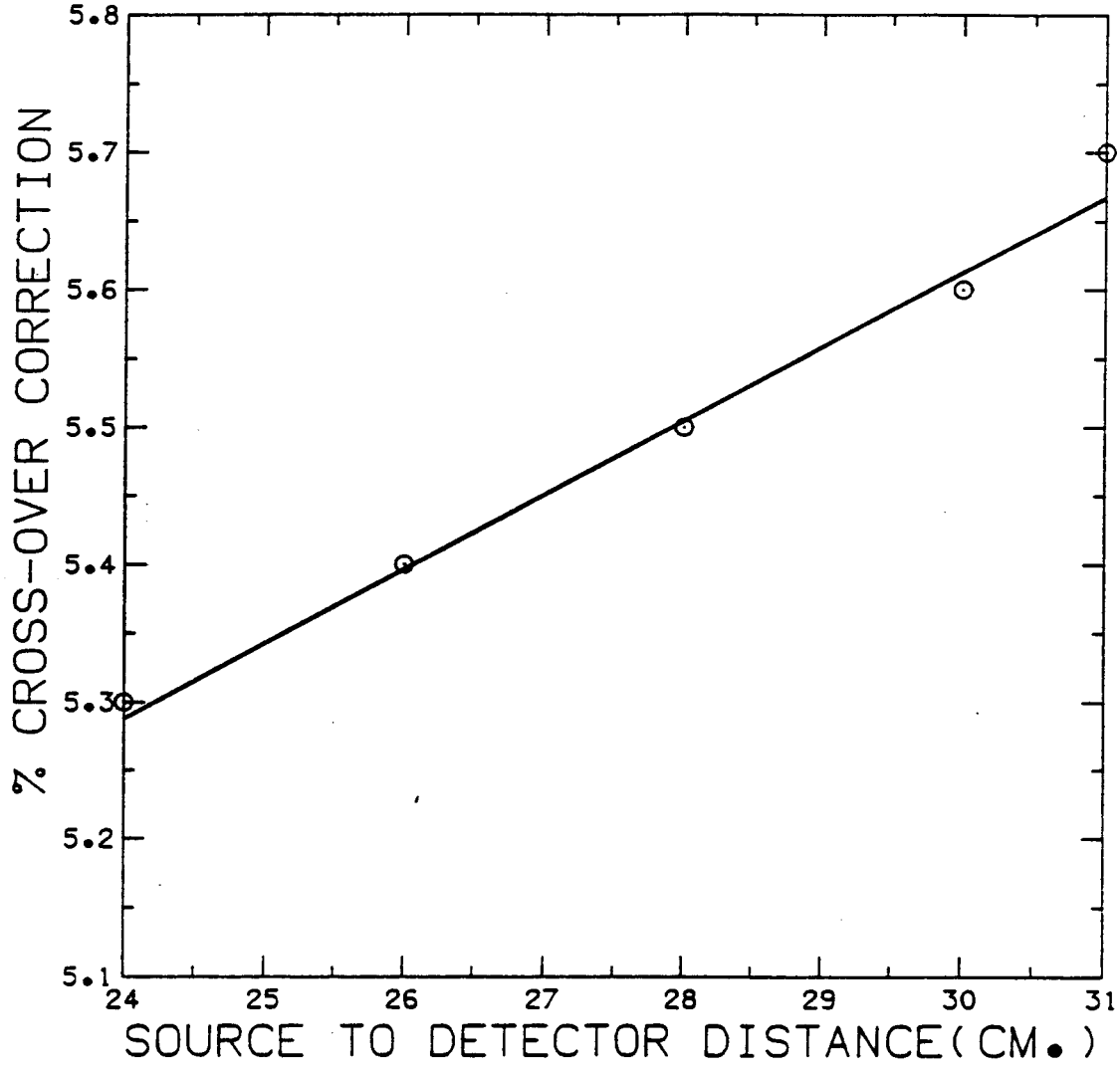

Figure 4-2 The relationship between the cross-over correction and the source-to-detector distance for the experimental geometry.

The transmission intensity of the 42.5 keV beam was determined by subtracting from the low energy counts the product of the percent cross-over (OX) and the high energy counts. This is given by:

$$*I_o^{42.5} = I_o^{42.5} - (OX) I_o^{103} \qquad (4\text{-}2)$$

A correction was also made for source decay. During sample periods of more than 2 hours the source would decay enough to cause the accuracy to decrease to less than 3%. When a correction for the decay was implemented, data sampling periods could be increased to 6 hours with no notable loss in accuracy or precision.

4.1.7 SCA Window Settings

The procedure for setting the SCA windows is outlined in appendix 3. Figure 4-4 shows the spectrum as detected by the experimental equipment. The pulse height analyzer was set to display 1024 channels. Using the 43 and 103 keV spectra peaks as data points, the energy per channel was determined to be .28 keV. The lower window was centered at 43 keV with limits of 25.5 and 62.5 keV which produced a width of 37 keV. The upper energy window was 62.5 to 145 keV with a peak at 103 keV. This corresponds to 13 and 30% of full scale for the low and high energy windows respectively.

4.1.8 Phase 1: Data Analysis

Before valid data can be acquired, certainty of exponential attenuation of the low energy photon beam must be realized in the range of absorber thicknesses to be studied. The above-mentioned corrections were applied for a complete combination of aluminum and water thicknesses, and the results are shown in figure 4-5. Because of the linearity of the 42.5 keV intensity using the 5.5% cross-over correction, the use of narrow beam mass attenuation coefficients is justified.

Table 4-1 shows the results of measurements on a two-component model taken from five, ^{153}Sm sources over a period of 8 weeks. The coefficient of variation indicates the precision and reproducibility of the data. Essentially, the precision throughout the range of aluminum thicknesses was less than 3%. The largest deviations in both accuracy and precision occurred at water thicknesses above 22.5 cm.. This may be due to the fact that the cross-over correction cannot be considered constant at absorber thicknesses above 20 cm. Also, there is the possibility that beam hardening of the X-rays grouped as 42.5 keV may justify the overestimate at large water and aluminum thicknesses.

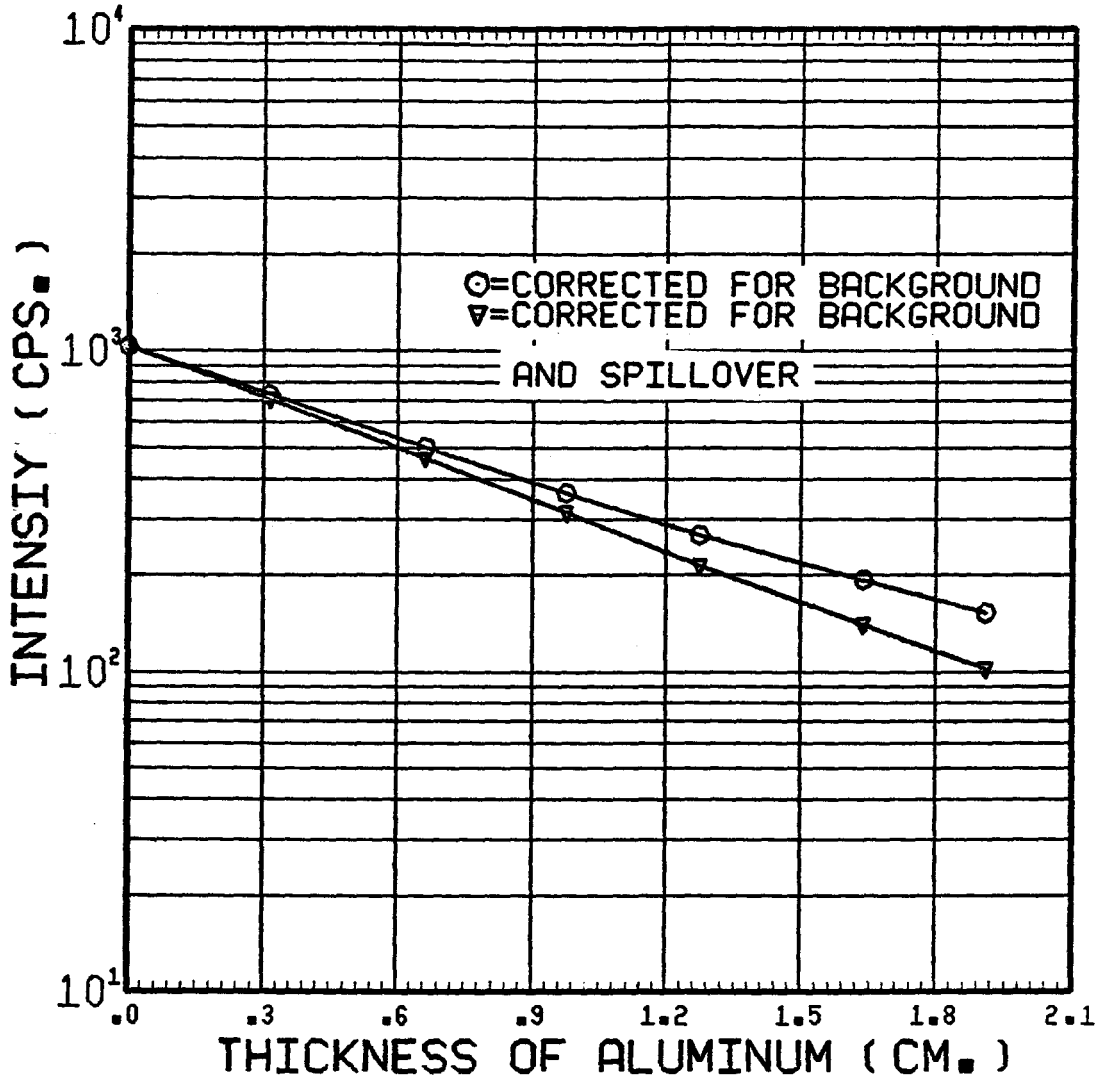

Figure 4-3 Transmission of the 42.5 keV photon beam through aluminum in 13 cm. of water with a 4.5% cross-over correction.

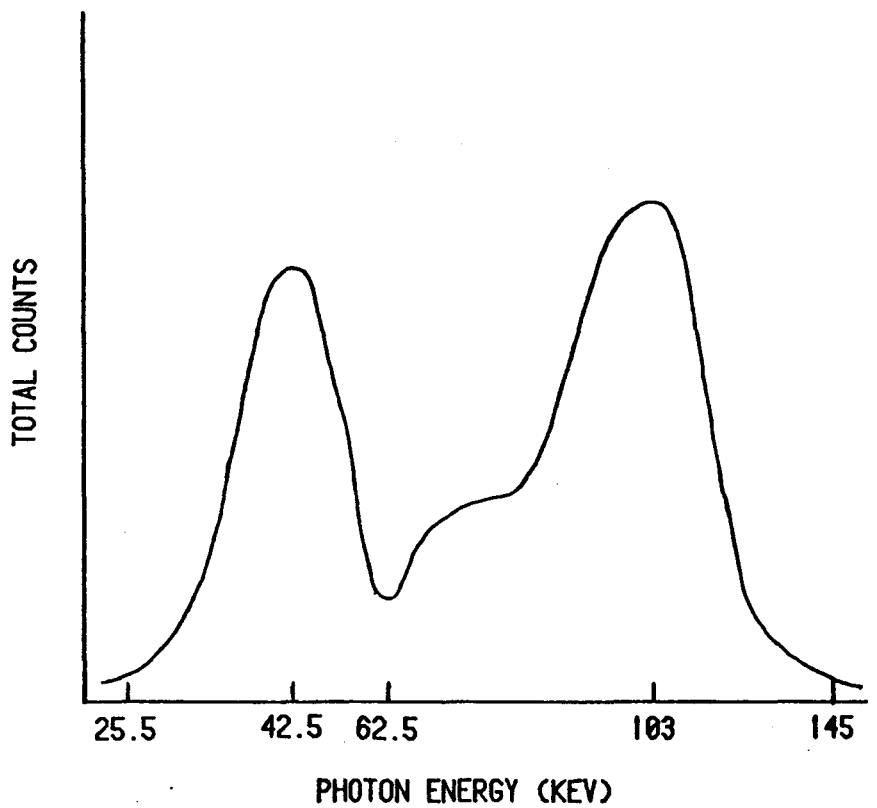

Figure 4-4 ^{153}Sm spectrum produced by the experimental apparatus.

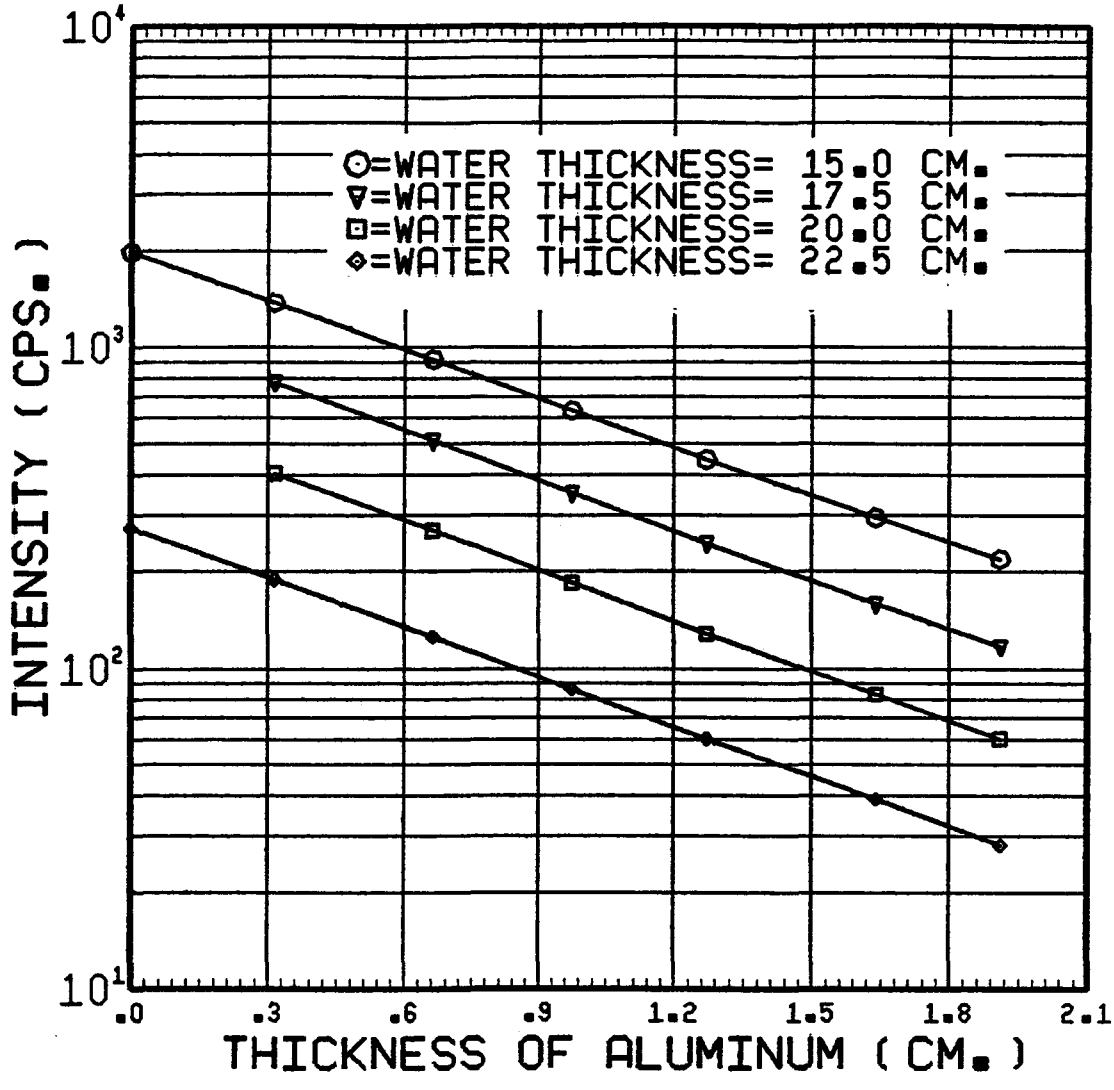

Figure 4-5 Corrected 42.5 keV transmission intensity for aluminum in various thicknesses of water.

True Aluminum Thickness (cm.)	Average Measured Aluminum Thickness % Coefficient of Variation				Accuracy %			
	Total Water Thickness (cm.)				Total Water Thickness (cm.)			
	22.5	20.0	17.5	15.0	22.5	20.0	17.5	15.0
.314	.300 5.0	.312 1.5	.313 1.7	.313 1.2	-4.5	-0.6	-0.3	-0.3
.662	.668 2.7	.666 0.8	.669 0.5	.673 1.2	1.0	+0.6	+1.2	+1.7
.974	.981 1.8	.989 1.2	.988 0.7	.988 1.3	+0.7	+1.5	+1.4	+1.4
1.272	1.28 2.5	1.28 0.9	1.28 1.1	1.28 1.3	+0.6	+0.6	+0.6	+0.6
1.636	1.66 2.4	1.66 1.7	1.66 1.4	1.65 1.2	+1.5	+1.5	+1.5	+0.9
1.908	1.93 2.3	1.91 1.8	1.90 1.3	1.90 0.9	+1.2	+0.0	-0.4	-0.4

Table 4-1 Precision and accuracy of DPA for the measurement of aluminum sample thicknesses in the ranging of .314 to 1.91 cm.

4.2 Phase 2:Stationary Measurements - Three-Component Model

Phase 1 of the experiment showed that ^{153}Sm could produce accurate, precise and reproducible results with a two-component model. Phase 2 was introduced to determine the effects of a third component on the accuracy and precision of results determined through a two-component model. As discussed previously, the only way to eliminate errors due to a third component was either to add an additional photon energy or keep the fat content constant. The latter of the two options was investigated in this paper.

4.2.1 Experimental Description

The effects of a non-uniform thickness of a third component in a two-component model was investigated. To accomplish this, the natural build-up of fat in the human body had to be simulated. The human body can have two forms of non-uniform fat: (1) The total thickness of the three components can increase with fat constituting a larger percentage of the total thickness as thickness increases; or (2) The total thickness can remain constant with the percent fat changing. An example of the latter occurs when the RST measurement (equation 2-13) is performed where there is no bone. The primary position for sampling where there is no bone is adjacent to the lower lumbar vertebrae. At this location, the beam of photons may pass through the kidney where normally a larger amount of fat resides than in the

lower lumbar region. An example of the former occurs when a very obese subject is scanned. In this case the total thickness from RST to BMC measurement as well as percent fat may not be constant.

The experimental configuration for phase 2 was the same as for phase 1 except for the addition of a third component, a change in source-to-detector distance and a modification of the cross-over correction. The third component added to simulate fat was polyethylene. A change in the source-to-detector distance from 30 to 31 cm. was required to accomodate the increased absorber thickness. Because of the change in geometry a new cross-over of 5.7 from 5.5% was implemented.

4.2.2 Phase 2: Data Analysis

Phase 2 data were acquired over a four week period with 3 sources of approximately 5 curie strength at the time of final irradiation. Each source was irradiated 36$\pm$.5 hours. The first segment of this experiment demonstrates the effect of a non-uniform fat layer (polyethylene) on the determination of aluminum thickness while keeping the total thickness constant. Figures 4-6 to 4-11 show the aluminum thickness as the polyethylene thickness was changed from the amount used in the RST measurement. Percent polyethylene

is given by:

$$\% \text{ Poly} = \frac{\text{Thickness of poly during BMC measurement}}{\text{Thickness of poly during RST measurement}} \times 100 \quad (4\text{-}3)$$

For example, if 3.26 cm. of polyethylene was used in the RST measurement, then 50% polyethylene would represent 1.63 cm. in the photon beam during aluminum measurement. The y-axis for these figures ranges from 50 to 150% of the true aluminum thickness and therefore allows comparison. As the true aluminum thickness increased, the range of error in the aluminum thickness estimate decreased for 50 to 150% change in polyethylene. This can be explained theoretically by considering equation 2-7. The term representing fat content is proportionally smaller for the same given polyethylene content in the BMC (i.e., m_f) and RST (i.e., m_{fo}) measurement compared to the term representing increasing aluminum thickness (i.e., equation 2-4). This results in a smaller error in bone mass (i.e., m_b). In addition, with lower percent polyethylene during BMC measurement than during RST measurement, the aluminum thickness was over-estimated. This is also in agreement with equation 2-7. Figures 4-12 and 4-13 show the error in aluminum thickness measurement for the percent change in polyethylene at 16.3% (3.26 cm.) and 8.3% (1.63 cm.) polyethylene in the RST measurement. Both figures demonstrate that the accuracy of the aluminum estimation increases as the amount of aluminum in the photon beam

increases. In addition, as the amount of polyethylene in the initial RST measurement increases, the error due to change in polyethylene during aluminum measurement increases. This indicates that the optimal situation for BMC measurement is on lean subjects. The result of a linear regression analysis is shown in figure 4-14. If the change in polyethylene content from the RST to the aluminum measurement is less than 50% at 16.3% initial RST polyethylene content, measurements of aluminum (bone) above 1.8 g/cm^2 (.662 cm. of aluminum) should be accurate to within 10% of the true aluminum (BMC) value.

The second experiment in this phase involved observing the effect of increasing polyethylene (fat) thickness as the total thickness was increased. Since female fat content normally varies between 20 and 40%, a similar range of polyethylene was used in conjunction with aluminum thicknesses between .314 and .974 cm. (.848 to 2.62 g/cm^2). Figures 4-15 through 4-17 show the error in the true aluminum thickness for percent change in polyethylene (fat) content from RST to aluminum (BMC) measurement. Again, for a given change in polyethylene there is a larger error for smaller aluminum thicknesses. The kink in the curves is present because at negative changes in polyethylene, total thickness was kept constant whereas at increasing percent polyethylene the total thickness was not constant. Intuitively, this is justifiable because for an increase in total absorber

thickness, polyethylene (fat) replaces air. Conversely, for decreases in percent polyethylene, water is replaced by polyethylene. Since polyethylene has a much greater linear attenuation coefficient than air, yet almost the same attenuating ability as water, the larger error at increasing total thickness (positive change in polyethylene) compared to constant total thickness is justified. In addition, as the percentage polyethylene in the initial RST measurement increases from 20 to 40%, the error in aluminum thickness is greater for a given percent change in polyethylene. This indicates that the highest accuracy of aluminum (BMC) measurement will occur in cases where there is low polyethylene (fat) and high aluminum (BMC) content.

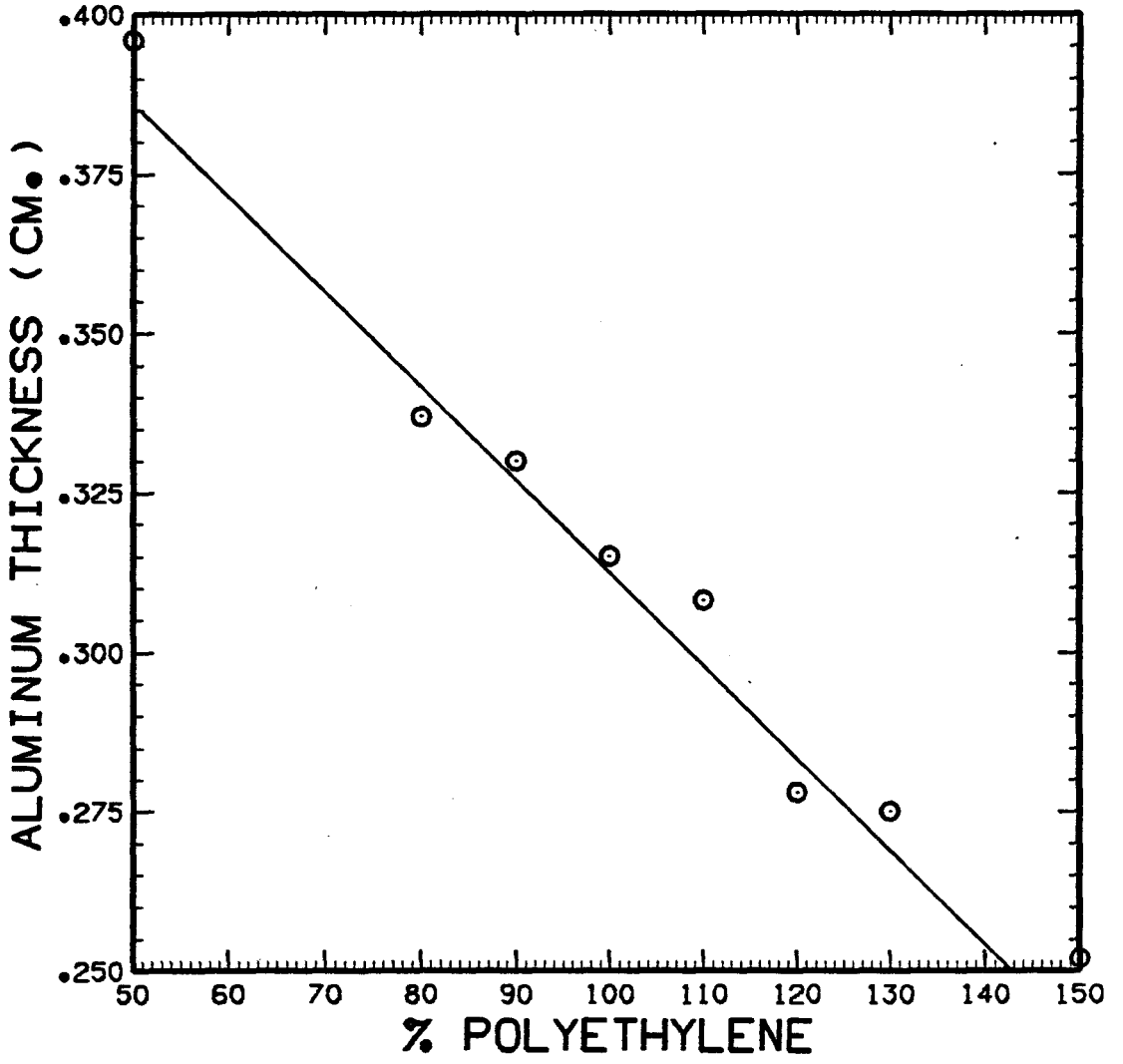

Figure 4-6 Aluminum thickness versus % polyethylene.

Total absorber thickness= 20 cm.

RST polyethylene thickness= 3.26 cm.

True aluminum thickness= .314 cm.

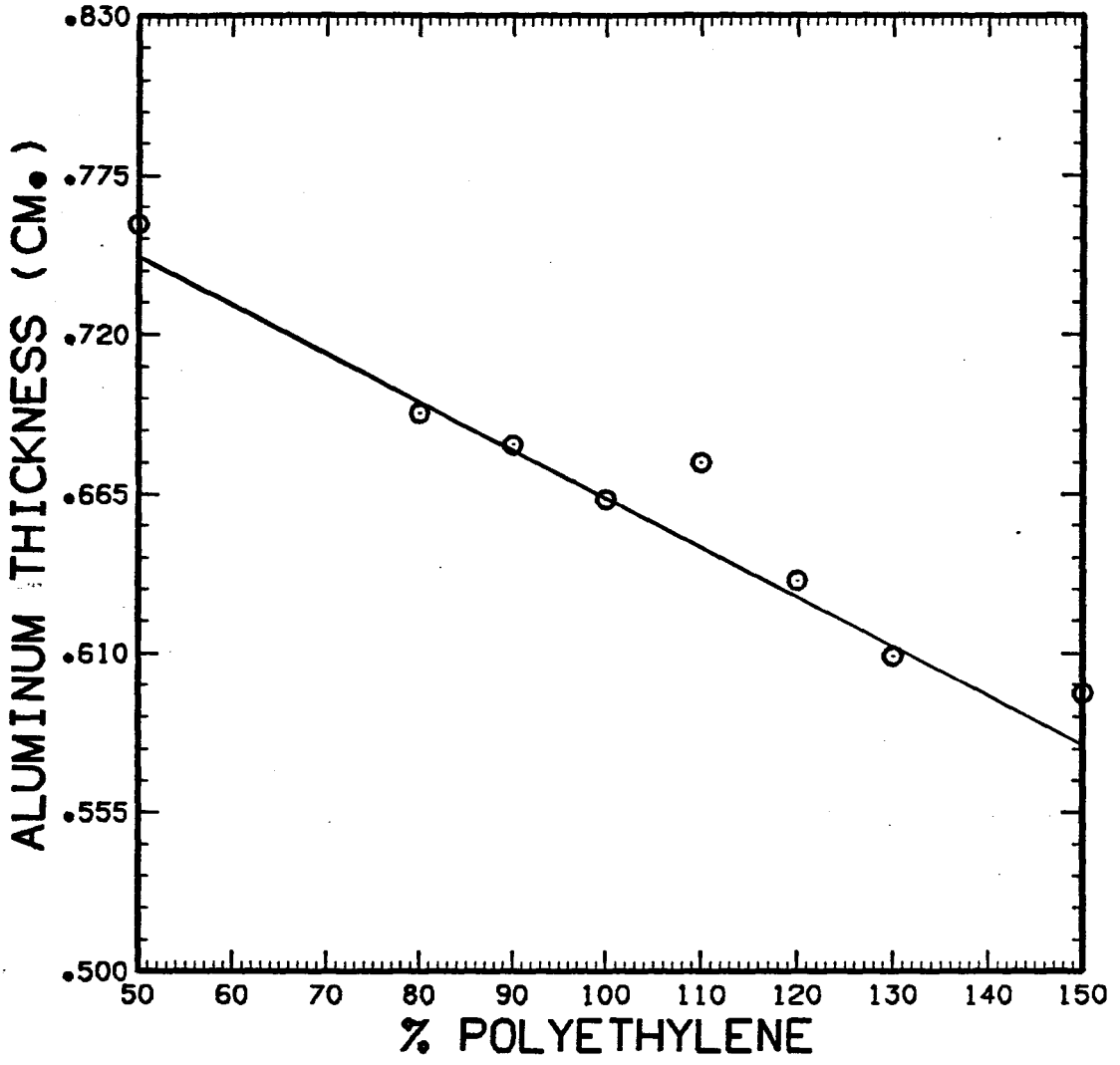

Figure 4-7 Aluminum thickness versus % polyethylene.

Total absorber thickness= 20 cm.

RST polyethylene thickness= 3.26 cm.

True aluminum thickness= .662 cm.

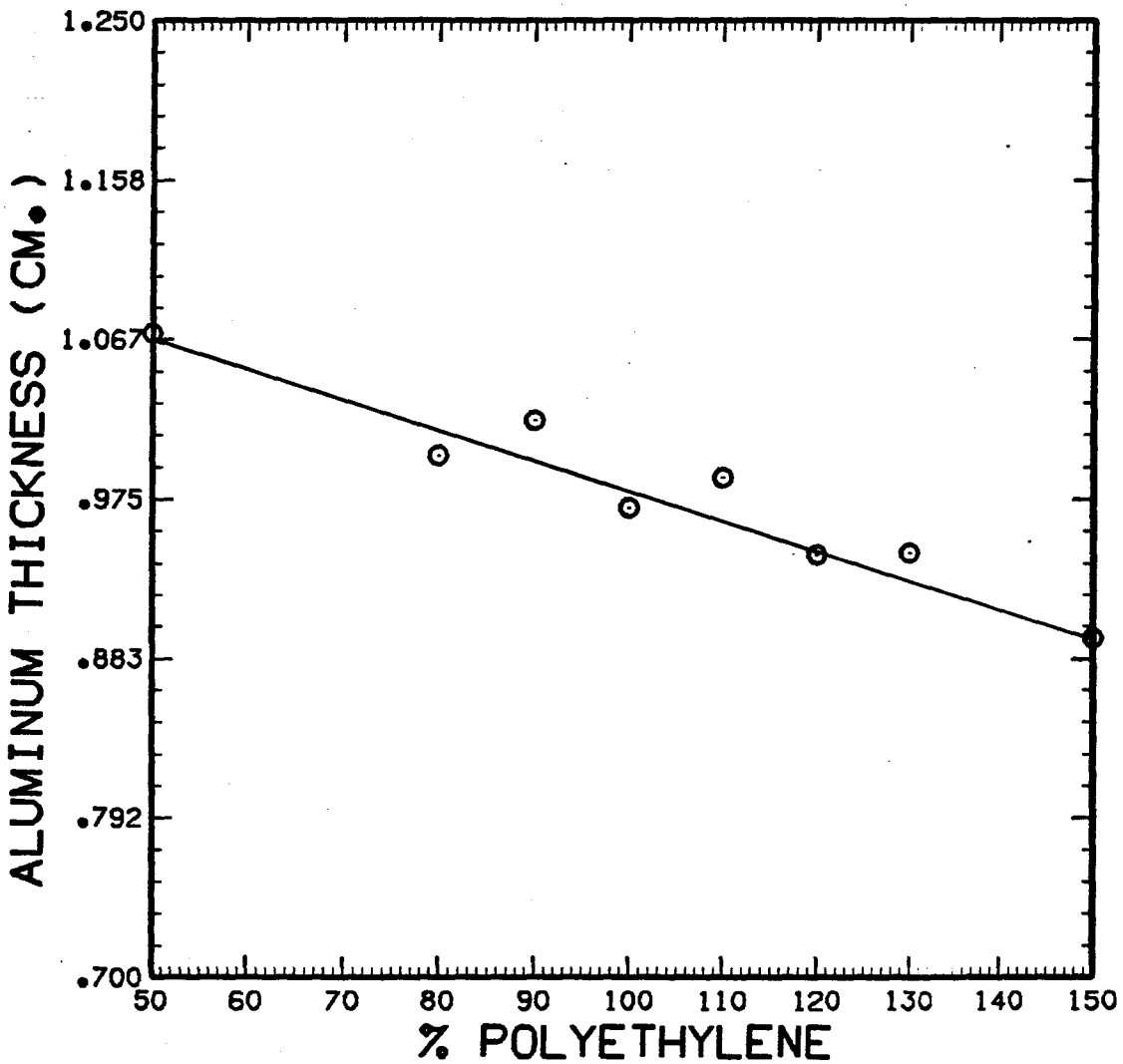

Figure 4-8 Aluminum thickness versus % polyethylene.

Total absorber thickness= 20 cm.

RST polyethylene thickness= 3.26 cm.

True aluminum thickness= .974 cm.

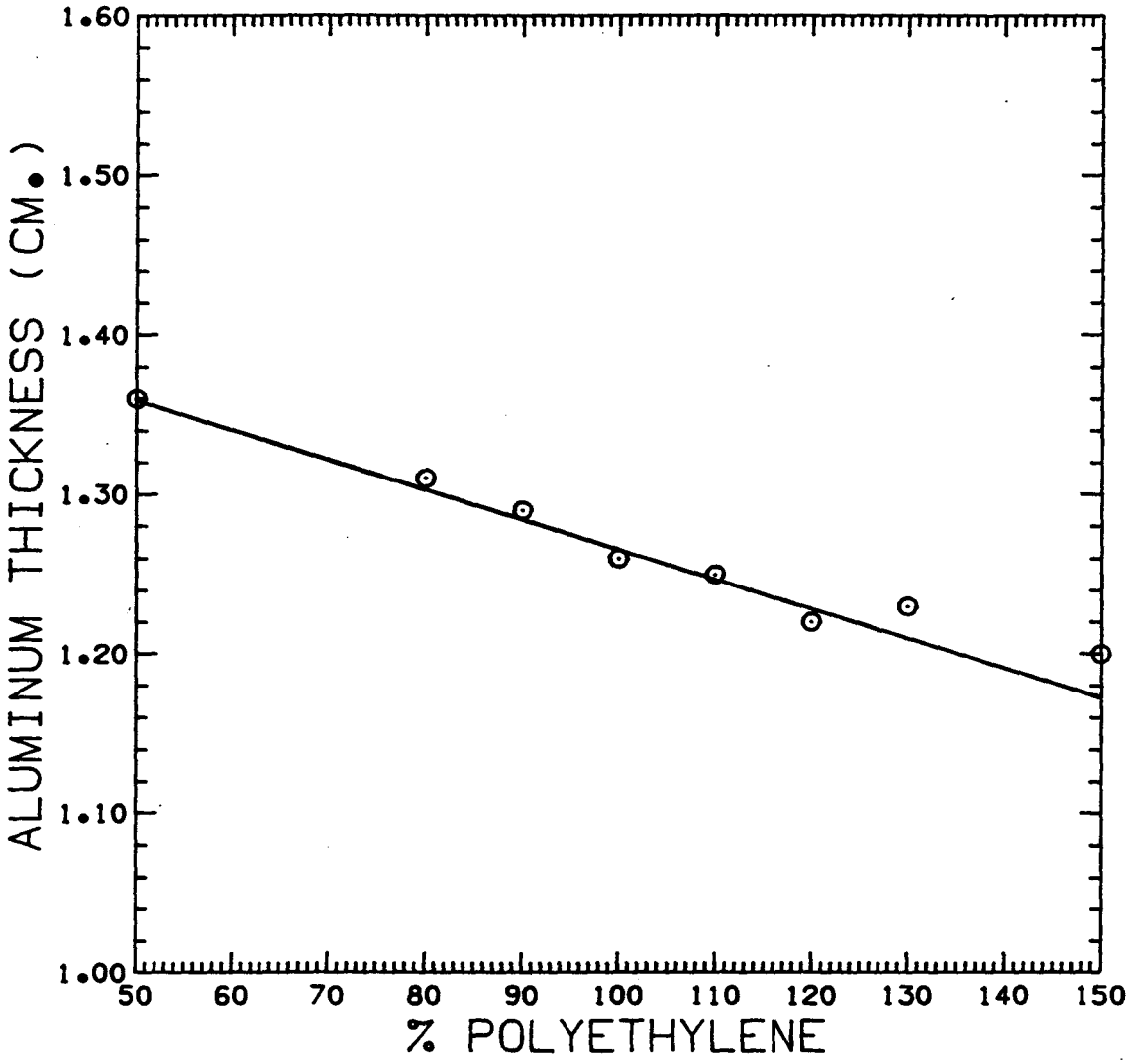

Figure 4-9 Aluminum thickness versus % polyethylene.

Total absorber thickness= 20 cm.

RST polyethylene thickness= 3.26 cm.

True aluminum thickness= 1.27 cm.

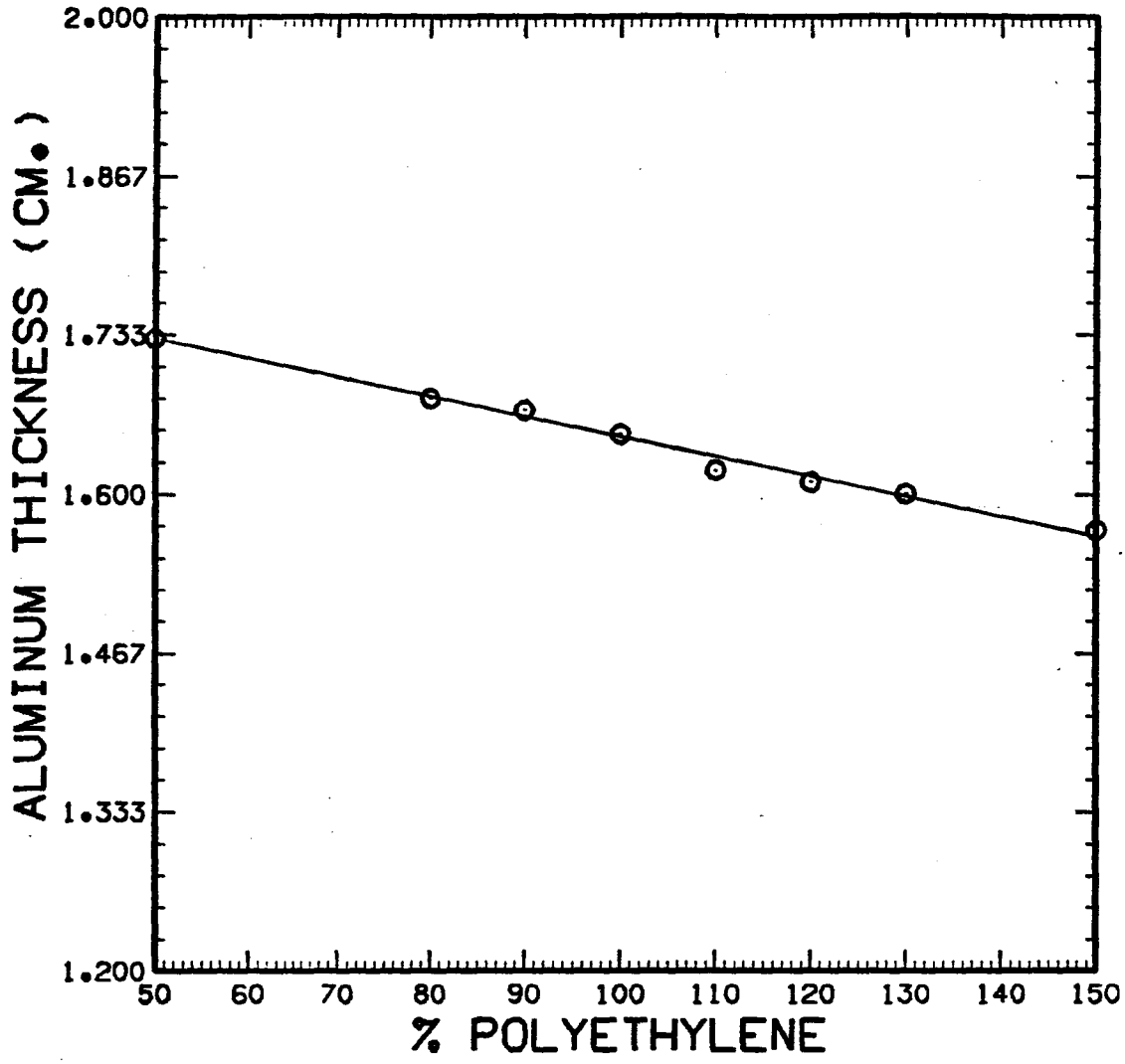

Figure 4-10 Aluminum thickness versus % polyethylene.

Total absorber thickness= 20 cm.

RST polyethylene thickness= 3.26 cm.

True aluminum thickness= 1.64 cm.

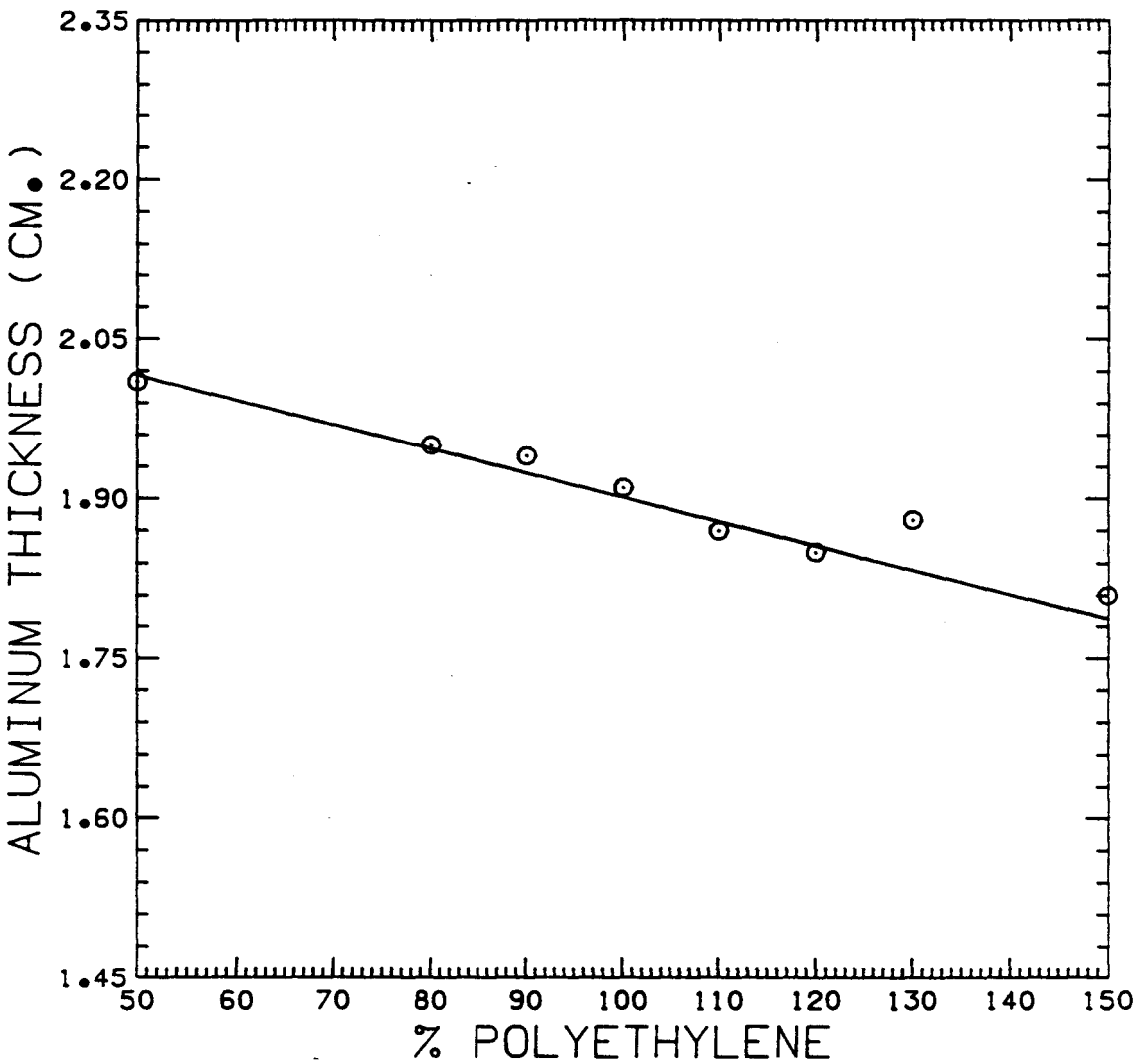

Figure 4-11 Aluminum thickness versus % polyethylene.

Total absorber thickness= 20 cm.

RST polyethylene thickness= 3.26 cm.

True aluminum thickness= 1.91 cm.

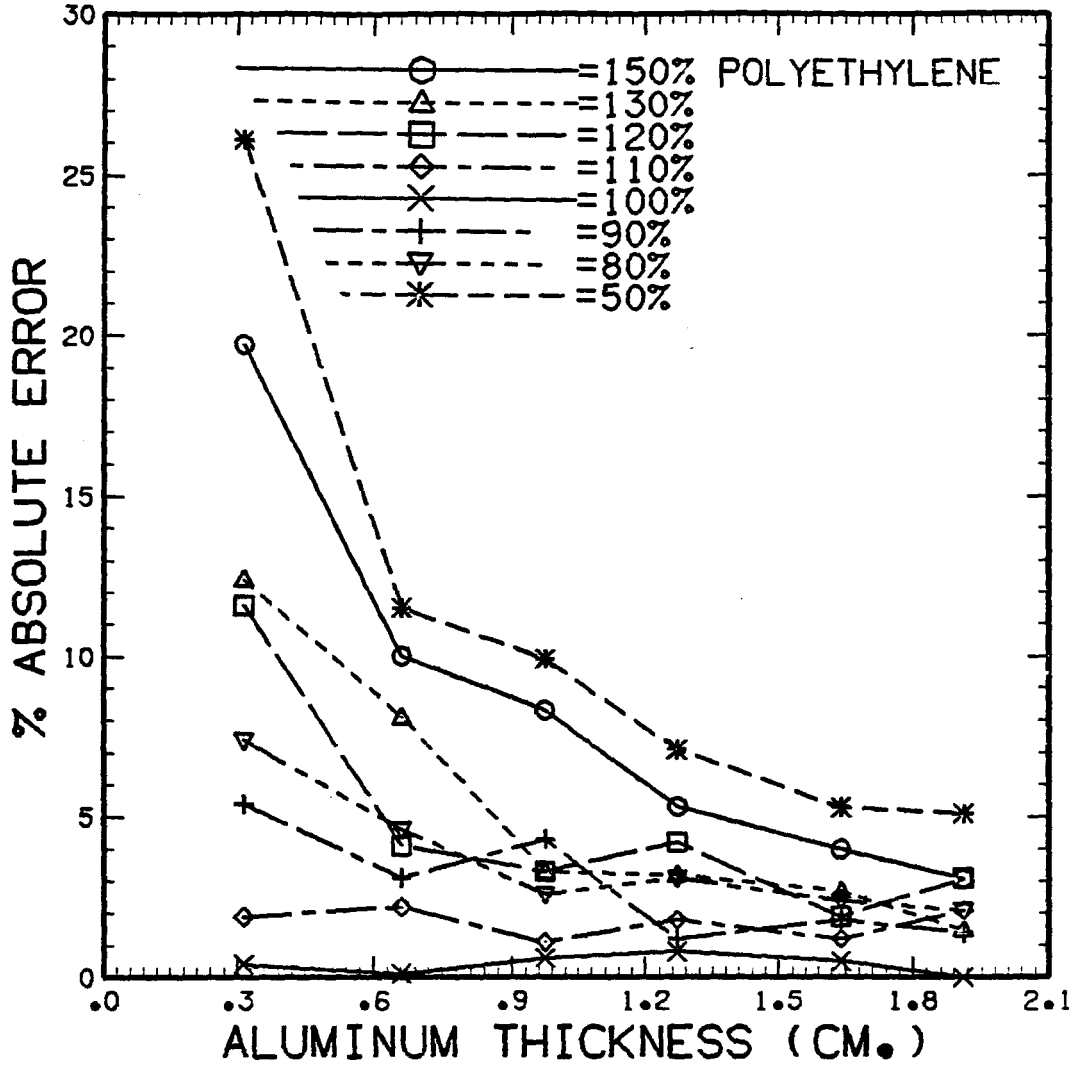

Figure 4-12 % error in measured aluminum thickness for 50 to 150 % polyethylene.
Total absorber thickness= 20 cm.
RST polyethylene thickness= 3.26 cm.

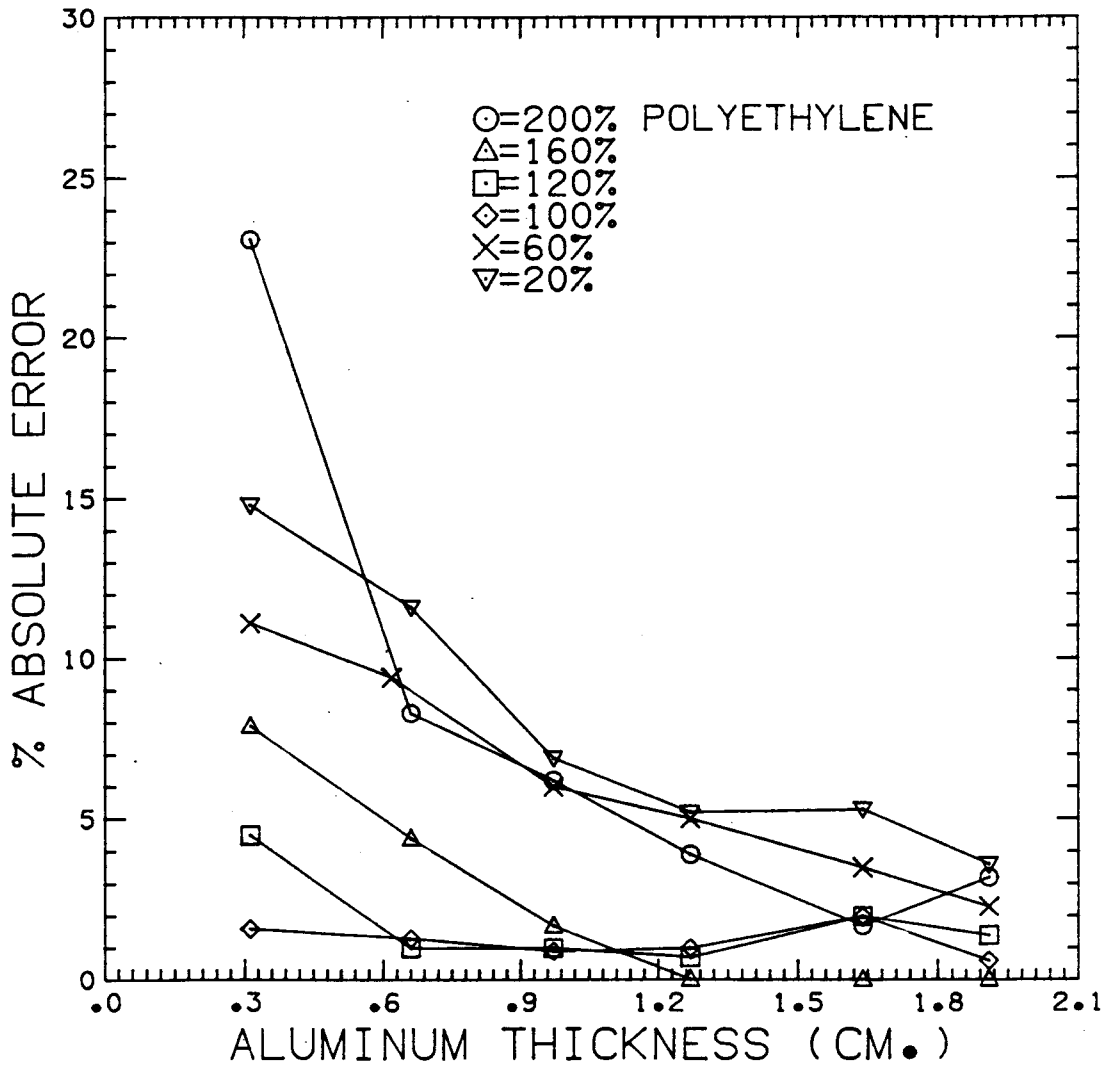

Figure 4-13 % error in measured aluminum thickness for 50 to 150 % polyethylene.
Total absorber thickness= 20 cm.
RST polyethylene thickness= 1.63

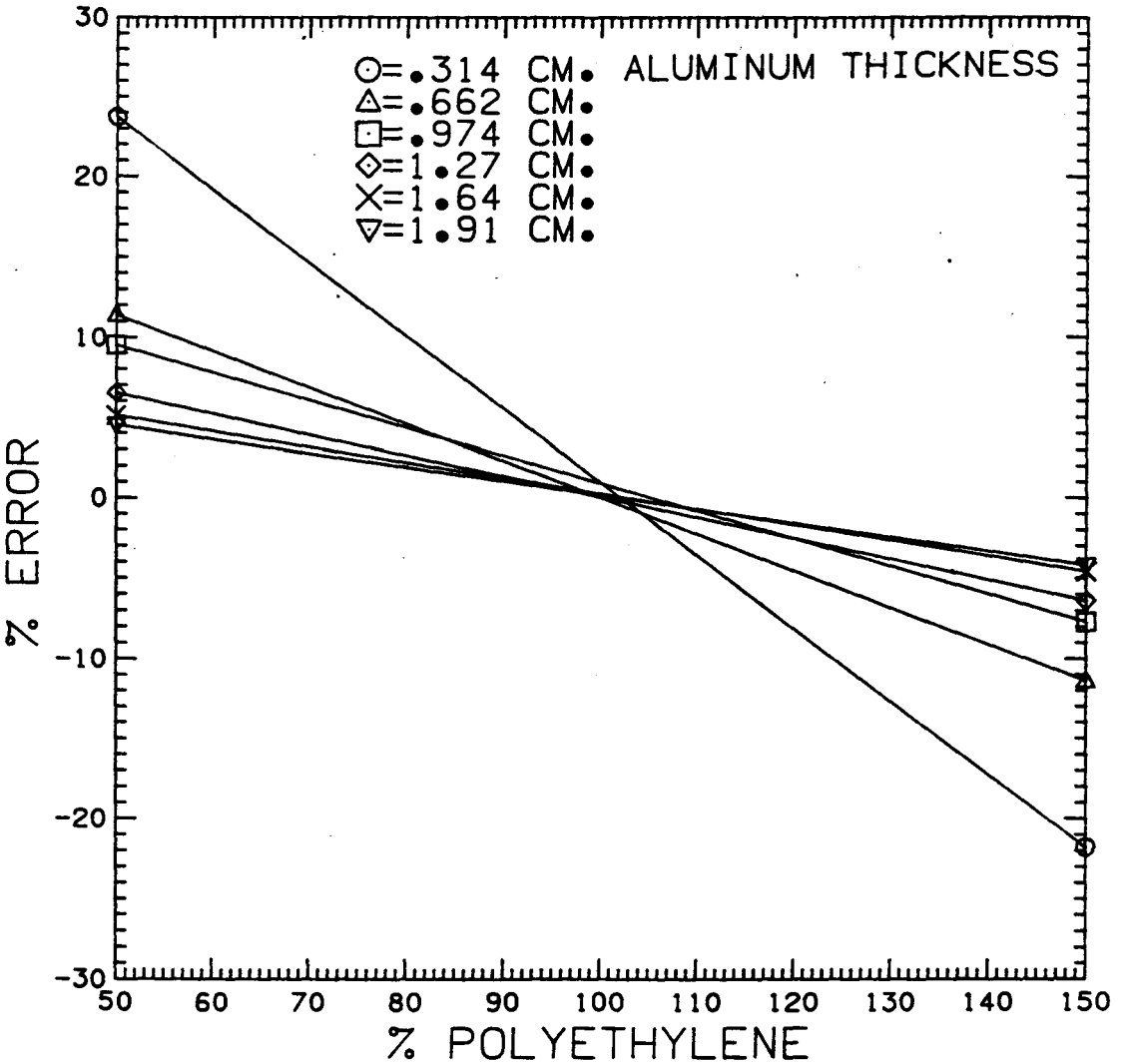

Figure 4-14 Linear regression of error in aluminum thickness versus % polyethylene for a range of aluminum thickness of .314-1.91 cm. Total absorber thickness= 20 cm. RST polyethylene thickness= 3.26 cm.

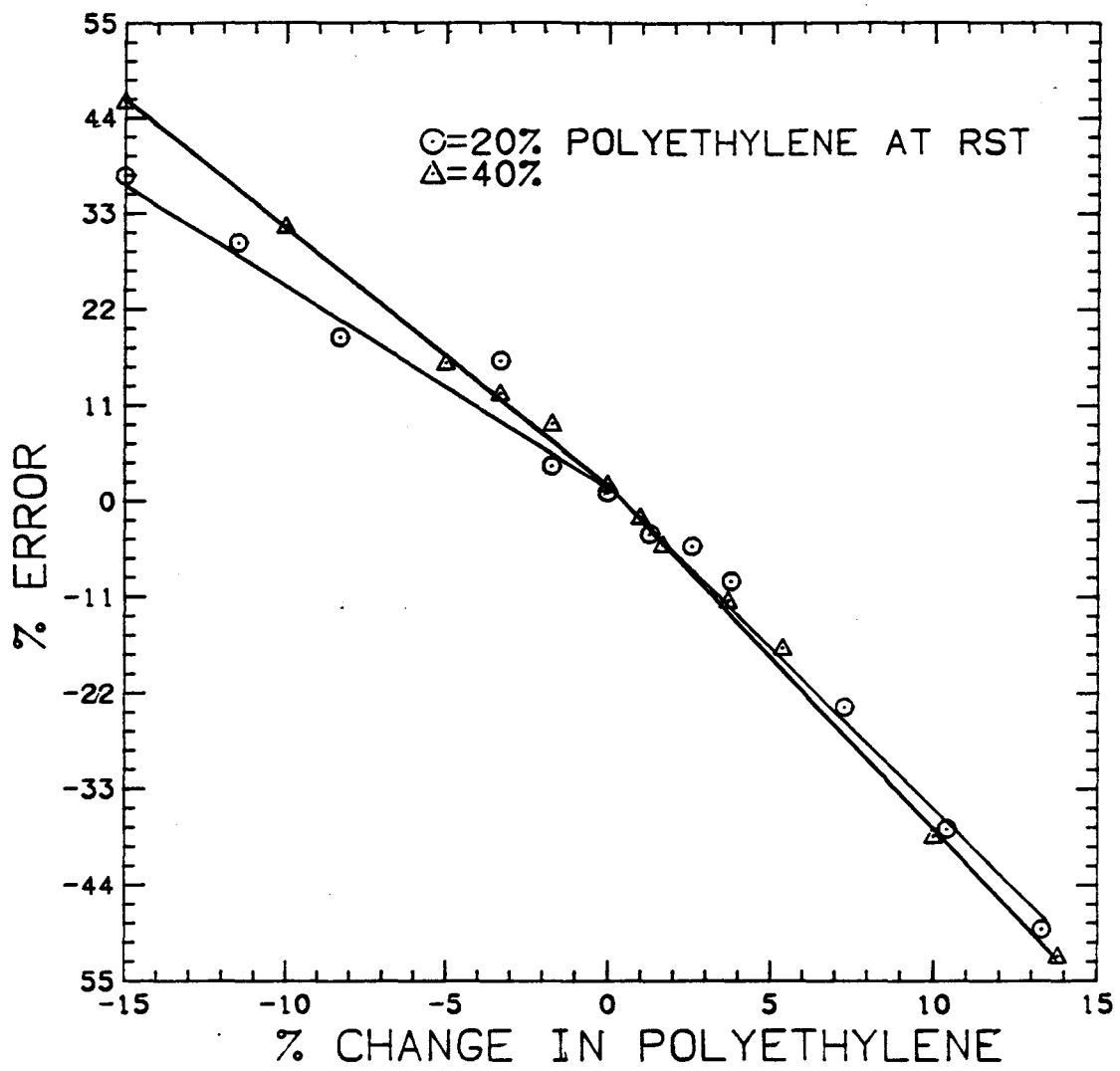

Figure 4-15 % error in aluminum thickness versus % change in polyethylene from RST to BMC measurement.
Total absorber thickness at RST measurement= 20 cm.
Aluminum thickness= .314 cm.

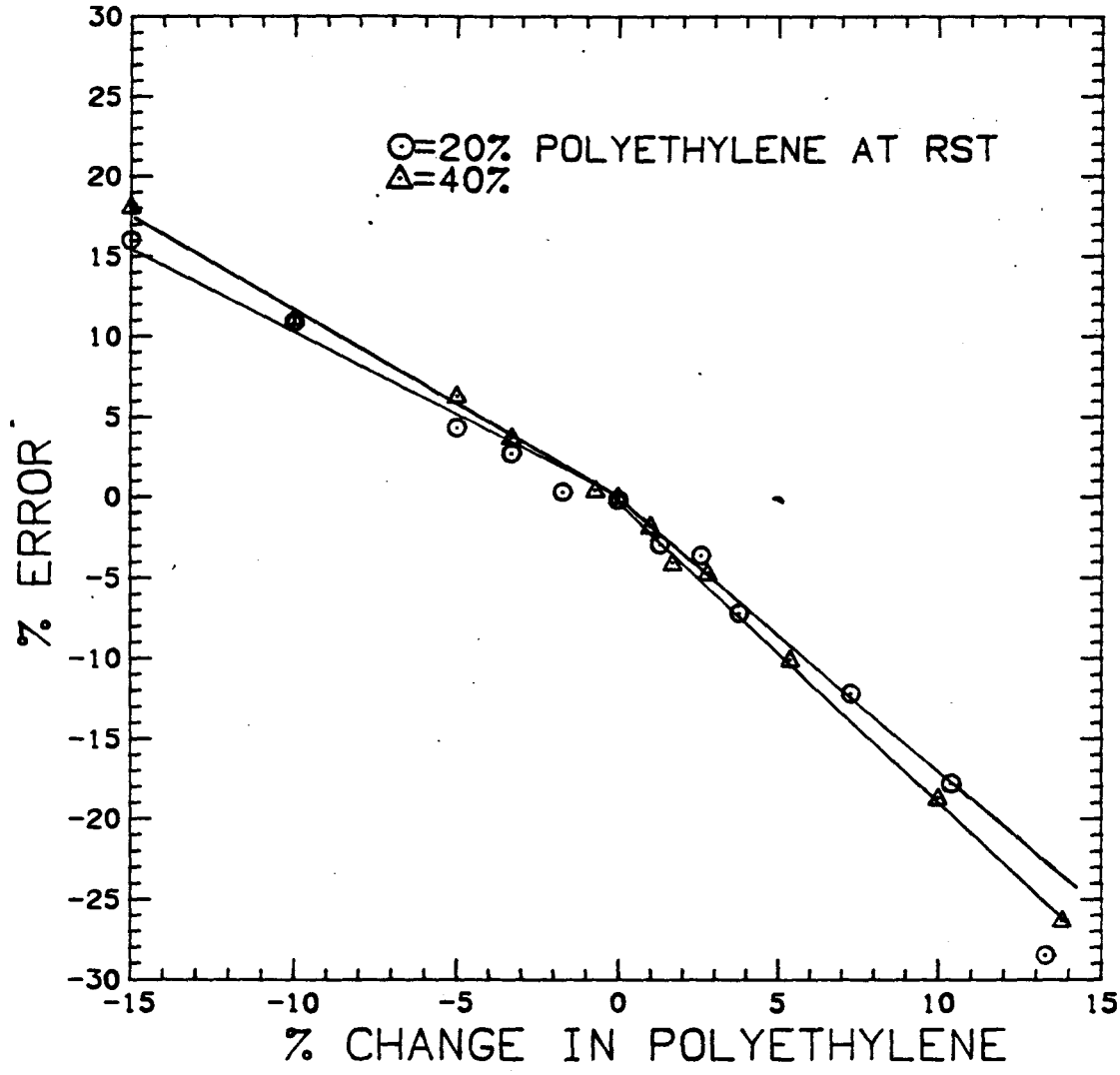

Figure 4-16 % error in aluminum thickness versus % change in polyethylene from RST to BMC measurement.
Total absorber thickness at RST measurement= 20 cm.
Aluminum thickness= .662 cm.

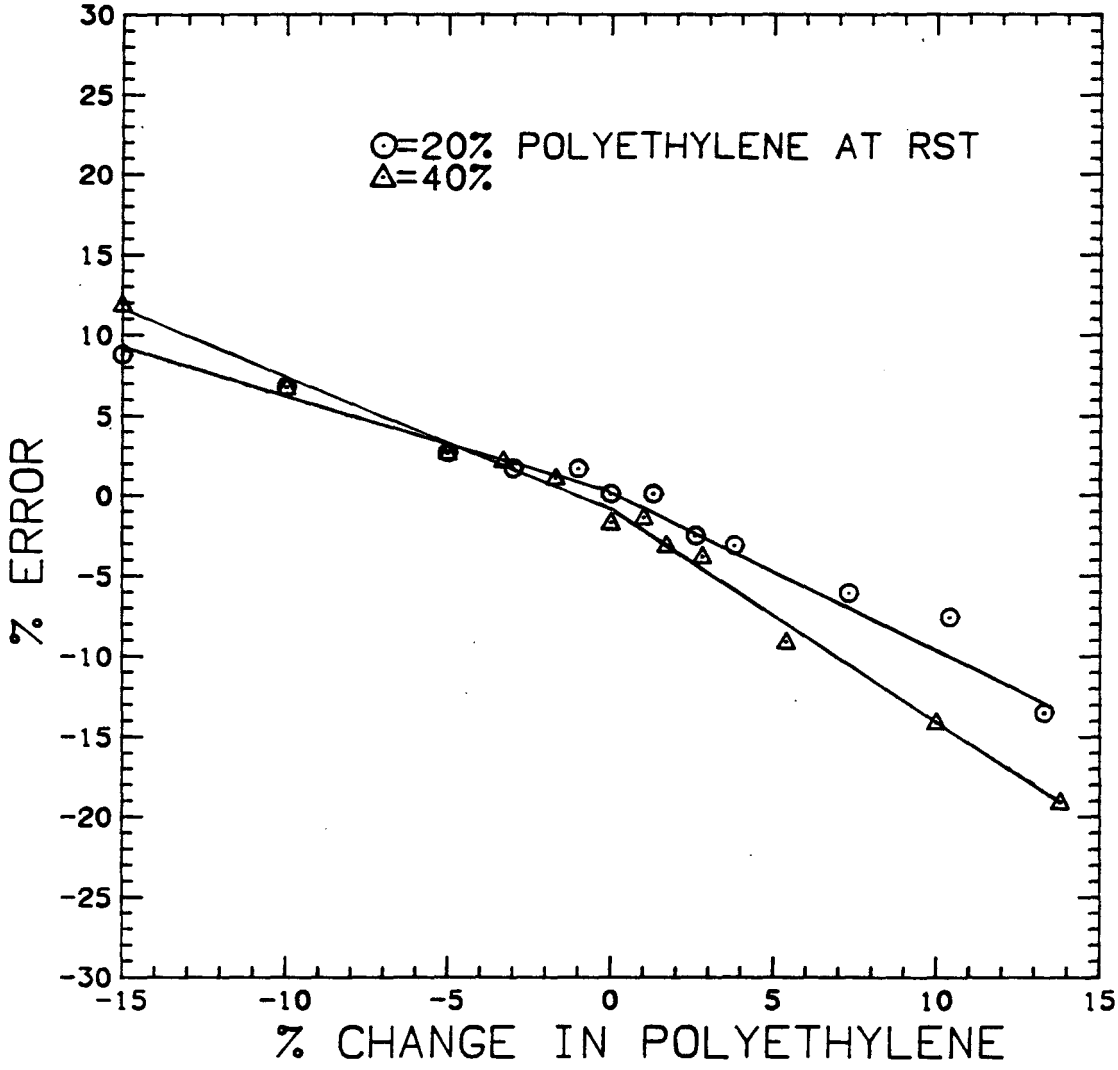

Figure 4-17 % error in aluminum thickness versus % change in polyethylene from RST to BMC measurement.
Total absorber thickness at RST measurement= 20 cm.
Aluminum thickness= .974 cm.

4.3 Phase 3: Motional Measurements - Two-Component Model

The purpose of phase 3 was to initiate sampling of data during motion of the rectilinear scanner. Prior to data collection, several system characteristics were determined as outlined in appendix 6. Subsequently, the dose for optimal scan speed and sample distance within a transverse scan was determined for this experimental geometry.

4.3.1 Experimental Description

The only deviation in the method from previous experiments was the addition of motion while collecting data. Figure 4-18 illustrates the scanning pattern that was used to acquire data. The pattern was in both the x and y directions because a rectilinear scan, as opposed to scanning over one transverse path, distributes the dose over a greater area. Hence a higher activity source can be used that will produce the same dose to a particular area that is irradiated. In addition, exact simulation of the procedure to be used in clinical studies will eliminate or reduce anomalies at an earlier stage in the overall experimental process.

If X is the transverse direction and Y is the longitudinal direction then x_k, the position of the kth data point is:

$$x_k = x - \frac{x_s}{2} \qquad (4\text{-}4)$$

where x is the absolute distance from the start scan Y-axis

and x_s is the sample space distance. The average BMC value at the X_k position summed over n transverse scans is given by:

$$BMC_k = \frac{\sum_{i=1}^{n} BMC(x_k, y_i)}{n} \qquad (4\text{-}5)$$

The total number of samples in the X direction is m. Each BMC_k can be calculated and plotted as a function of its displacement from the Y-axis in the X direction. To perform the analysis and acquisition using equation 4-5, the program SCANDPA was implemented.

The program SCANDPA (appendix 9) samples in the continuous mode although some researchers have used the point-to-point method (Roos[6]). Continuous sampling ideally has a constant speed and sample distance whereas the point-to-point method samples at discrete spatial intervals and requires stationary acquisition of data. For the continuous scanning mode, the sample distance, sample time and speed are all interrelated. At each sample location x_k, the sample time for x_s and low and high energy counts were recorded. After the scan, the data were used to calculate the thickness (mass) for each of the m x n samples using equation 2-12. These results were then averaged using equation 4-5. This produced a thickness (mass) profile that indicates the average thickness (mass) at each x_k as shown in

figure 4-19.

Alternately, the program ANALYSIS was used as a stand-alone unit for the display of previously acquired files. The display was either on the VDT (video display terminal) or a plotter. ANALYSIS produced exactly the same results as the program in SCANDPA.

4.3.2 Phase 3: Data Analysis

To optimize the sampling of data, the scan velocity and sample space must be determined. Table 4-2 shows a summary of selected values of sample speed, sample distance, distance between transverse scans and total scan time as used by other workers. The researchers quoted give little explanation for their choices. Figures 4-19 through 4-24 show the variation of sample speed while holding the sample space and total sample time constant at .5 cm and 23.5$\pm$1.0 min. respectively. The aluminum plates were placed in the water tank filled with 20 cm. of water, and scanned 23 cm. across and approximately 5 cm. longitudinally. The range of speeds were from a dial setting of 40 to 90 (.19 to .81 cm/sec). This range was chosen since below a dial setting of 40 the transverse motor would not produce uniform motion. At a dial setting of above 90 the data sample frequency for a "reasonably" sized sample space were too low. A "reasonable" sample space was considered to be less than 20% of the width of the object. The square box drawn on the plots indicate

the true dimensions of the aluminum plate which are .484 cm. thick and 6.35 cm. wide. At slightly above and below the .484 cm. line, two lines are drawn to indicate the 5% error. On both sides of the plate the thickness estimates are approximately zero and give a good indication of the accuracy of the measured initial counts, RST measurement and corrected attenuation coefficients. The plots show that at the edges of the plate the thickness is underestimated. This was due to the finite beam width that caused the beam to impinge on the aluminum and water simultaneously. Resultingly, the averaging that occurs because of the "partial volume effect" underestimates the aluminum thickness. The plots do not indicate, with any high degree of confidence, that better data could be obtained by choosing one particular speed over another in the range tested. Figures 4-25 to 4-30 illustrate the effect of a constant dial setting of 60 and total scan cycles of 16 while varying the sample distance from .3 to 1.3 cm. At the sample spacings of .9, 1.1 and 1.3 cm., the spacing is quite visibly too large because of the underestimate of aluminum thickness at the edges. At .3 cm the sampling rate is quite high with large statistical fluctuation. Therefore, the sample space could be set to .5 or .7 cm. with a scan speed dial setting of 60 to produce optimal results for this experimental geometry.

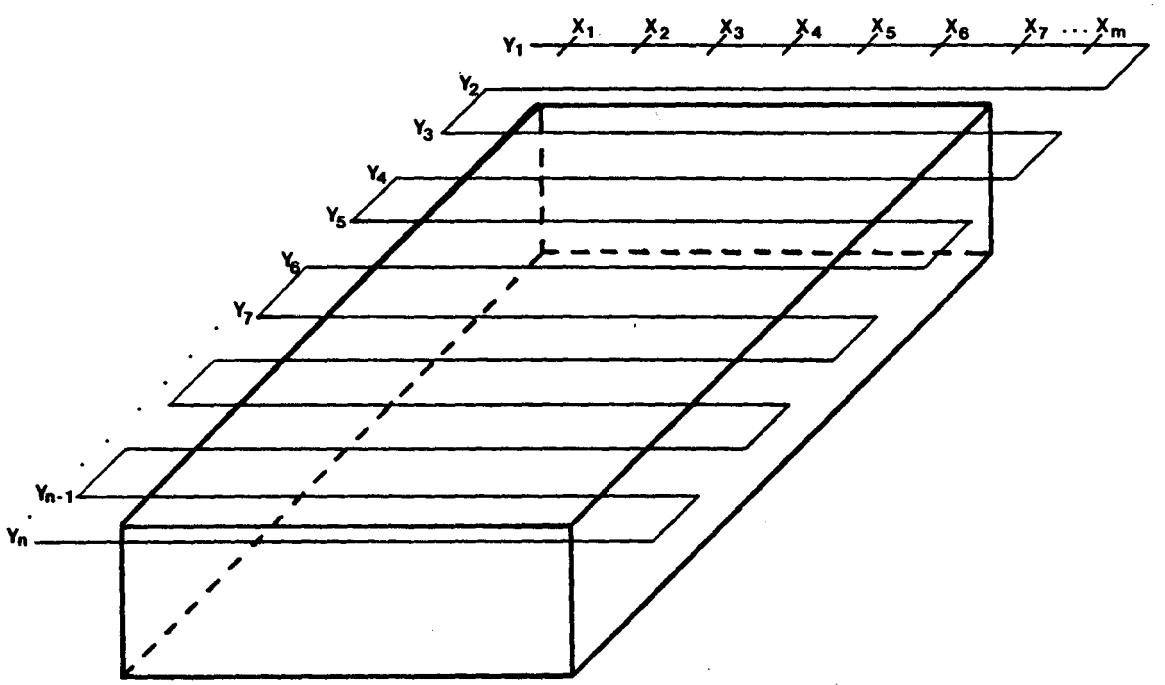

Figure 4-18 Scan pattern for the acquisition of data.

Researcher	Speed (mm/s)	Tran. (cm.)	Long. (mm.)	Sample time min.
Krolner[8]	4	12.0	4	25
Smith[15]	5	12.0	4	20
Dunn[10]	12	-	4.5	-
Roos[6]	4	16.0	-	25

Table 4-2 Summary of values used for motional scanning parameters.

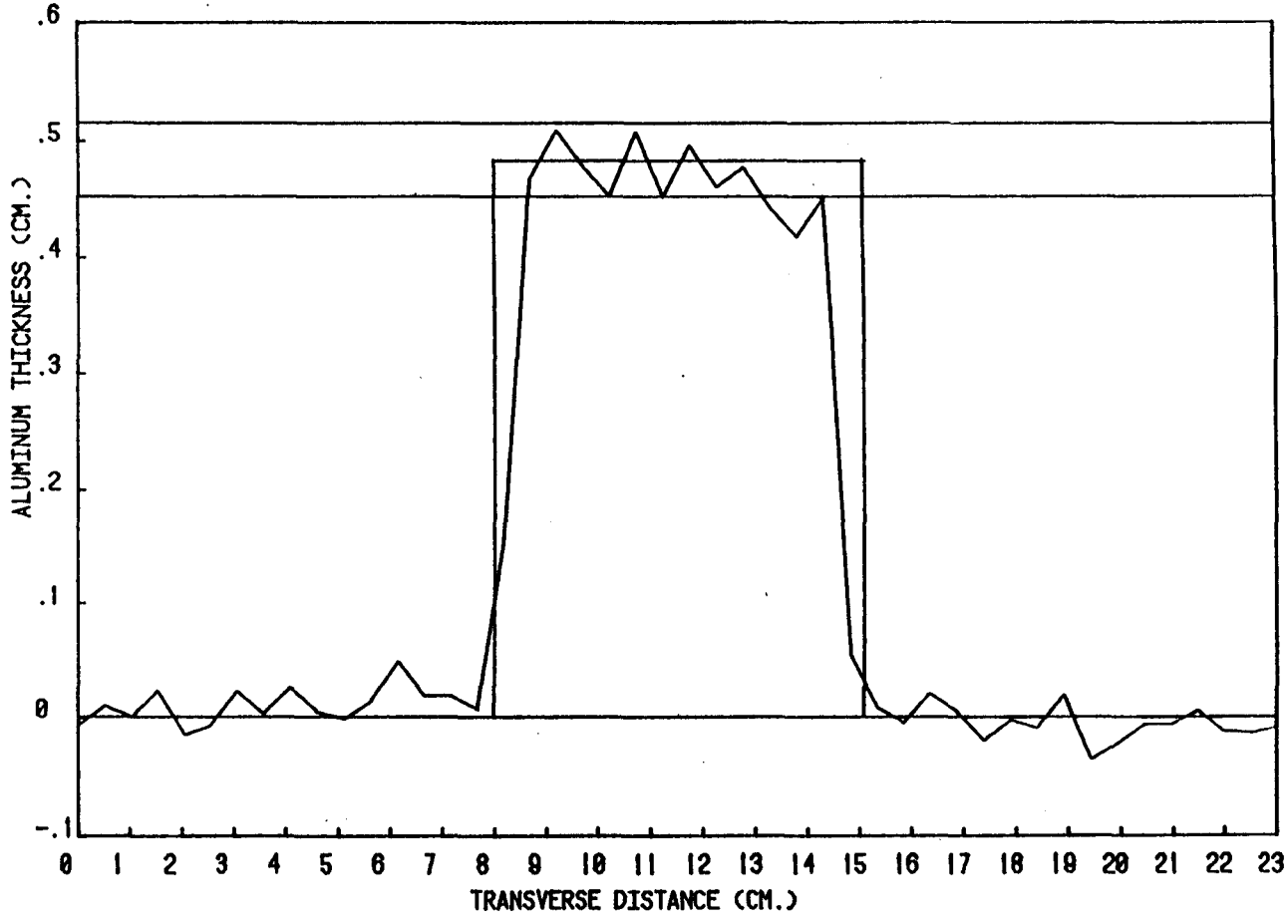

Figure 4-19 Aluminum thickness versus transverse distance
for a constant sample distance of .5 cm.
Scan time= 24.5 minutes
Transverse speed= .19 cm./sec.
Number of cycles= 7
Scan speed dial setting= 40

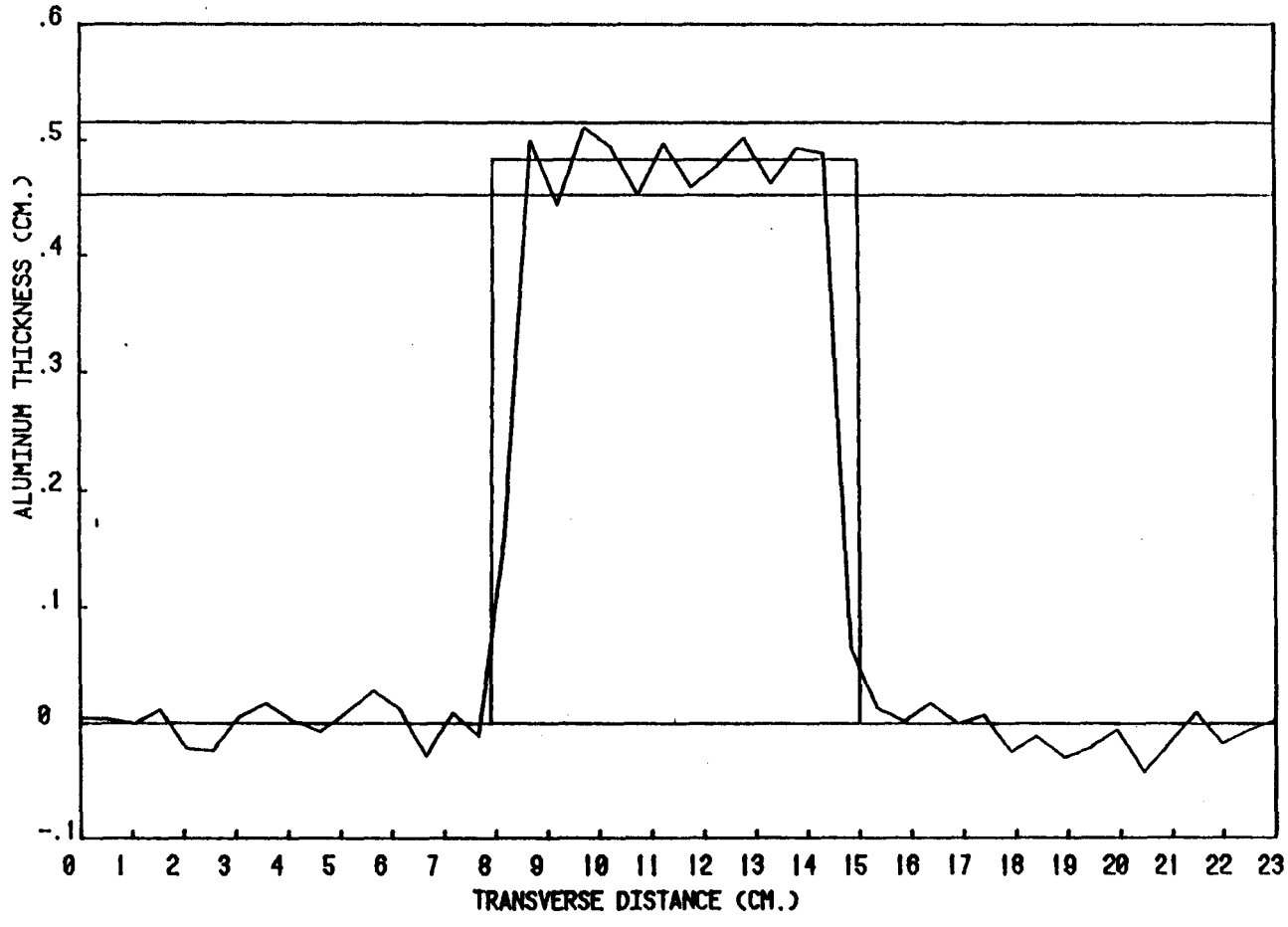

Figure 4-20 Aluminum thickness versus transverse distance for a constant sample distance of .5 cm.
Scan time= 23.3 minutes
Transverse speed= .32 cm./sec.
Number of cycles= 10
Scan speed dial setting= 50

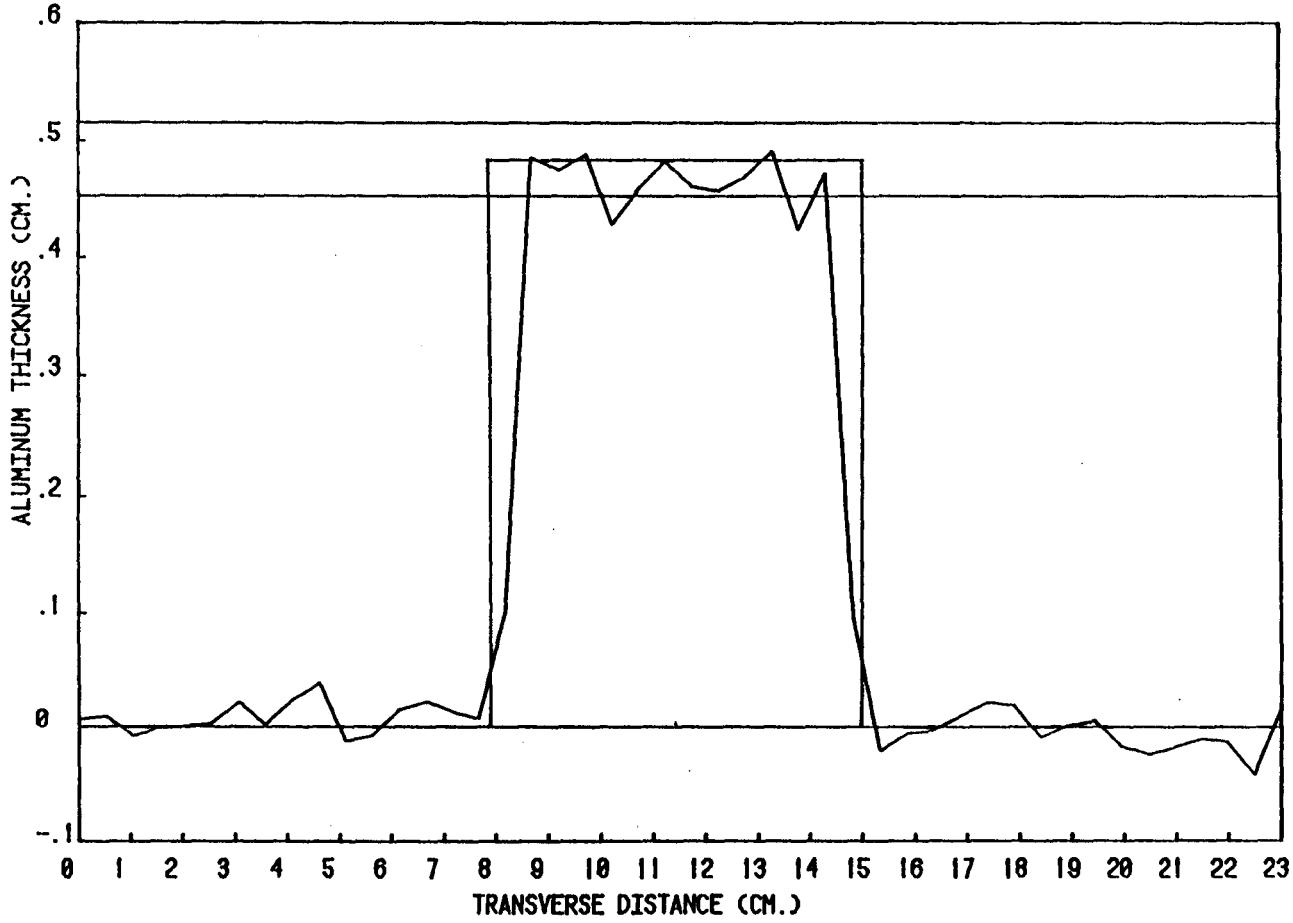

Figure 4-21 Aluminum thickness versus transverse distance for a constant sample distance of .5 cm.
Scan time= 24.0 minutes
Transverse speed= .44 cm./sec.
Number of cycles= 14
Scan speed dial setting= 60

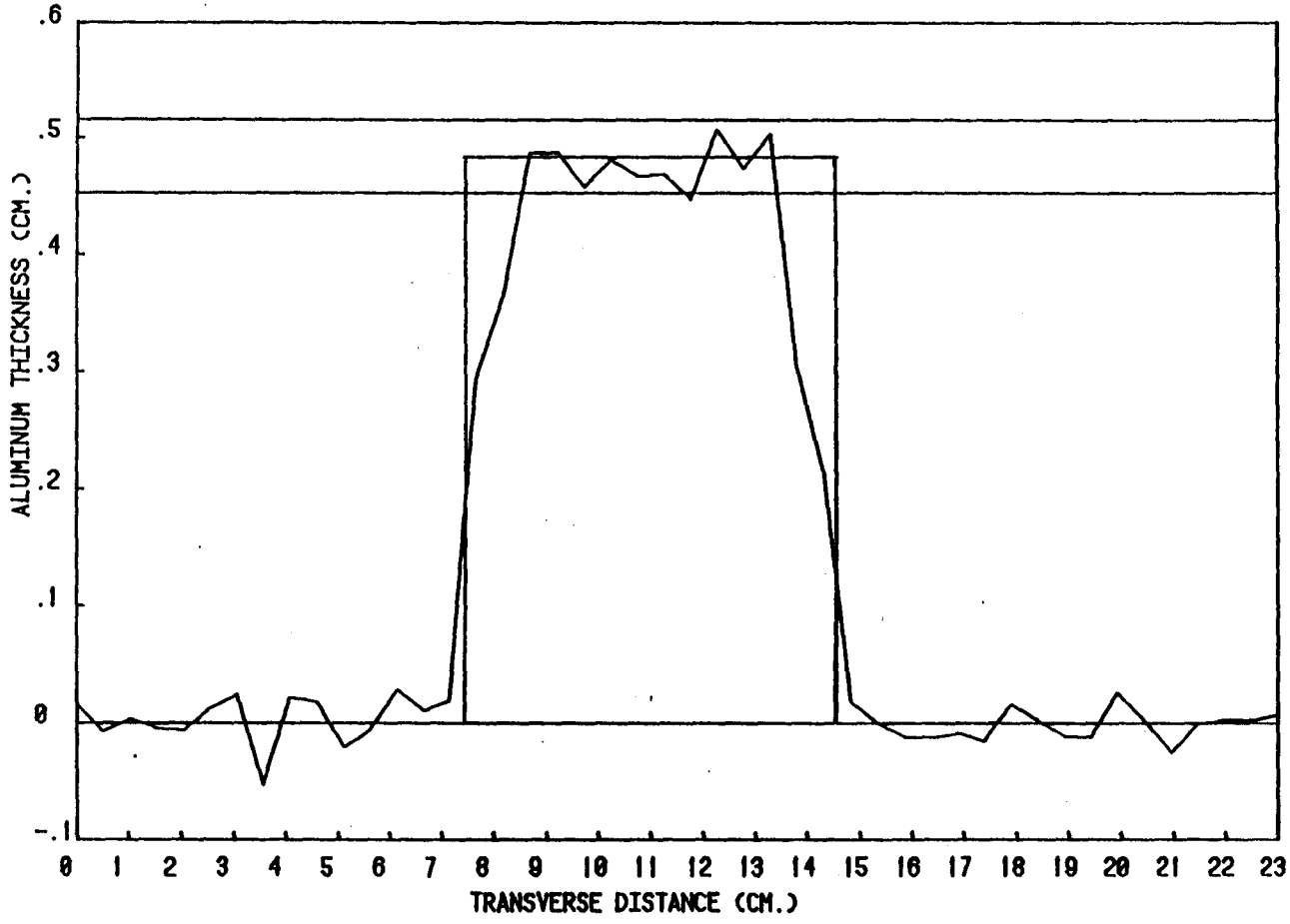

Figure 4-22 Aluminum thickness versus transverse distance
for a constant sample distance of .5 cm.
Sample time= 24.5 min.
Transverse speed= .56 cm./sec.
Number of cycles= 18
Scan speed dial setting= 70

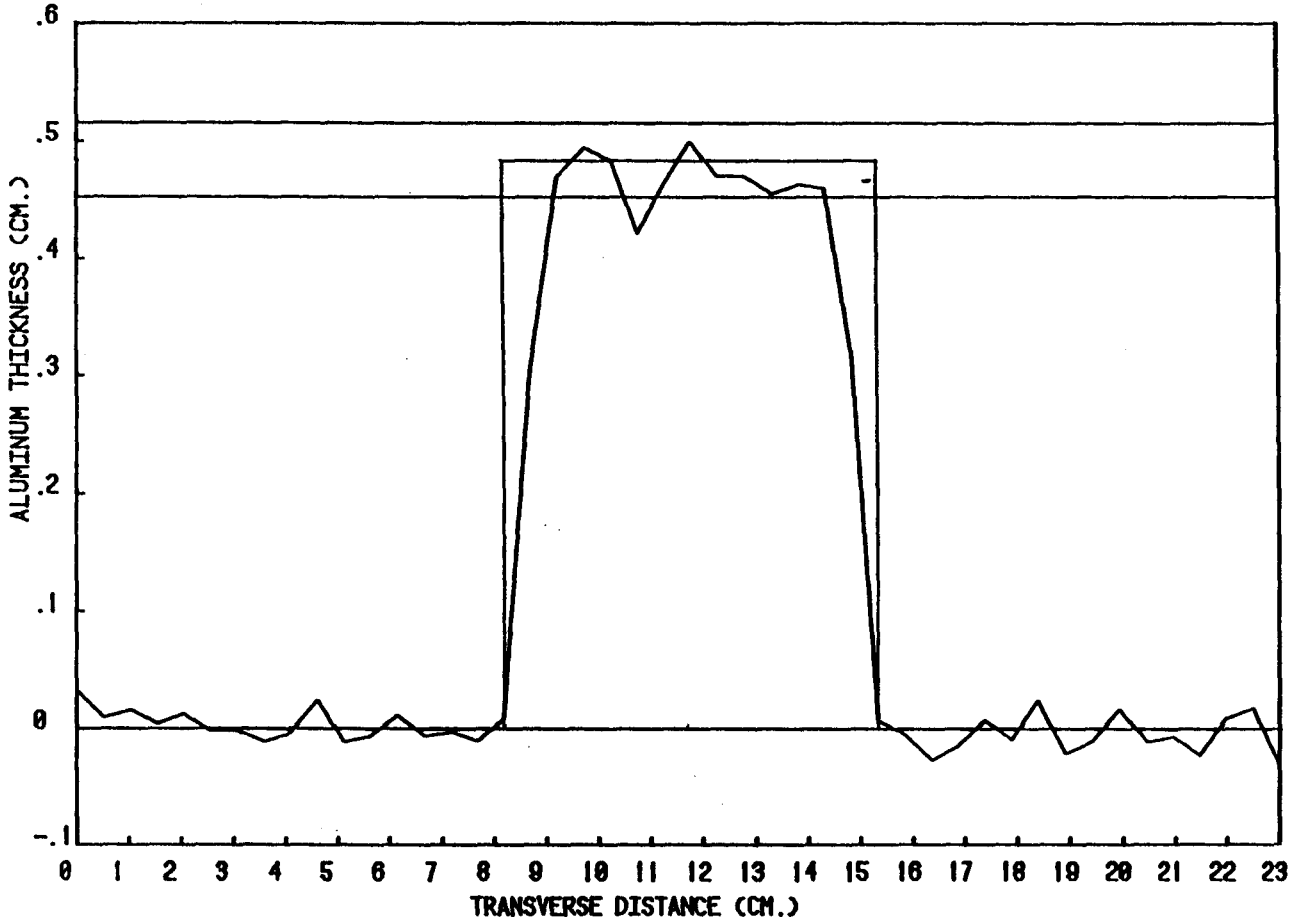

Figure 4-23 Aluminum thickness versus transverse distance
for a constant sample distance of .5 cm.
Scan time= 23.5 minutes
Transverse speed= .69 cm./sec.
Number of cycles= 20
Scan speed dial setting= 80

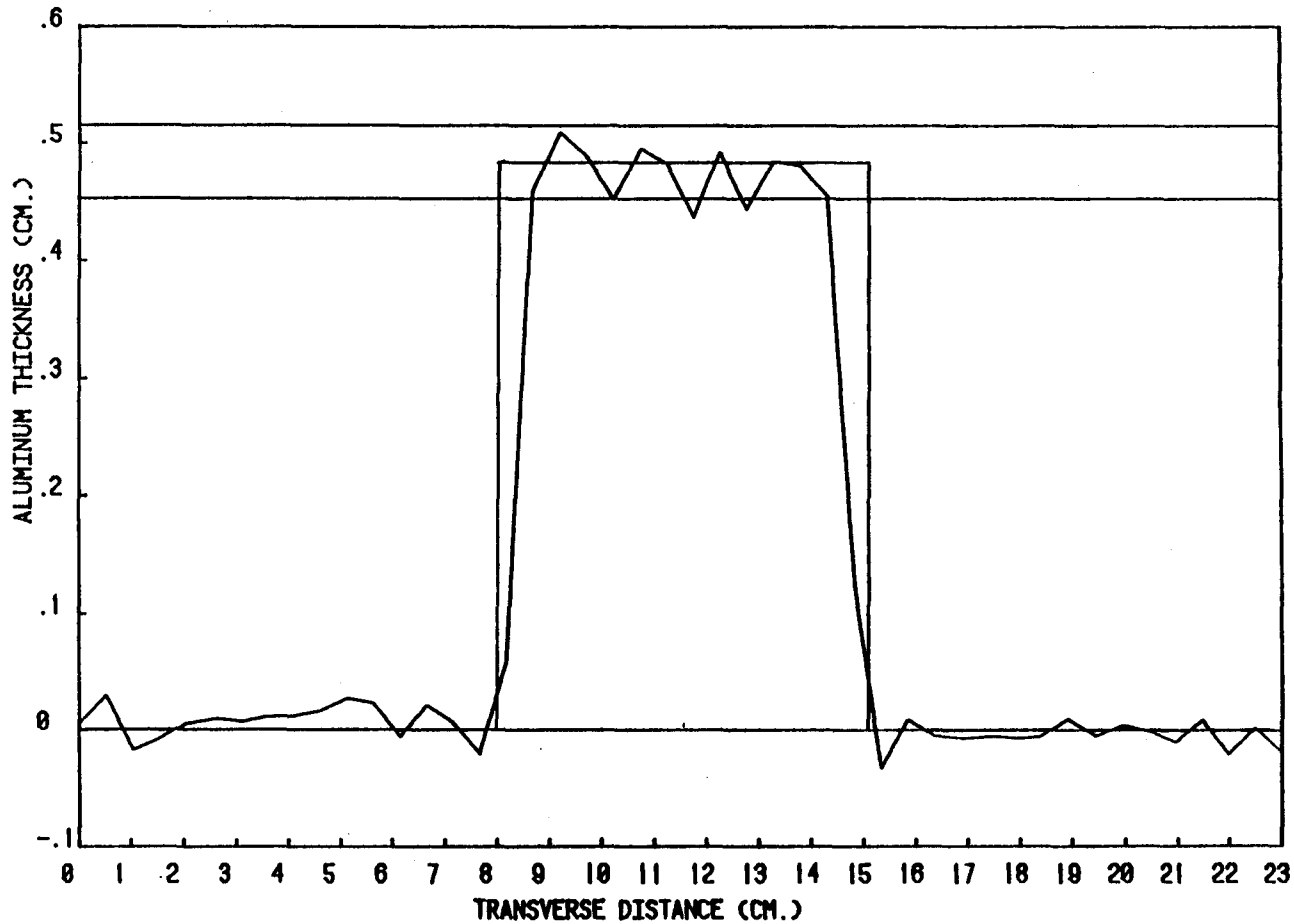

Figure 4-24 Aluminum thickness versus transverse distance
for a constant sample distance of .5 cm.
Scan time= 23.5 minutes
Transverse speed= .81 cm./sec.
Number of cycles= 22
Scan speed dial setting= 90

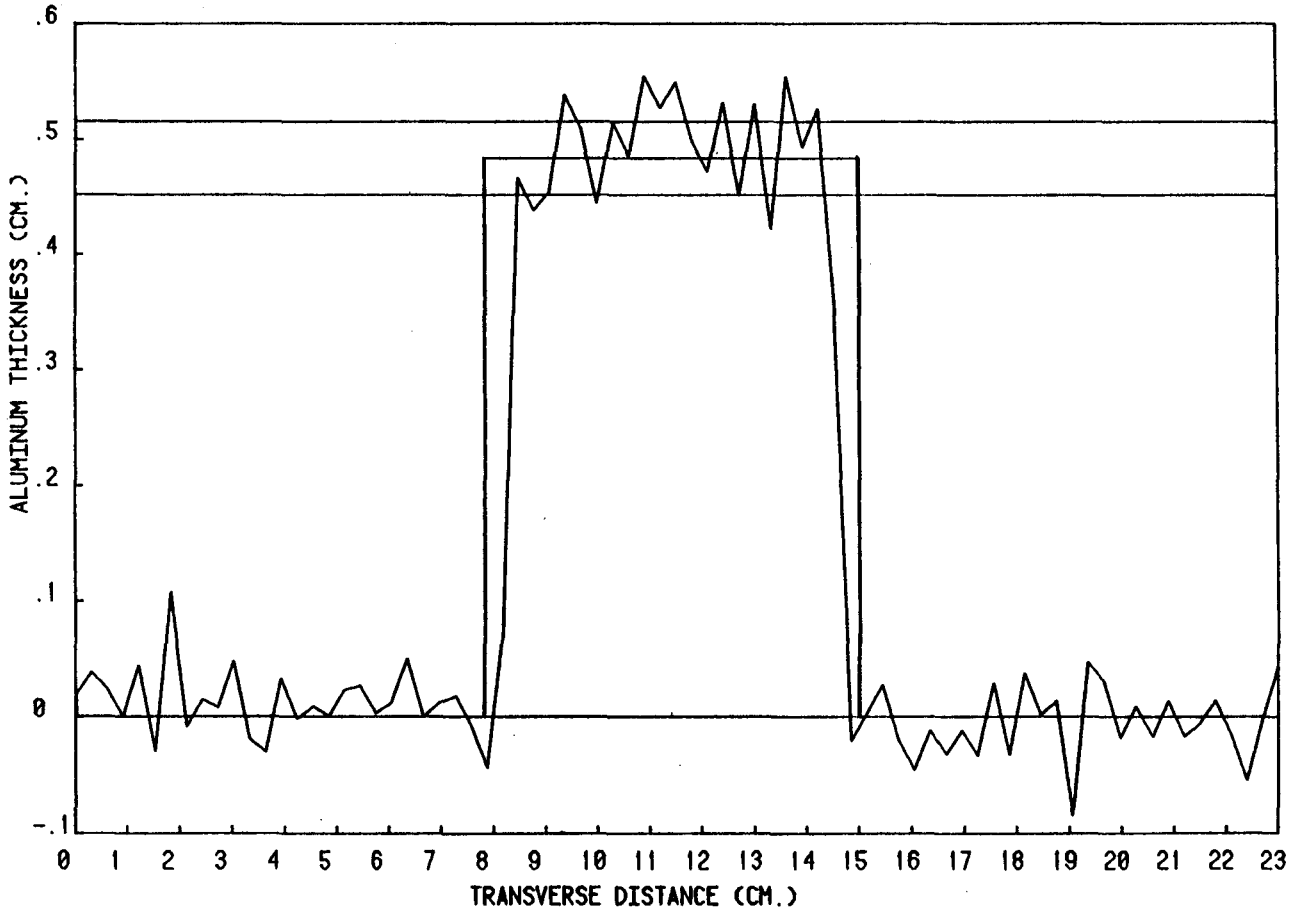

Figure 4-25 Aluminum thickness versus transverse distance
for 1 of 6 sample distances.
Total Scan time= 28.0 minutes
Number of cycles= 16
Sample time= .68 seconds
Sample distance= .3 cm.

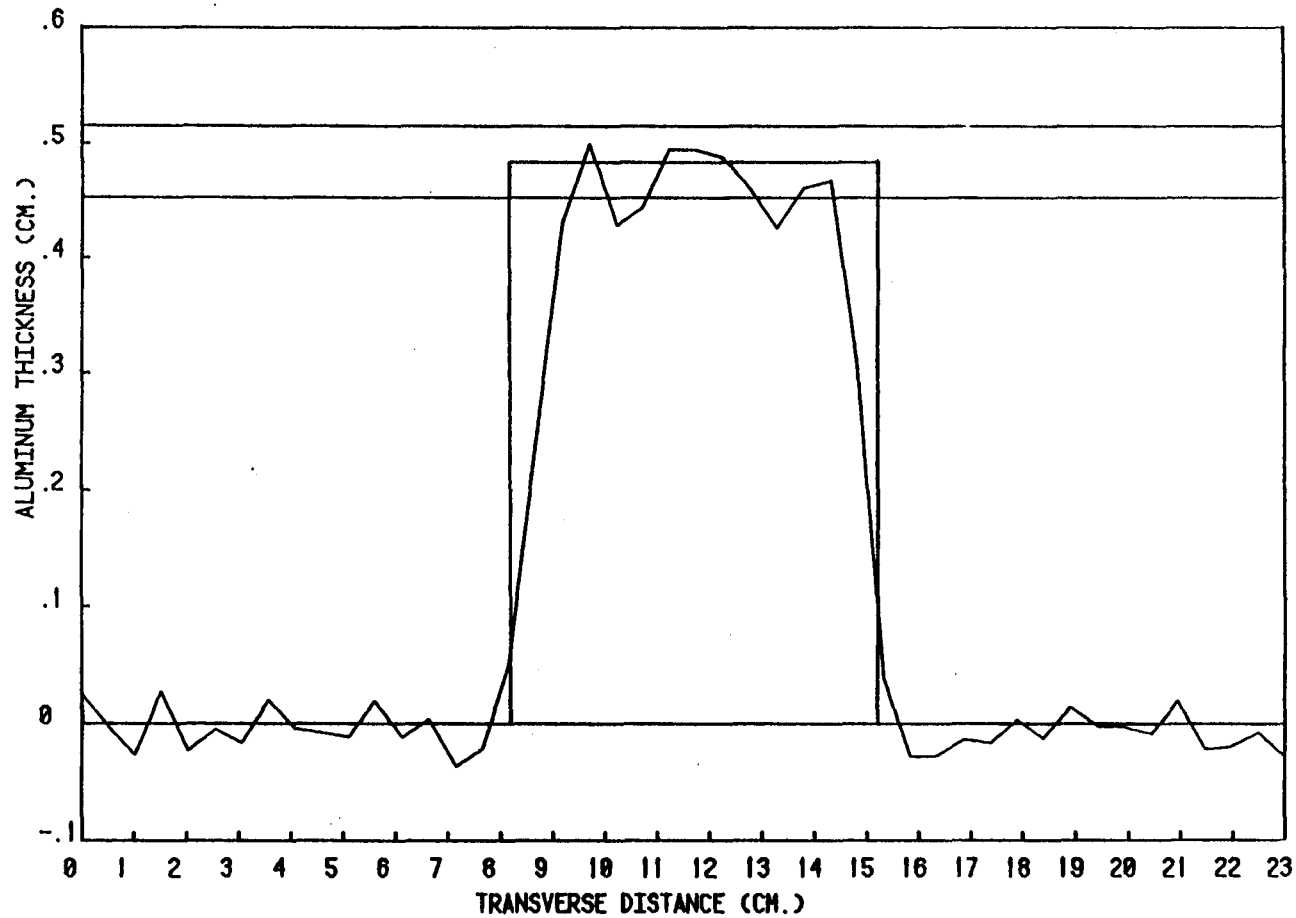

Figure 4-26 Aluminum thickness versus transverse distance for 1 of 6 sample distances.
Total Scan time= 28.0 minutes
Number of cycles= 16
Sample time= 1.1 seconds
Sample distance= .5 cm.

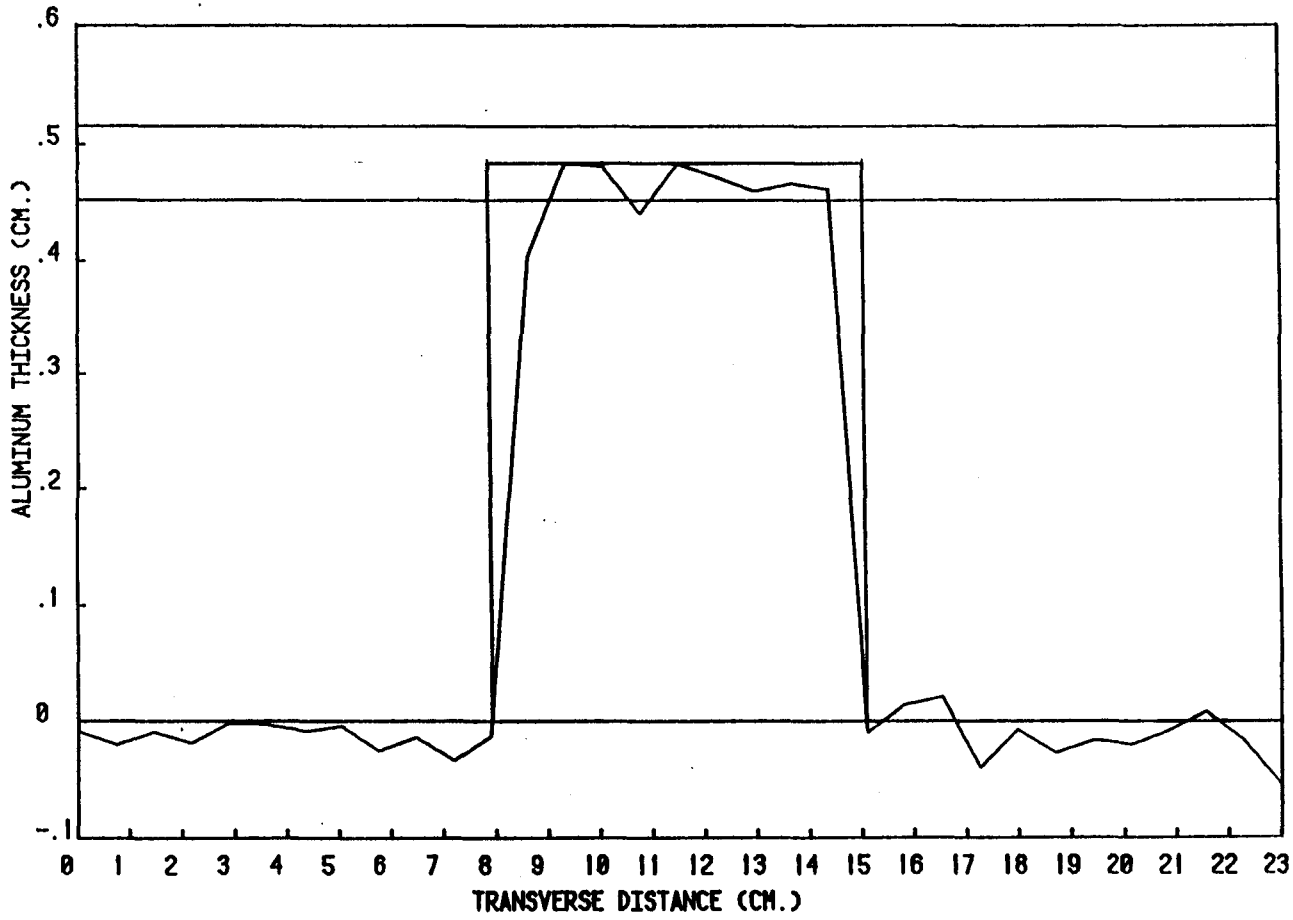

Figure 4-27 Aluminum thickness versus transverse distance
for 1 of 6 sample distances.
Total Scan time= 28.0 minutes
Number of cycles= 16
Sample time= 1.6 seconds
Sample distance= .7 cm.

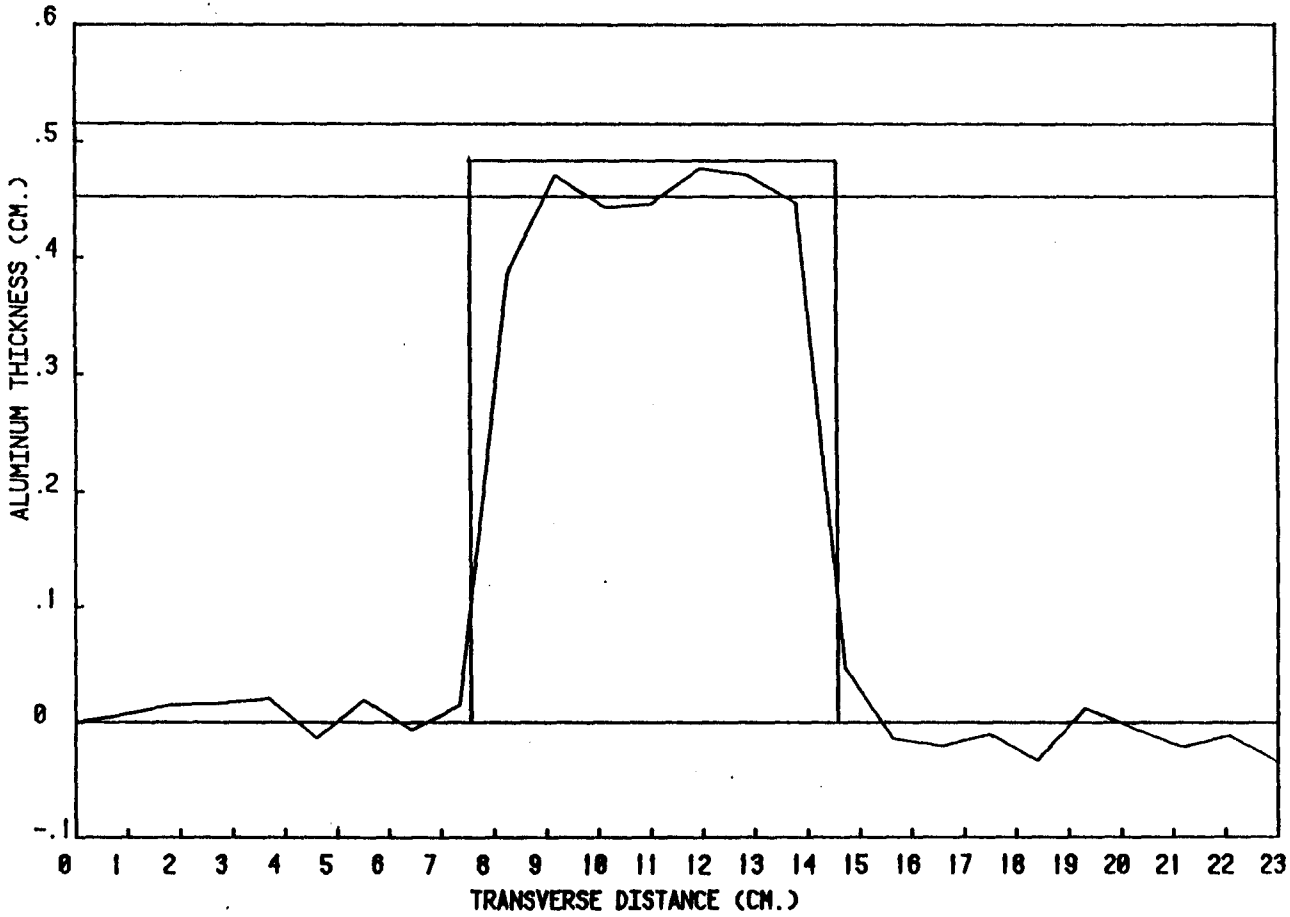

Figure 4-28 Aluminum thickness versus transverse distance
for 1 of 6 sample distances.
Total Scan time= 28.0 minutes
Number of cycles= 16
Sample time= 2.0 seconds
Sample distance= .9 cm.

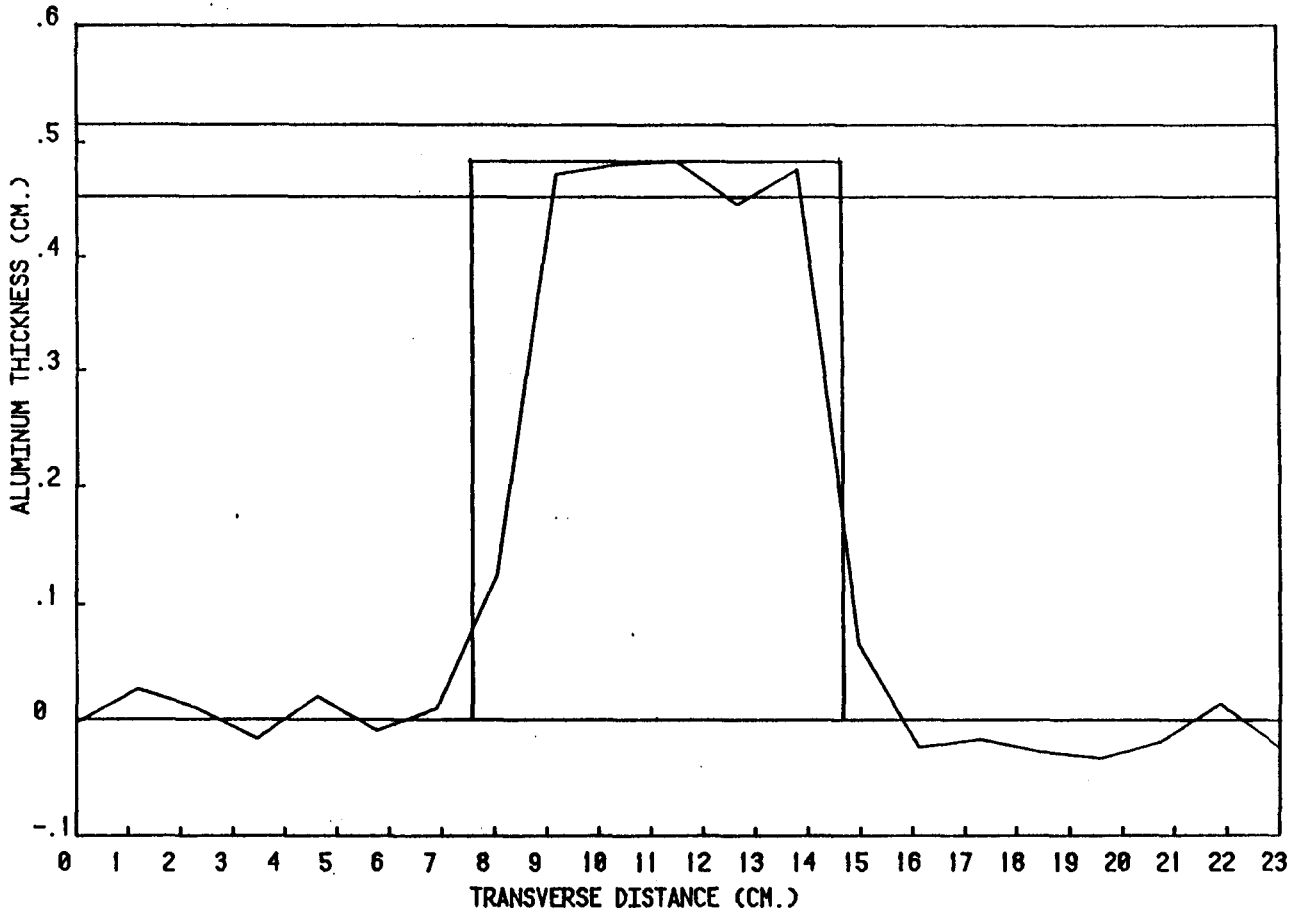

Figure 4-29 Aluminum thickness versus transverse distance for 1 of 6 sample distances.
Total Scan time= 28.0 minutes
Number of cycles= 16
Sample time= 2.5 seconds
Sample distance= 1.1 cm.

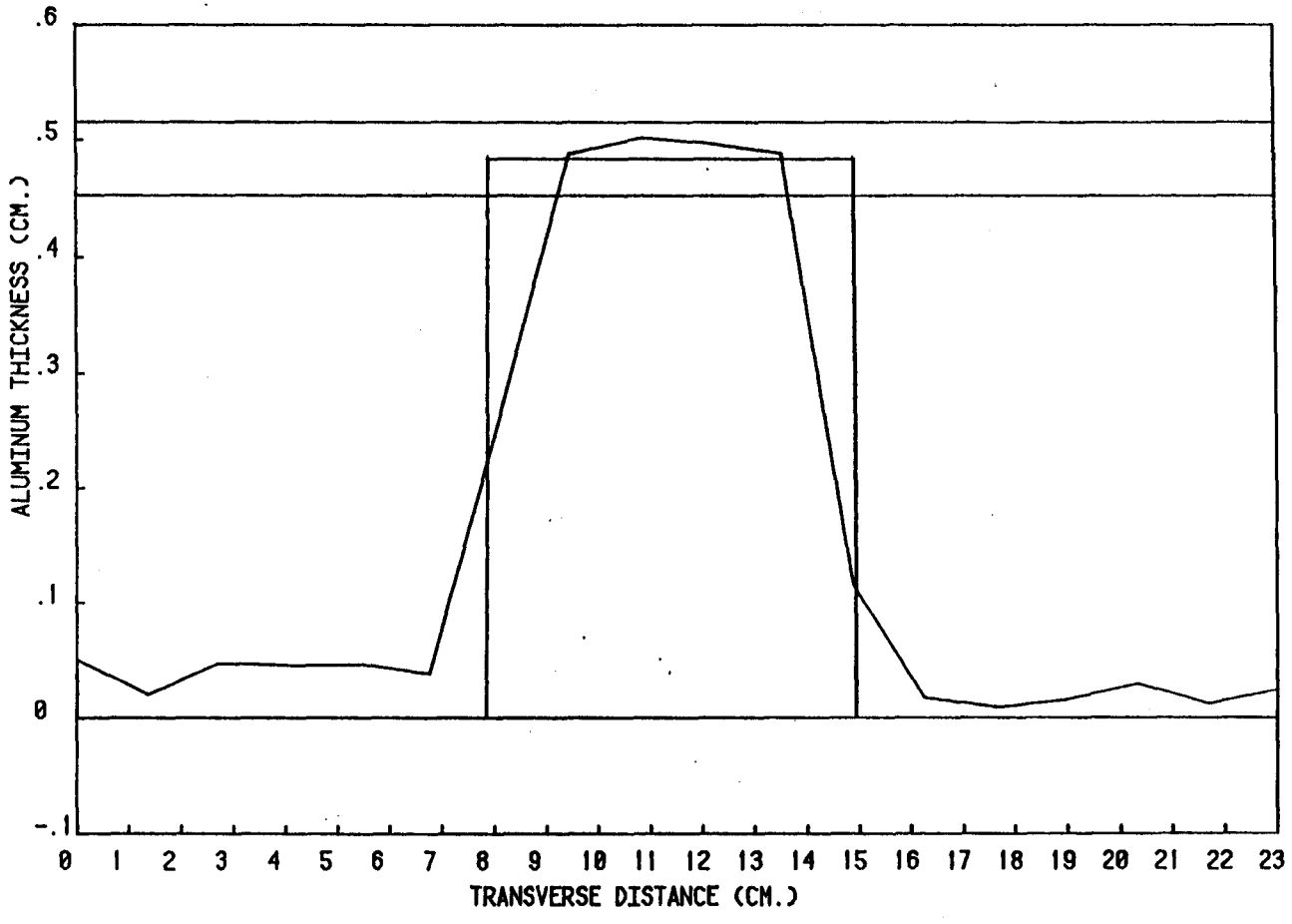

Figure 4-30 Aluminum thickness versus transverse distance
for 1 of 6 sample distances.
Total Scan time= 28.0 minutes
Number of cycles= 16
Sample time= 3.0 seconds
Sample distance= 1.3 cm.

The last part of phase 3 required the determination of the dose that would be imparted during in vivo studies. The dose to any particular body component within the scan was calculated (appendix 10) and compared to measured values at 8 cm. above the source's top end. This distance is representative of the mid-lumbar vertebrae to source distance. The measured values were determined for a 44 hour irradiation and 49 hour "cool-down" period so that the first clinical scan could be at 8:30 Monday morning and the source could be used until Friday at 5:00 in the afternoon. Table 4-3 shows the comparison of the calculated and measured dose to bone and muscle for the optimal sampling rate. To obtain the measured values, thermoluminescent dosimeters (TLD) were used. The large difference between the calculated and measured values arises because the calculated values were determined by assuming that the full beam of photons were incident on a sample space for the entire sample time (e.g., 1.5 sec.). However, for motional studies only part of the beam is incident on a particular point at any given time. Therefore, the calcuated values are the worst-case maximum doses. The measured values should be underestimates of the true dose due to alignment difficulties of the TLDs with the photon beam. Figure 4-31 shows the dose rate as a function of count rate for 103 keV photons. Figure 4-32 shows the relationship between the time after irradiation and the count rate corrected for source decay, cross-over, and background.

From these two plots, the approximate dose to a subject can be determined at any time during the week provided that the source has had an irradiation time of 44 hours.

Component	Dose (mRad)		Difference %
	Calculated	Measured	
Bone	6.2	4.0	35
Muscle	1.4	.88	37

Table 4-3 Comparison of calculated and measured doses at the optimal sample rate for bone and muscle.

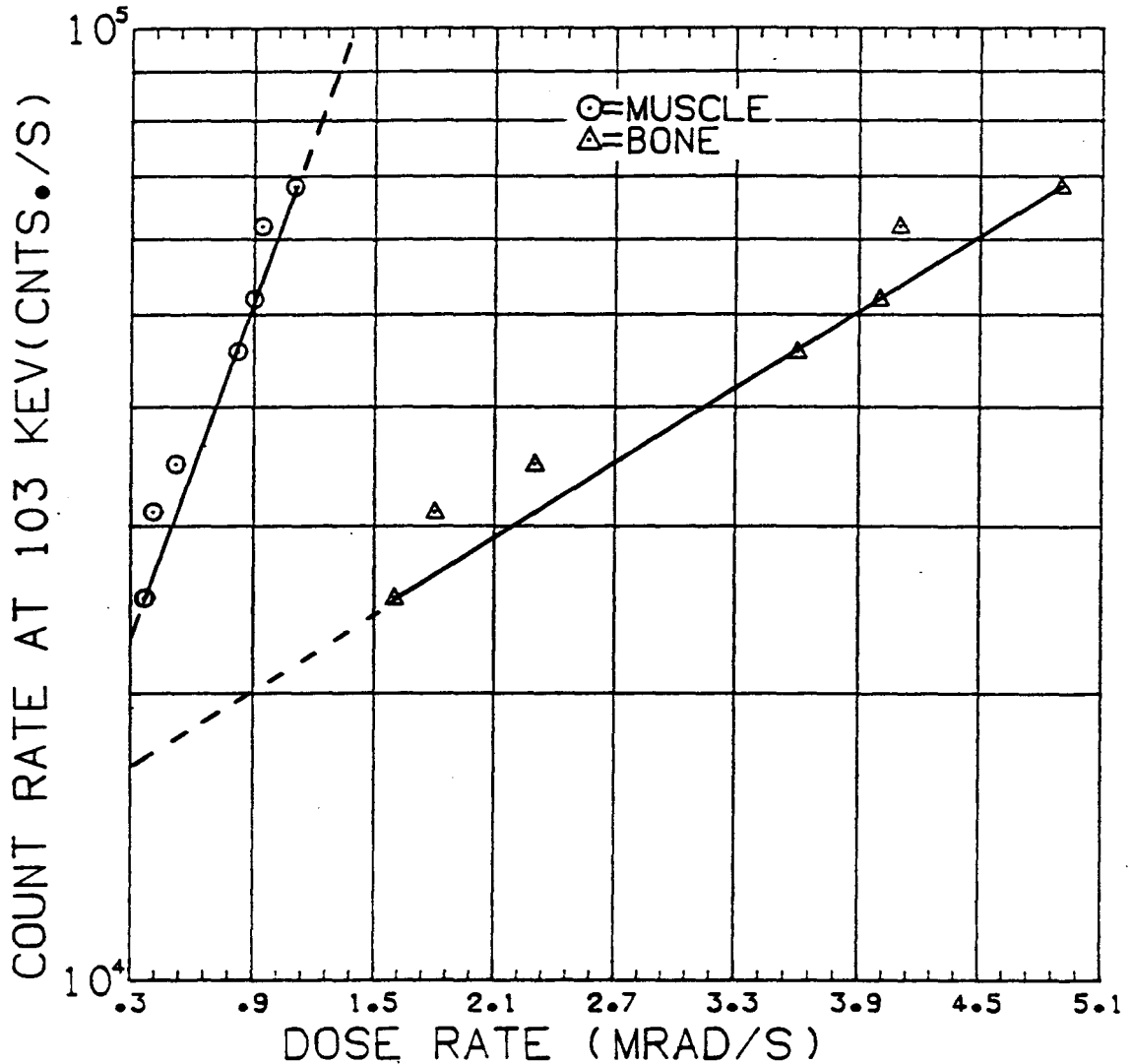

Figure 4-31 The relationship between the count rate and the dose rate for a ^{153}Sm source irradiated for 44 hours.

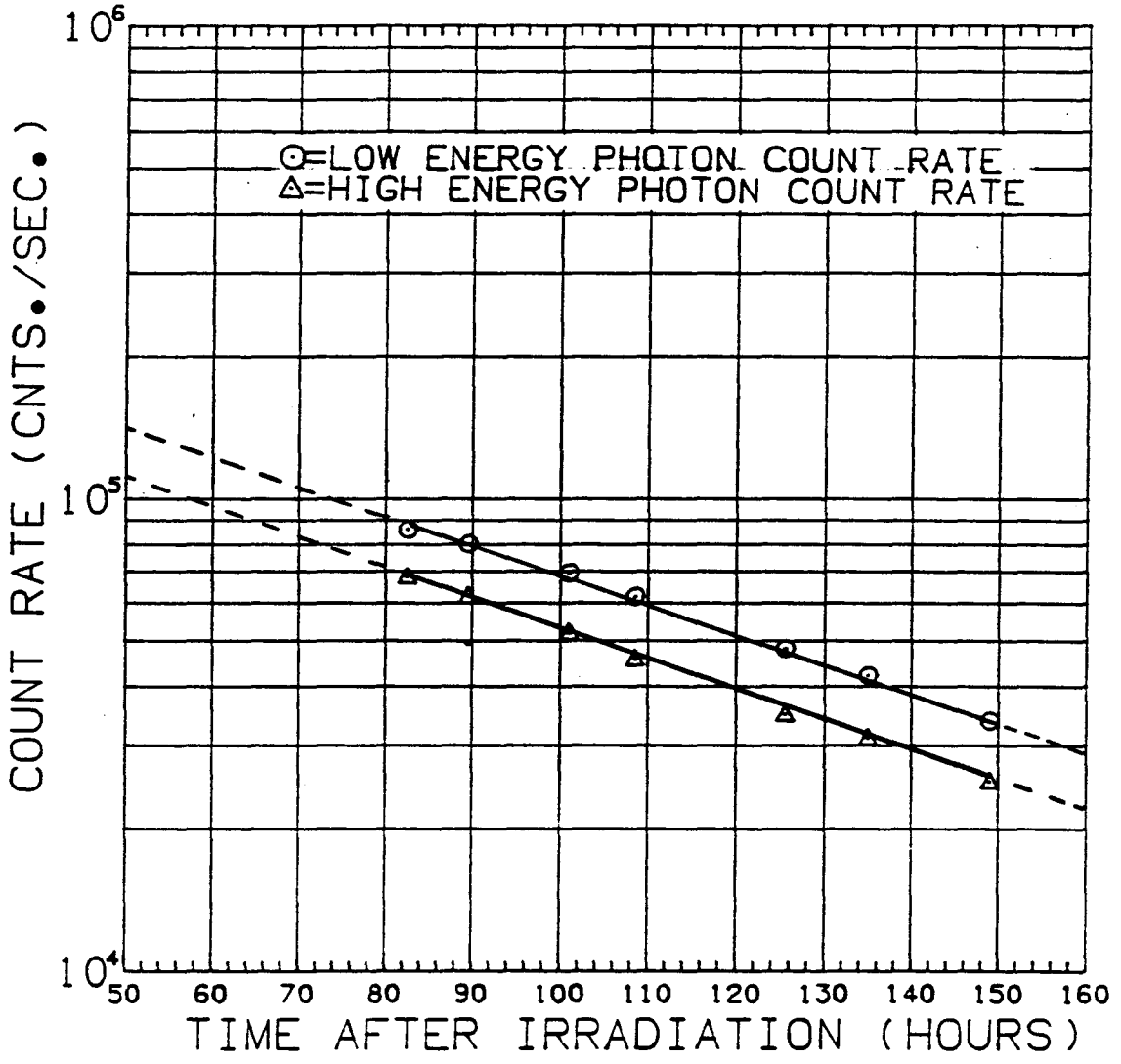

Figure 4-32 The relationship between the photon count rate and the time after source irradiation.

Chapter 5

Monte Carlo Simulation of DPA

The computer simulation of the experimental procedure is beneficial for several reasons. First and foremost, it allows the opportunity to understand the theory through a simulation of actual physical events. Secondly, parameters can be adjusted within the simulation to find the optimal experimental configuration if the model accurately describes the physical events. Lastly, the simulation can provide a comparison between experimental and theoretical results.

5.1 Monte Carlo Method

Monte Carlo analysis is used in many areas of science and engineering where direct analytical solutions are impossible or very difficult to obtain, and in situations where the predominant phenomenon is of a random nature. Examples of these areas are the solution of differential equations, the determination of species proliferation in genetics, the modelling of traffic flow, the investigation of particle interaction with matter, and traditionally, the simulation of games of chance.

The fundamental requirement and most crucial element of the Monte Carlo method is a large supply of "high quality" random numbers. High quality refers to a high degree of randomness. However, mathematicians have never been able to give a precise definition of randomness. Even though a

precise definition for randomness does not exist, it is possible to determine if a sequence of numbers is random. This can be accomplished by arguing that a sequence is not random if it fails one of a prescribed series of tests for randomness. The generation of random numbers can be categorized into three basic methods: (1) drawing samples from preconstructed tables; (2) monitoring the output of a physical device or process; and (3) calculation using a mathematical algorithm. The first option is seldom used today because storing in secondary memory and calling is very inefficient from a memory access time perspective. Likewise, monitoring of physical devices in some instances will have a repeated pattern that will provide a high correlation between samples drawn. Therefore, this method has limited use. Implementation of a mathematical algorithm creates a software pseudo-random generator. The disadvantage of this is that after a certain number of elements are drawn the sequence will repeat. This is called the period. If the period of a sequence is large compared to the number of draws, the periodic behaviour is of no practical consequence.

5.2 Theory for Simulation of Photon Interaction

To simulate the physical interaction of photons (particles) two processes must be understood; namely, the mathematical calculation of photon coordinates and the methods of modelling their interactions.

5.2.1 Coordinates System for Monte Carlo Calculations.

In classical physics, to determine the exact position of a photon (particle), the photon's coordinates must be related to the original coordinate system. Therefore, for each interaction in the photon's history, a rotation and translation must be performed. Let the z axis be the direction of the photon before the first collision as shown in figure 5-1. The position of the first interaction is:

$$[X]_o=(x_o,y_o,z_o) \tag{5-1}$$

where [] indicates a vector. The particle leaves this point at angle θ_o with respect to the $\bar{z}_1$ axis and angle ϕ_o with respect to the $\bar{x}_1$ axis and travels to P_1 where the next interaction occurs. At P_1

$$x_1=R_1 Sin\theta_o Cos\phi_o \tag{5-2}$$

$$y_1=R_1 Sin\theta_o Sin\phi_o \tag{5-3}$$

$$z_1=R_1 Cos\theta_o \tag{5-4}$$

in the coordinate system with unit vectors $\bar{x}_1,\bar{y}_1,\bar{z}_1$. A new coordinate system is defined at P_1 with P_1 as the origin. This coordinate system is defined with unit vectors $\bar{x}_2,\bar{y}_2,\bar{z}_2$ where $\bar{z}_2$ is parallel to the direction of R_1.

For a right handed system the unit vector $\bar{z}_2$ is given as:

$$\bar{z}_2 = \frac{1}{R_1}(x_1\bar{x}_1 + y_1\bar{y}_1 + z_1\bar{z}_1) \tag{5-5}$$

The unit vector $\bar{y}_2$ must be normal to the plane defining $\bar{z}_1$ and $\bar{z}_2$. Therfore $\bar{y}_2$ is given by:

$$\bar{y}_2 = \frac{\bar{z}_1 \times \bar{z}_2}{|\bar{z}_1 \times \bar{z}_2|} \tag{5-6}$$

Lastly, the unit vector $\bar{x}_2$ is defined by $\bar{y}_2$ and $\bar{z}_2$:

$$\bar{x}_2 = \bar{y}_2 \times \bar{z}_2 \tag{5-7}$$

In matrix form so that unit vectors $\bar{x}_2, \bar{y}_2, \bar{z}_2$ are defined in terms of $\bar{x}_1, \bar{y}_1, \bar{z}_1$:

$$\begin{bmatrix} \bar{x}_2 \\ \bar{y}_2 \\ \bar{z}_2 \end{bmatrix} = \begin{bmatrix} \text{Cos}\theta_o\text{Cos}\phi_o & \text{Cos}\theta_o\text{Sin}\phi_o & -\text{Sin}\theta_o \\ -\text{Sin}\phi_o & \text{Cos}\phi_o & 0 \\ \text{Sin}\theta_o\text{Cos}\phi_o & \text{Sin}\theta_o\text{Sin}\phi_o & \text{Cos}\theta_o \end{bmatrix} \begin{bmatrix} \bar{x}_1 \\ \bar{y}_1 \\ \bar{z}_1 \end{bmatrix} \tag{5-8}$$

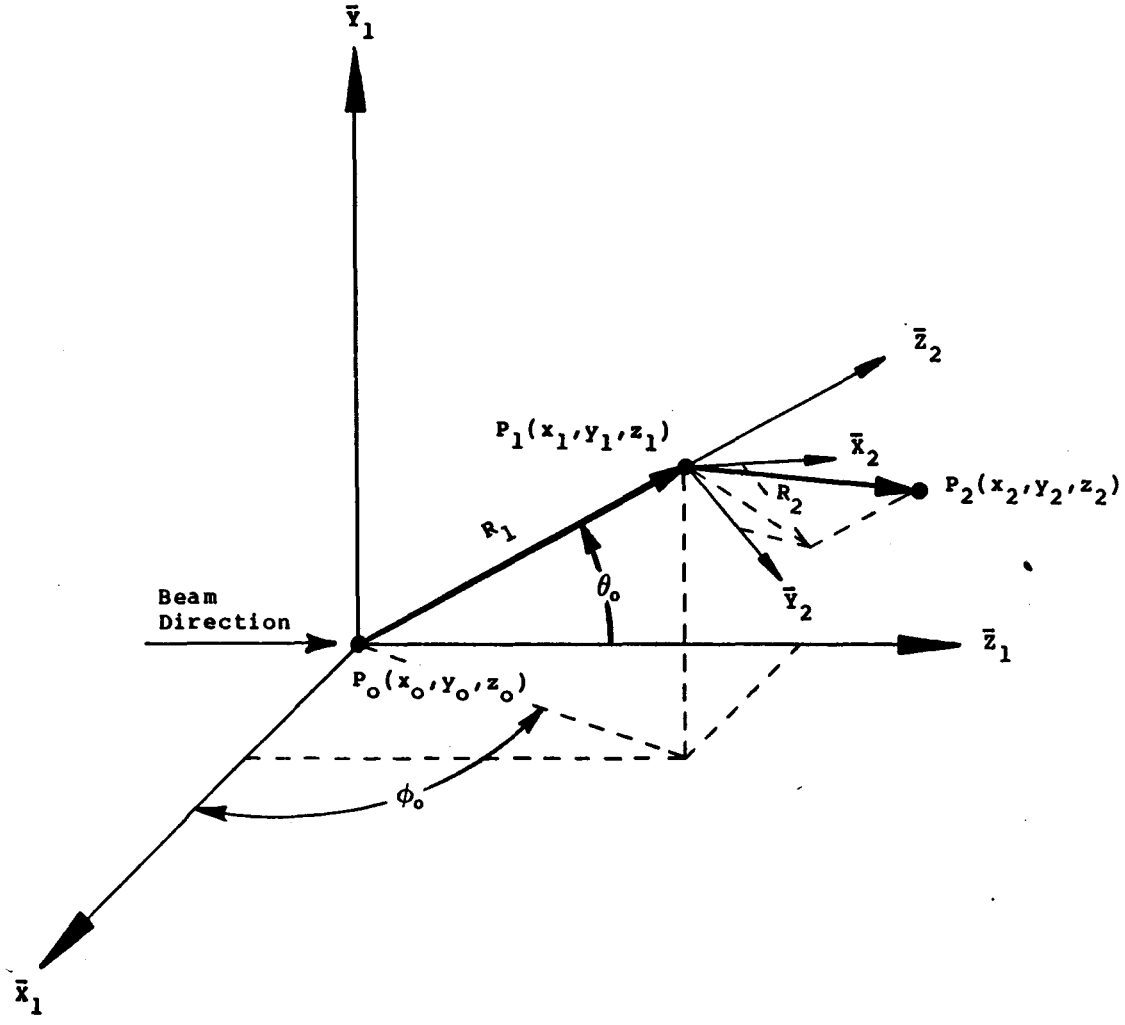

Figure 5-1 Coordinate system for particle position determination.

The coordinates of P_2 in the $(\bar{x}_2,\bar{y}_2,\bar{z}_2)$ system are:

$$\begin{bmatrix} x_2 \\ y_2 \\ z_2 \end{bmatrix} = R_1 \begin{bmatrix} \mathrm{Sin}\theta_1\mathrm{Cos}\phi_1 \\ \mathrm{Sin}\theta_1\mathrm{Sin}\phi_1 \\ \mathrm{Cos}\theta_1 \end{bmatrix} \tag{5-9}$$

The coordinates of P_1 in the $(\bar{x}_1,\bar{y}_1,\bar{z}_1)$ system are:

$$[x]_1=[\mathrm{TINV}(\theta_o,\phi_o)][R_1] \tag{5-10}$$

where $[R_1]=(0,0,R_1)$ and $[\mathrm{TINV}(\theta_o,\phi_o)]=[T(\theta_o,\phi_o)]^{-1}$ is the inverse transformation matrix and is given by:

$$\begin{pmatrix} \mathrm{Cos}\theta_o\mathrm{Cos}\phi_o & -\mathrm{Sin}\phi_o & \mathrm{Sin}\theta_o\mathrm{Cos}\phi_o \\ \mathrm{Cos}\theta_o\mathrm{Sin}\phi_o & \mathrm{Cos}\phi_o & \mathrm{Sin}\theta_o\mathrm{Sin}\phi_o \\ -\mathrm{Sin}\theta_o & 0 & \mathrm{Cos}\theta_o \end{pmatrix} \tag{5-11}$$

in matrix form. For rotation only, the coordinates of P_2 are:

$$[x]_2=[\mathrm{TINV}(\theta_o,\phi_o)][\mathrm{TINV}(\theta_1,\phi_1)][R_2] \tag{5-12}$$

The coordinates for P_2 when both rotation and translation are included are given by:

$$[x]_2=[x]_o+[\mathrm{TINV}(\theta_o,\phi_o)][R_1]+[\mathrm{TINV}(\theta_o,\phi_o)][\mathrm{TINV}(\theta_1,\phi_1)][R_2] \tag{5-13}$$

The coordinates of the third point P_3 in the absolute coordinates system are:

$$[x]_3=[x]_2+[\mathrm{TINV}(\theta_o,\phi_o)][\mathrm{TINV}(\theta_1,\phi_1)][\mathrm{TINV}(\theta_2,\phi_2)][R_3] \tag{5-14}$$

In general, the coordinates of the n^{th} scatter is:

$$[x]_n=[x]_{n-1}+[TP(\theta,\phi)]_{n-1}[R_n] \quad (5\text{-}15)$$

where

$$[TP(\theta,\phi)]_{n-1}=[TINV(\theta_o,\phi_o)]...[TINV(\theta_{n-1},\phi_{n-1})] \quad (5\text{-}16)$$

Equation 5-15 can be used to determine the position of a particle in three dimensional space relative to the initial coordinates.

5.2.2 Photon Interaction Model

Photon interactions for energies below 1 MeV consist of the photoelectric effect and Compton scattering. To simulate the interaction of photons with matter two parameters must be generated; the path length and, for Compton events, the scattering angle.

To generate the random distance which a photon travels between interactions, the laws governing the physical phenomena must be determined. For photons, the exponential probability law is valid. The probability that a photon travels a distance dx without an interaction is:

$$\exp(-ux)dx \quad (5\text{-}17)$$

The probability that a photon will have an interaction in dx is:

$$u\exp(-ux)dx \tag{5-18}$$

The cumulative probability F(x) is given as:

$$F(x)=\int p(x)dx \tag{5-19}$$

where F(x) is normalised to $0< F(x) <1$. Inserting equation 5-18 and $F(x)\cong r$ into equation 5-19 the result is:

$$x=-\frac{1}{u}\ln(1-r) \tag{5-20}$$

However, $0<1-r<1$ is equivalent to $0<r<1$ and therefore:

$$x=-\frac{1}{u}\ln(r) \tag{5-21}$$

Equation 5-21 can be used to determine the path length of a photon in an attenuating material.

The second factor that must be determined is the scattering angle when a Compton event occurs. The equation

for Compton scattering is given by:

$$E' = \frac{E}{1+E(1-\cos\theta)} \qquad (5\text{-}22)$$

where E' and E are respectively the scattered and initial photon energies in units of electron mass energies and θ is the angle of photon scatter. Rearranging for the angle produces:

$$\cos\theta = 1 - \frac{(E-E')}{ExE'} \qquad (5\text{-}23)$$

Equation 5-23 is difficult to use directly in a simulation environment because random numbers cannot be implemented easily without an appropriate probability density function (pdf). However, in 1929 Klein and Nishina[35] devised a theory that produced a Compton scattering probability density function F(E) that is vital for Monte Carlo studies of photon transport. Their basic theory has been verified experimentally by Meitner[36] and Hofstadter[37] with departures occurring predominantly at low and high energies.

The departure of Klein-Nishina pdf at low energy occurs because of the assumption that the electrons are free and at rest. Resultingly, electron binding effects are not compensated for correctly. At high energies there is a possibility of an additional photon (double Compton effect)

and radiative corrections associated with emission and re-absorption of virtual photons. Previously, much effort has been directed at the development of methods to sample the Klein-Nishina pdf. These methods may be categorized as follows:

1/ The rejection technique (e.g., the Kahn method (Kahn[38])).

2/ Solution of the inverse cumulative distribution function by numerical approximation such as Newton's method as investigated by Cavanaugh and Chilton[39].

3/ The creation of approximate expressions of the inverse cdf. (e.g., the Carleson method (Cashwell and Everett[40])).

4/ Selection of the new energy by means of a cdf, and correction by means of a weight adjustment (Cavanaugh and Chilton[39]).

5/ The direct sampling technique (e.g., the Koblinger method (Koblinger[41])).

To determine the optimal sampling technique of the Klein-Nishina pdf for Monte Carlo studies, the following factors must be considered:

1/ Sampling will be repeated thousands of times which can result in significant computer time.

2/ Economy in consumption of random numbers.

3/ Suitability of the technique to the photon energy range of interest.

The Carleson method was chosen for three main reasons: (1) The method requires only one random number per trial which is not true for the other methods; (2) It is based on an approximation of the true cdf; and (3) The method is recommended for photon energies below 5 MeV. The equation for the Carleson method that utilizes random numbers and approximates the equation for Compton scattering is:

$$E' = \frac{E}{1+SX+(2E-S)X^3} \qquad (5\text{-}24)$$

where x is a random number between 0 and 1 and S is:

$$S = \frac{E}{1+.5625E} \qquad (5\text{-}25)$$

All energies are divided by the rest mass of an electron (.511 MeV).

5.3 Monte Carlo Simulation of DPA

The simulation of DPA employs a three-dimensional model to determine the optimal geometry. Figure 5-2 shows the simulation graphics and the geometrical parameters that are variable from within the software developed. These

parameters are:

1/ Source depth (D1).

2/ Source collimator exit width (s).

3/ Source collimator exit to detector collimator entrance distance (x).

4/ Detector collimator entrance height (D2).

5/ Detector collimator depth (D3).

6/ Detector collimator entrance width (D4).

Figure 5-3 shows the flow-chart for the overall approach of determining the thickness of one of the materials. The initial counts are included for each thickness determination unless there is no change in geometry. Figures 5-4 and 5-5 display the flow-charts for the initial and attenuated counts. The following assumptions apply to the program: (1) Unlike the experimental procedure where the RST value is determined by scanning a section with no bone, the RST value is an input to the simulation program; (2) There is neither provision nor need for consideration of cross-over correction since the low and high energy counts are determined in separate cycles; and (3) The beam is monoenergetic. While the scattering model and quality of the random numbers are of vital importance, the correction for particle motion across two or three materials is equally as critical.

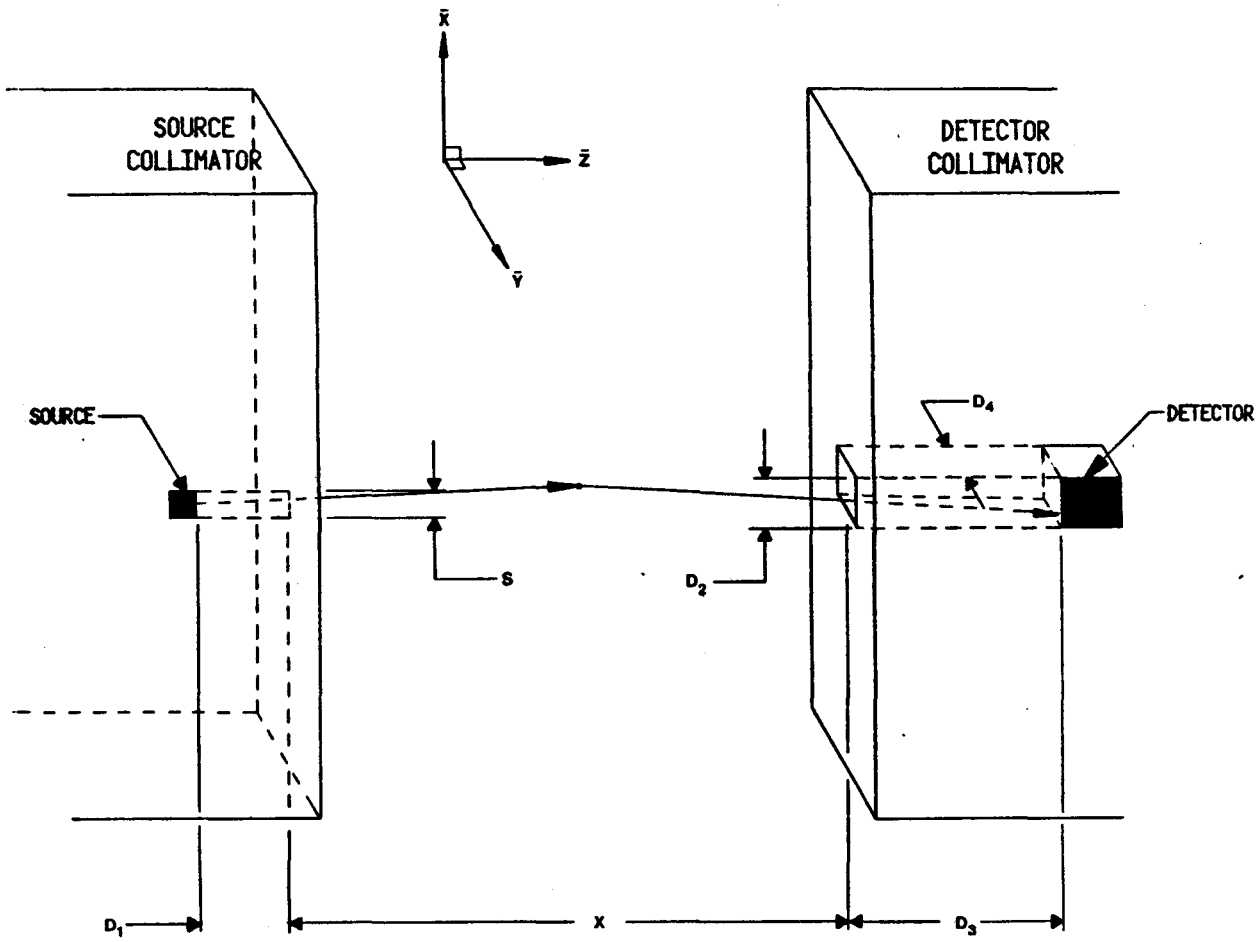

Figure 5-2 Pictorial of the DPA simulation geometry and parameters.

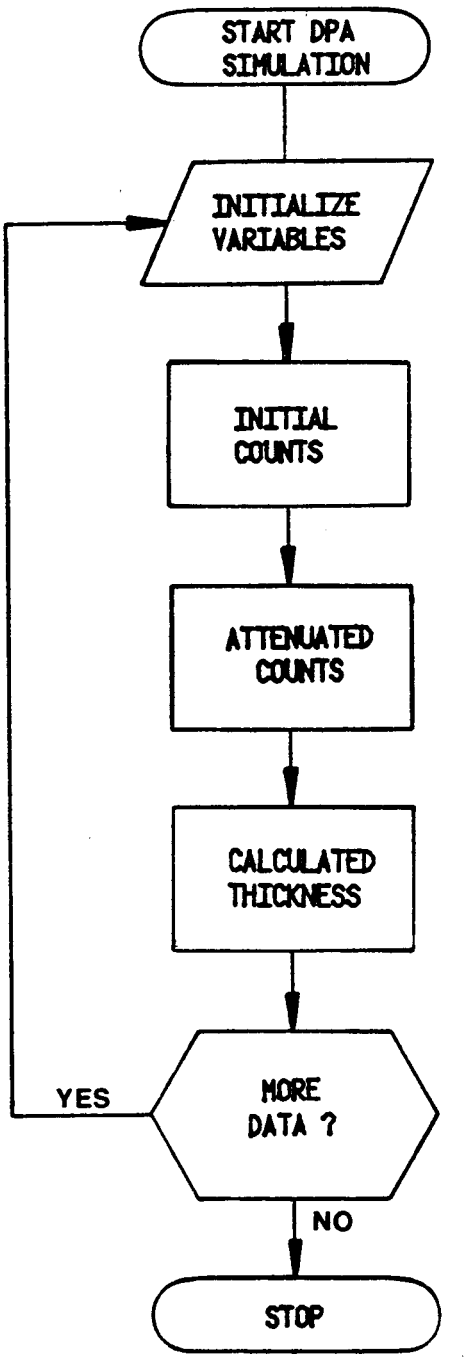

Figure 5-3 Flow-chart of the overall DPA simulation.

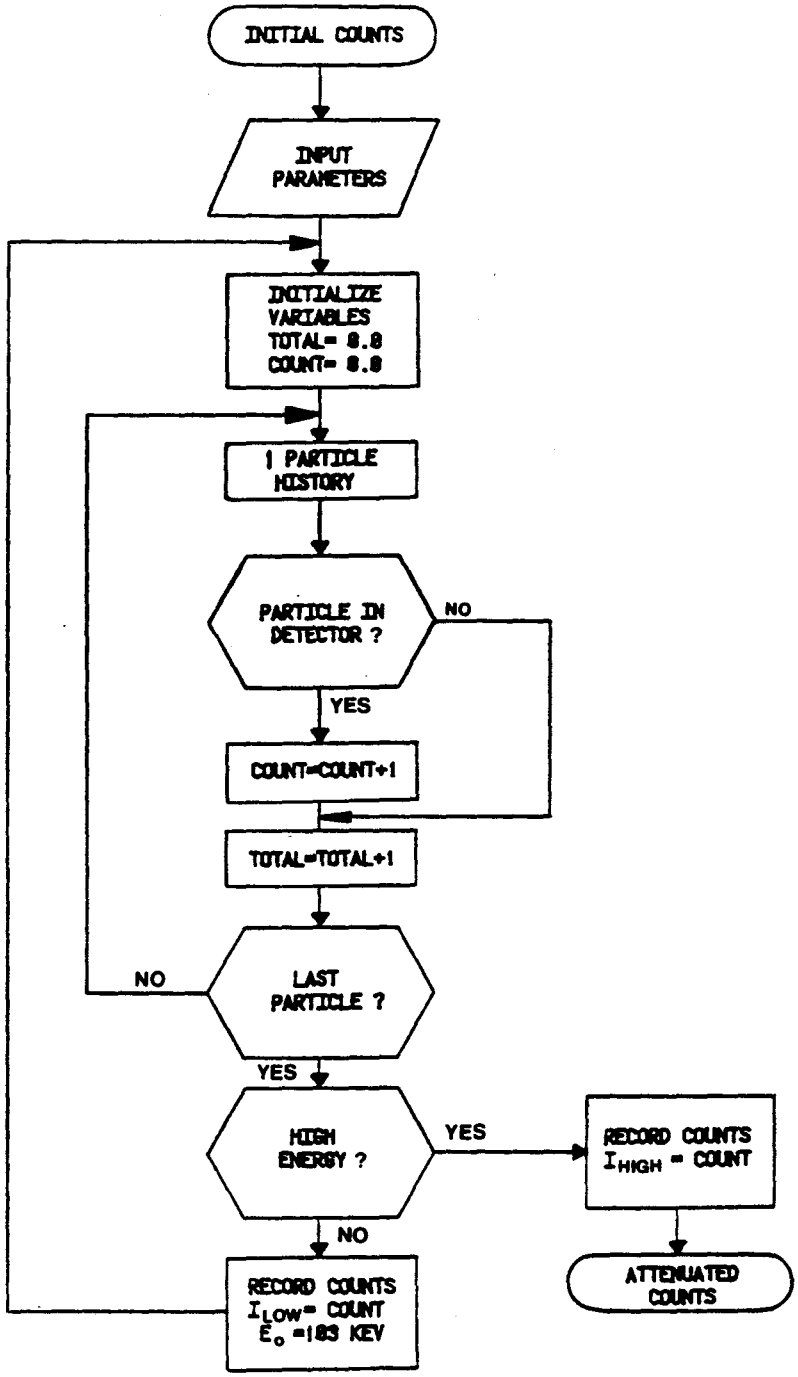

Figure 5-4 Flow-chart of the initial count section.

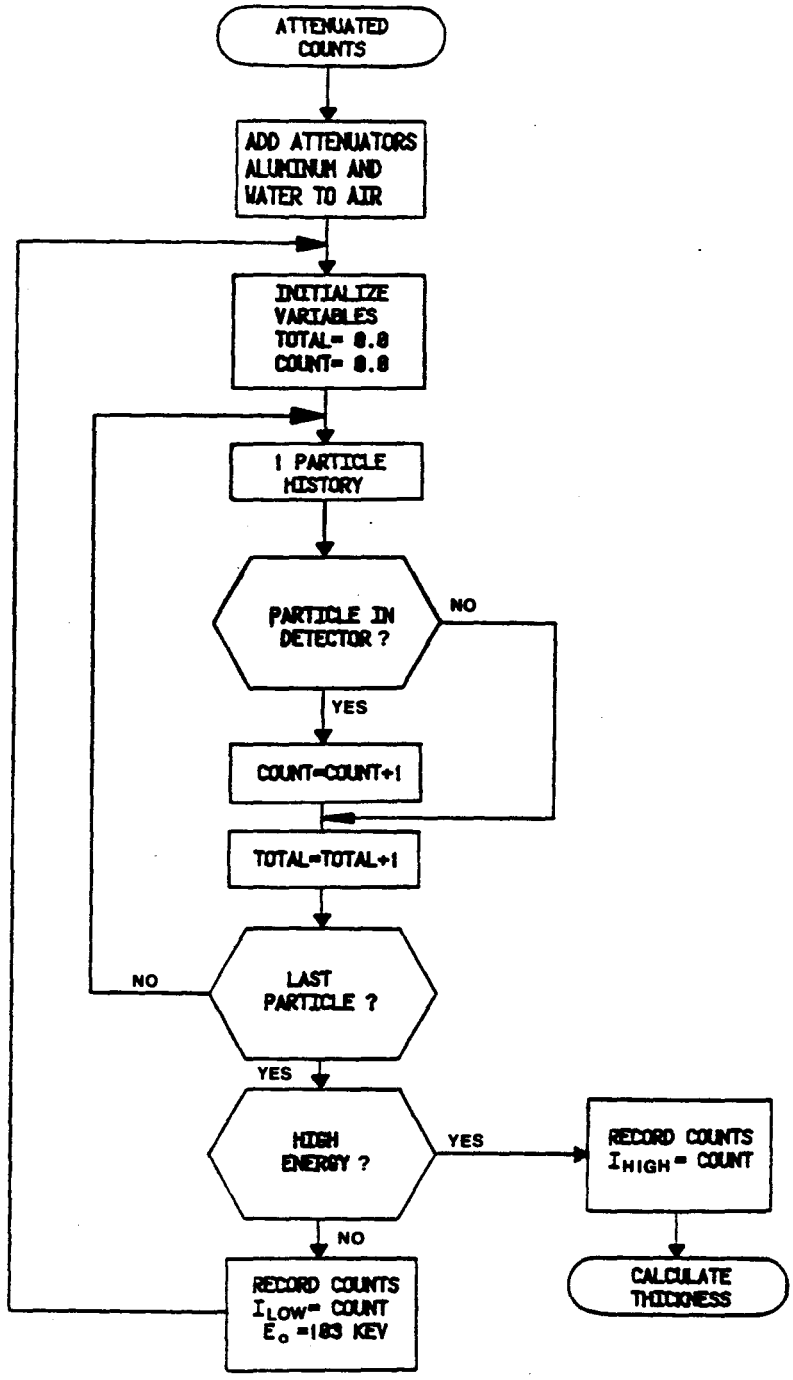

Figure 5-5 Flow-chart of the attenuated counts section.

5.3.1 Photon History

A photon history is the duration of time for which either the photon exists and does not exceed the predetermined simulation spatial boundaries, the photon energy does not fall below the minimum energy set to simulate an energy "window", or it is not annihilated. Figure 5-6 shows the flow-chart for one photon history. Two types of interactions may occur; namely, photoelectric or Compton interaction. Photoelectric interaction will cause annihilation of the photon and a new history to start while Compton events will cause only an energy loss. The starting point of the particle is randomly selected at the source as set by predetermined collimator dimensions. The path length is calculated using attenuation coefficients determined from equations that are functions of photon energy. The equations for various materials are in appendix 4 and are derived from data given by Hubbell[34]. Central to the determination of path length, type of event, amount of energy loss and angle of scatter in a Compton interaction is the need for random numbers. Once the type of event and new position are determined, a check for material boundary crossing must be performed.

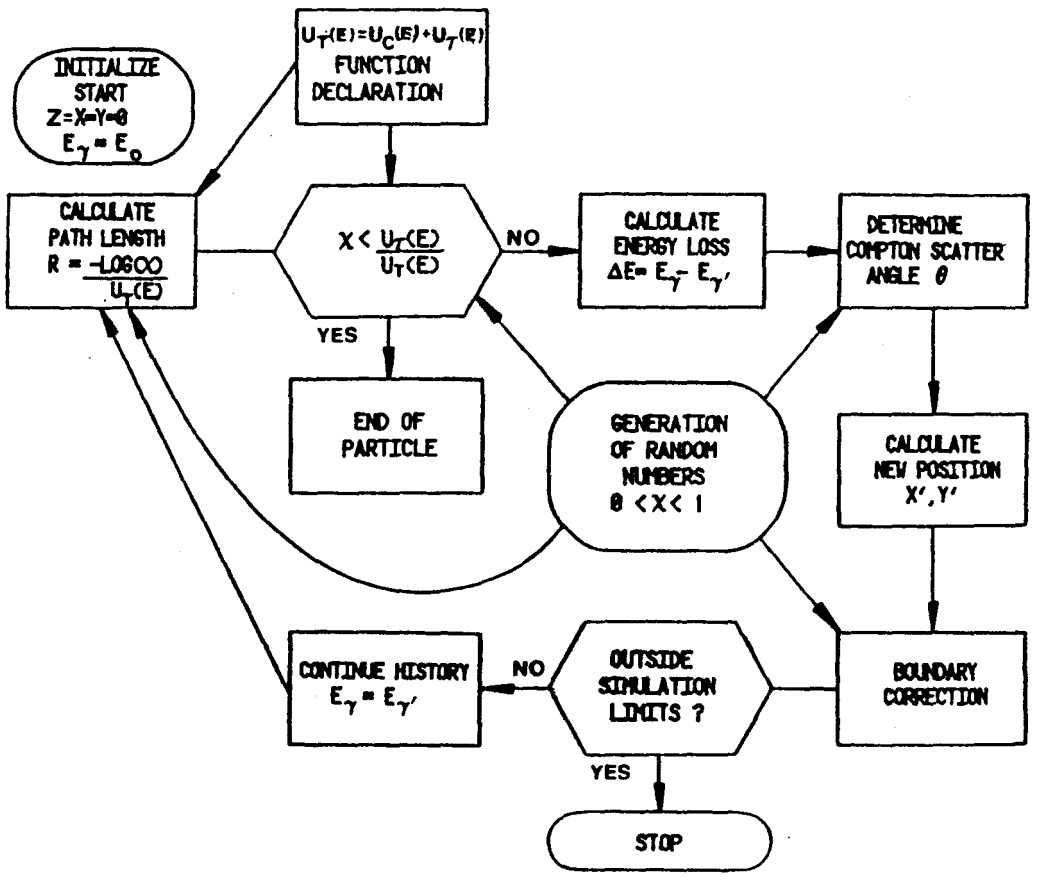

Figure 5-6 Flow-chart for the generation of a photon's history.

5.3.2 The Boundary Correction

A boundary correction is required for photons that pass from one material into another material because the path length is normally generated by assuming that the photon is travelling in one material. Figure 5-7 shows the z and x component of a particle travelling through two and three materials. This process is given mathematically by:

$$\sum_{i=1}^{n} u_i r_i = \ln(\chi) \qquad (5\text{-}27)$$

If no boundary is crossed than equation 5-21 is valid for the range. However, when one boundary is crossed the range is given by:

$$R = -\frac{\ln(\chi)}{u_2} + \left(1 - \frac{u_1}{u_2}\right) r_1 \qquad (5\text{-}28)$$

When two boundaries are crossed the range is given by:

$$R = -\frac{\ln(\chi)}{u_3} + \left(1 - \frac{u_2}{u_3}\right) r_2 + \left(1 - \frac{u_1}{u_3}\right) r_1 \qquad (5\text{-}29)$$

where r1 and r2 are crossing boundary H_1:

$$r_1 = \frac{H_1 - Z}{\cos\theta} \qquad (5\text{-}30)$$

$$r_2 = \frac{H_2 - H_1}{\cos\theta} \qquad (5\text{-}31)$$

Intuitively, the correction for a photon crossing one boundary can be described as:

$$\begin{bmatrix}\text{TOTAL}\\ \text{PATH}\\ \text{LENGTH}\end{bmatrix} = \begin{bmatrix}\text{PATH LENGTH}\\ \text{IN M1 \& M2}\\ \text{ASSUMING U2}\end{bmatrix} - \begin{bmatrix}\text{PATH LENGTH}\\ \text{IN M1}\\ \text{ASSUMING U2}\end{bmatrix} + \begin{bmatrix}\text{PATH LENGTH}\\ \text{IN M1}\\ \text{ASSUMING U1}\end{bmatrix} \quad (5\text{-}32)$$

Figure 5-8 shows the flow-chart for the boundary correction. The correction for boundary crossing by the photons is made during the attenuated counts since only air is present during the unattenuated counts.

5.4 Simulation Results

The experimental geometry was simulated with only minor changes. A line source was used instead of a circular source because a .2 cm. diameter was much smaller then the distance from the source to detector. Therefore, this assumption should have minimal practical consequences. A square collimator detector, as opposed to a circular collimator, was used for simplicity. To reduce the number of random numbers required, the source to detector collimator distance was reduced from 31 to 20 cm..

The detector was made like a "bull's-eye". An account was made of the number of counts in the succeedingly smaller collimators ranging from 2.0 cm. to .2 cm. by increments of .2 cm.. The minimum number of counts at 2.0 cm. was 2500 in the detector at the lower energy. The number of photon

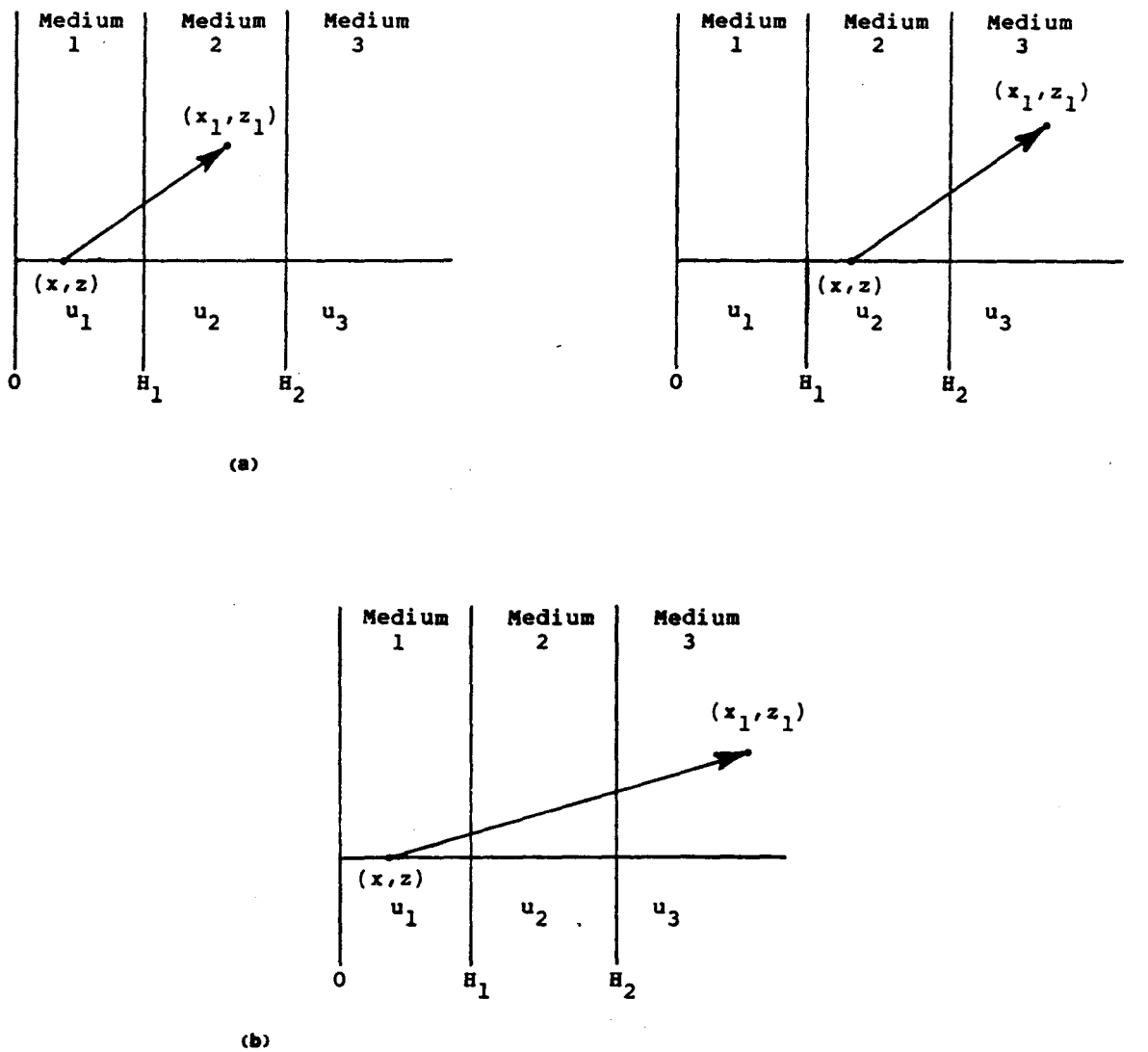

Figure 5-7 A graphical representation of the boundary correction. (a) shows the geometry for a particle crossing one boundary, (b) shows the geometry for a particle crossing two boundaries.

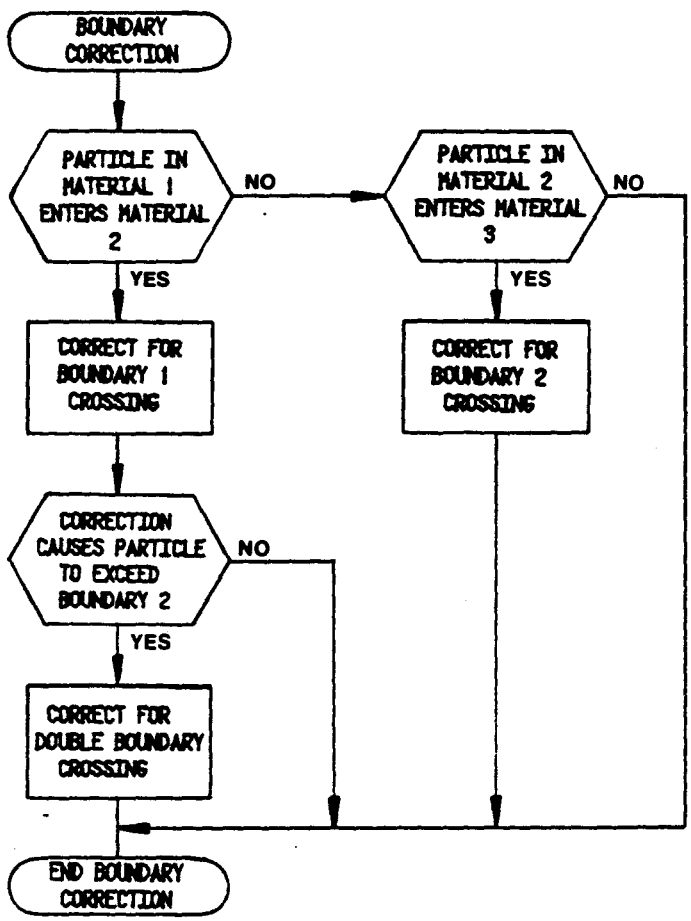

Figure 5-8 Flow-chart for the boundary correction.

histories required to produce the above value were recorded and applied to the high energy photon cycle. At 6 and 11 cm. of water, 1.7 x 10^5 and 5.6 x 10^5 random numbers were used respectively. These values included both the high and low energy counts with 5 random numbers selected per photon history. The total time to simulate 6 to 11 cm. of water was approximately 6 days.

The three ways that a photon's history may be terminated are by: the photon travelling outside the spatial boundary, it losses sufficient energy to fall below the preset energy window, or it annihilating due to photoelectric interaction. The last method of termination is governed by the materials in use and subsequently may not be changed by the user. For the acquired data, the lower limit on the 42.5 and 103 keV photons was set to 20 and 60 keV respectively. This allowed the detector collimator to be the limiting factor in rejecting photons. The spatial boundary was made large enough that any photon at the boundary would have limited probability of entering the detector collimator. The boundary parallel to the initial direction of the photon was approximately 10 times the dimensions of the detector collimator.

The results of using water and aluminum as attenuators in the simulation are shown in figure 5-9. The true aluminum thickness was .3 cm. (.81 g/cm^2) which represents the minimal amount of BMC before bone fractures occur. The water range

of 6 to 11 cm. tested was far below the average thickness of 20 cm. for a man. This was done to conserve time and random numbers. At a collimation of .6 cm. or less the uncertainty in the aluminum thickness estimate was large. This indicated that the use of collimator dimensions below .6 cm. for this simulation geometry would require a greater amount of photon histories to achieve statistical significance. For collimator dimensions between 1.0 and 2.0 cm. at water levels of 6 to 7 cm. the estimates were constant and were thus representative of narrow beam geometry. At 9 cm. of water and above, the thickness estimate for 1.0 to 2.0 cm. collimators deviates from linearity. This indicated that the collimators effectiveness at rejecting multiply scattered photons had deteriorated. Due to a near constant estimate of aluminum thickness in the range of .6 to 1.0 cm. there was evidence that minimal multiple scattering was detected. In addition, as the collimator dimensions increased so did the precision. This is in agreement with experimental results since at larger collimations there are more counts due to multiple scattering. Resultantly, the precision increased and accuracy decreased as the collimation size increased.

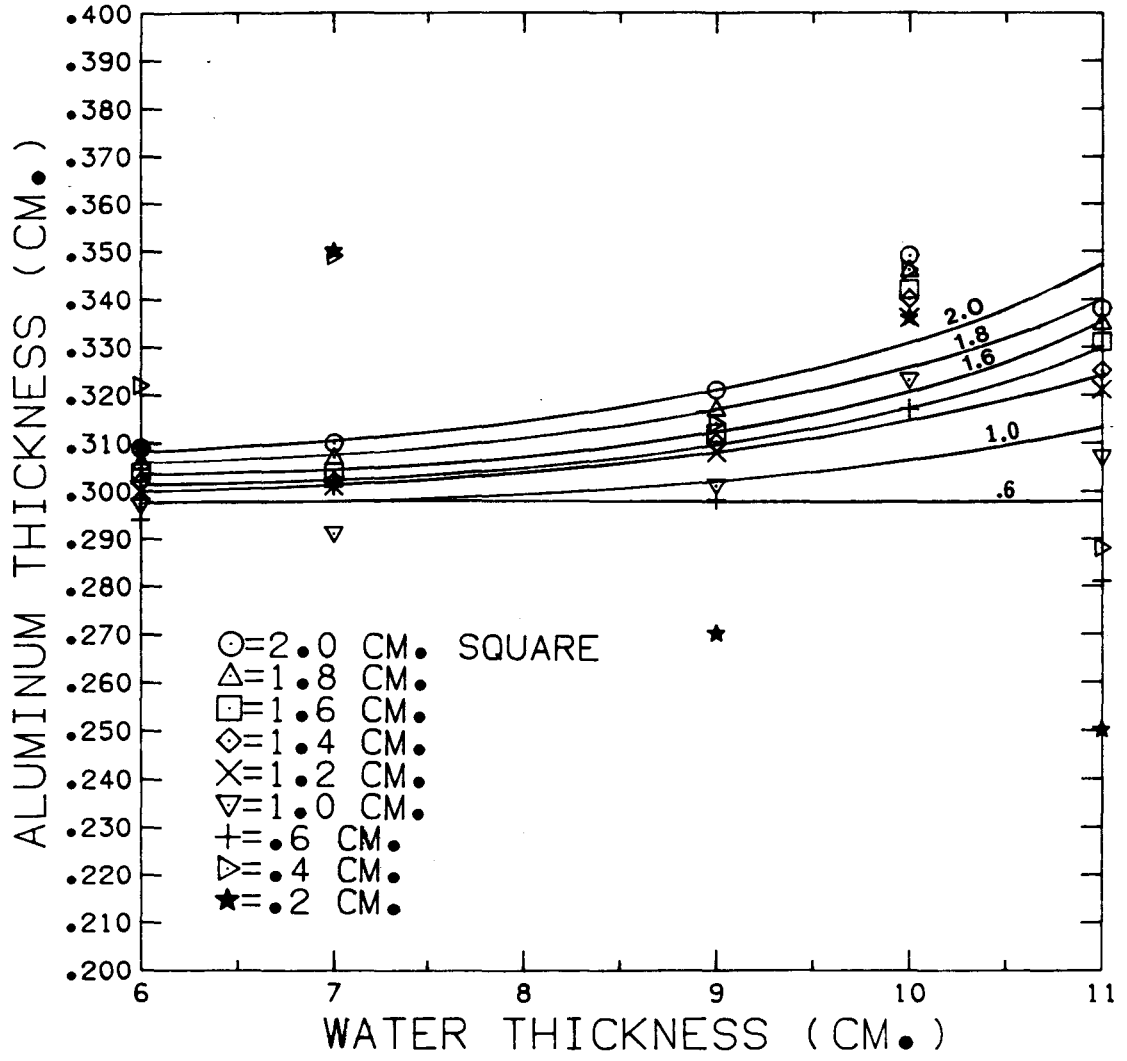

Figure 5-9 Simulation of .3 cm. of aluminum in 6 to 11 cm. of water for a range of detector sizes from .2 to 2.0 cm.

Conclusion

For stationary measurements the experimental apparatus using ^{153}Sm produced precision and accuracy of less than 2% for most total absorber thicknesses in the range of 15 to 22.5 cm.. However, at absorber thicknesses greater than 22.5 cm. accuracy and precision deteriorated. Lowering of the accuracy was caused by either beam hardening of the polychromatic ^{153}Eu X-rays with energies centered at 42.5 keV or the cross-over correction becoming non-linear above 20 cm. The precision was lowered because either the measured count rate was low in comparison to the background and caused large statistical fluctations, or the cross-over correction was non-linear. To obtain valid results, four corrections were included; namely, cross-over, dead-time, source decay, and background.

Unlike other researchers that use the copper or aluminum filter technique, an iterative procedure was used to produce a viable cross-over correction. Cross-over as a function of source-to-detector distance varied only slightly from 5.3% at 24 cm. to 5.7% at 31 cm. of total absorber thickness. This small difference was probably due to increased detection of multiply scattered photons.

Dead-time was determined to be 2.0 us. using two methods. The dead-time characteristics were representative of a non-paralyzable system. Thus to correct for dead-time losses the equation for this model was used. Because of the

high count rate through air and the large dead-time that would ensue, the initial counts were not measured directly but through a "standard". To increase precision and accuracy the ratio of high to low counts was optimized by using polyethylene (density of .930±.005 g/cm^3) as a standard.

The effects of a fat simulator (polyethylene) on the thickness measurements of a bone simulator (aluminum) for two *in vivo* situations were simulated. One occurs when the total absorber thickness is constant but percent fat changes while in the second both the total absorber thickness and the percent fat change. For both cases, as the true aluminum thickness increased the accuracy of the thickness estimate increased. With a lower percent polyethylene during BMC measurement than during RST measurement, the aluminum thickness was over-estimated. Also a difference in the amount of polyethylene between the RST and BMC measurement caused a larger error in the BMC estimate as the amount of polyethylene in the RST measurement increased. Therefore, for two people, one with a small and the other with a large amount of fat around the kidneys, the error in BMC measurement should be less for the former case. Quantitatively, if the percent change in polyethylene from the RST to BMC measurement is less than 50% at 16.3% RST polyethylene content, measurements of aluminum(bone) above 1.8 g/cm^2 (.662 cm. of aluminum) should be accurate to within 10% of the true aluminum(BMC) value for this experimental

geometry.

Motion was incorporated into the data sampling process and three stages were involved; (1) Finding the optimal sampling speed for the experimental equipment; (2) Determination of the optimal sample distance; (3) Measuring the dose that would be imparted during in vivo studies and comparing the results to calculated values.

A sample speed range of .19 to .81 cm./sec. was tested because at higher speeds inertial effects were substantial while at lower speeds the transverse motors would not produce constant motion. The optimal sample length was determined to be in the range of .5 to .7 cm. with a scan speed of 4.4 mm./sec. This was chosen because at smaller sample lengths the statistical fluctations between spatial samples were so great that the data became invalid. At sample rates above this range, the sample space was so wide that the thickness (BMC) profile did not accurately describe the object's spatial profile. This included underestimation of object edges due to "partial volume effects".

Dose calculations for the optimal speed and sample length were made and compared to measured values. A ^{153}Sm source irradiated for 44 hours with a 49 hour "cool-down" period was used for dose measurements. For a .5 cm. sample length and speed of .44 cm/sec (dial setting 60) the measured estimate of dose to bone and muscle was 4.0 and .88 mRad as calculated at 8 cm. above the source's top end. This is

representative of a typical mid-lumbar to source distance in clinical situations. The doses were measured using TLD'S and gave values approximately two-thirds of those calculated. The discrepancy arises because the calculations involved the assumption that the full photon beam is incident on a particular area for the full sample time. The measured values are underestimates because of difficulties in beam alignment.

The Monte Carlo simulation of DPA for this experimental geometry indicated that detector collimation less than .6 cm. was suspect to wide statistical fluctations due to reduced counts when compared to larger collimations. Above detector collimation of 1.0 cm. the reduced ability of the collimator to reject multiply scattered photons lowered the accuracy in the aluminum thickness estimate. However, as the collimation dimensions increased a increase in detected photons also increased the precision. In the range of .6 to 1.0 cm. detector collimation, the thickness estimate was approximately constant indicating optimal detector collimator entrance size.

Improvements and Further Study

The two main areas that require further study are the introduction of the developed system to clinical scrutiny and technical changes that may perhaps increase the efficiency of the system. Recognition must be given to the fact that these

two categories are not mutually exclusive. Also, improvements and more in-depth analysis can be performed on the Monte Carlo simulation of the experimental system.

There are several changes that can be made that may optimize the experimental system. First, to perform any long term reproducibility experiments a technique must be incorporated in hardware or software to correct for repositioning errors. Whether in vivo or in vitro studies are initiated to compare data from the same subject taken at different times chronologically, the data must be in the same spatial area for valid comparison. Secondly, the iterative technique was used in lieu of the filter technique for determination of the cross-over correction. To determine the optimal technique a comparison could be performed. Thirdly, the experimental geometry may require some change depending on the intended use of the system. Increasing the source and detector collimator width can lower the source activity required. However, this is at the expense of increasing the multiple scattering of photons resulting in a non-linear cross-over correction. If wider source collimation is used then the source upper face surface area could be increased. This would promote less self-absorption within the source. In addition, a larger NaI crystal would provide a higher efficiency and therefore reduce the required activity of the source.

Clinically, several studies must be done to prove the

technique. Firstly, a study to show that the same subjects can be measured with reproducible results. This requires, as stated above, that a good technique be implemented to correct for repositioning errors. Secondly, the effects of fat on measurements were performed in vitro and an in vivo study should be implemented to verify that precision greater than 3% can be obtained. After the basic clinical viability of the technique has been established, specific studies may be executed. For example, investigation of combining peripheral or spinal measurements with total skeletal measurements and analysing the feasiblity of using the ratio as a disease indicator. In addition, a more in-depth study of fat effects on thickness (BMC) estimation with different experimental collimations could be performed.

The Monte Carlo simulation provided some limited direction in experimental optimization. The major weakness of the model was the long run time required to obtain results and that the simulated detector collimator was square rather than circular. To speed up the operation the program could be translated into fortran from basic. Because fortran is a compiled language on the Nova as opposed to a basic interpreter, a savings in run time of a factor of 10 could be realized. In addition, use of and comparison of other sources could be performed in the simulation.

References

1. Wahner, H.W., et al., "Noninvasive bone mineral measurements", Seminars in Nuclear Medicine, 13:3, 282, 1983.
2. Hansson, T., "Effect of combined therapy with sodium fluoride, calcium, and vitamin D on the lumbar spine in osteoporosis", J. Roentgenol., 126:1293, 1976.
3. Lagrelius, A., "Treatment with oral estrone sulphate in the female climacteric: III. Effects on bone density and on certain biochemical parameters", Acta Obstet. Gynecol. Scand. (Sweden), 60:5, 481, 1981.
4. Bartley, M.H., Arnold, J.S., Haslam, R.K., Lee W.S., "The relationship of bone strength and bone quantity in health, disease, and aging", J. Gerontol., 21:517, 1966.
5. Mather, S.B., "The effects of variation in specific gravity and ash content on the mechanical properties of human compact bone", J. Biomech., 1:207, 1968.
6. Roos, B., et al., "Dual photon absorptiometry in lumbar vertebrae, I. Theory and Method", Acta Radiologica, Ther. Phys. Biol., 13:266, 1974.
7. Wilson, C.R., Madsen, M., "Dichromatic absorptiometry of vertebral bone mineral content", Invest. Radiol., 12:180, 1977.

8. Krolner, B., Neilsen, S.P., "Measurement of bone mineral content (BMC) of lumbar spine, I. Theory and application of a new 2-dimensional dual photon attenuation method", Scand. J. Clin. Lab. Invest., 40:653, 1980.

9. Mazess, R.B., "Measurement of skeletal status by noninvasive methods", Calc. Tis. Int., 28:89, 1979.

10. Dunn, W., et al., "Measurement of bone mineral content in human vertebrae and hip by dual photon absorptiometry", Radiology, 136:485, 1980.

11. Reed, G.W., Phys. Med. Biol., 11:174, 1966.

12. Cameron, J.R., Sorenson, J., "Measurement of bone mineral in vivo: An improved method", Science, 142: 230, 1963.

13. Judy, P.F., "A dichromatic attenuation technique for the in vivo determination of bone mineral content", Ph.D, 1971.

14. Watt, D.E., "Optimum photon energies for the measurement of bone mineral and fat fractions", Br. J. Radiol., 48:265, 1975.

15. Smith, M.A., et al., "Comparison between ^{153}Gd and ^{241}Am, ^{137}Cs for dual photon absorptiometry of the spine", Phys. Med. Biol., 28:709, 1983.

16. Davis, M.W., Webber, C.E., "The reactor production of a low energy, high intensity photon beam", Nuclear Inst. Meth., 154:395, 1978.

17. Bhaskar, B.K., "Study of a new source for dual photon absorptiometry of the lumbar spine", M. Eng., 1984.

18. Krolner, B., "Assessment of vertebral osteopenia", Acta Radiologica Diagnosis, 521, 1982.

19. Atkinson, P.J., "Relevance of peripheral, axial or total skeletal mass measurement", Non-invasive bone measurements: methodical problems, Ed. Dequeker, 1982.

20. Schaadt, O., Bohr, H., "Bone mineral by dual photon absorptiometry. Accuracy - precision - sites of measurement", Non-invasive bone measurements: methodical problems, Ed. Dequeker, 1982.

21. Russell, R.G., "Osteoporosis", Endocrinology, Ed. Degroot, et al., N.Y., Grune and Stratton, 2:873, 1980.

22. Gallagher, et al., "The crush fracture syndrome in post-menopausal women", Clin. Endocr. Met., 2:293, 1973.

23. Schaadt, O., Bohr, H., "Skeletal metabolism", Lancet, II:914, 1980.

24. Schaadt, O., Bohr, H., "Photon absorptiometry with 153-Gadolinium and 125-Iodine in cortical and trabecular bone. A non-invasive in vivo measurement of the skeletal status and rate of bone loss", Calc. Tiss. Int., 335:182, 1981.

25. Krolner, B., Nielsen, S.P., Lund, B., et al., "Measurement of bone mineral content (BMC) of the lumbar spine, II. Correlation between forearm and lumbar spine BMC", Scand. Clin. Lab. Invest., 40:665, 1980.

26. Riggs, B.L., et al., "Differential changes in bone mineral density of the appendicular and axial skeleton with aging", J. Clin. Invest., 67:328, 1981.

27. Riggs, B.L., et al., "Changes in bone mineral density of the proximal femur and spine with aging. Differences between the post-menopausal and senile osteoporosis syndromes", J. Clin. Invest., 70:716, 1982.

28. Reifenstein, E. C., Albright, F., "The metabolic effects of steroid hormones in osteoporosis", J. Clin. Invest., 26:24, 1947.

29. Smith, M.A., Tothill, P., "The crossover correction in dual photon absorptiometry with ^{153}Gd", Phys. Med. Biol., 27: 1515, 1982.

30. Peppler, W.W., Mazess, R.B., "Total body bone mineral and lean body mass by dual photon absorptiometry: I. Theory and measurement procedure.", Calc. Tis. Int., 33:353, 1981.

31. Witt, R.M., Mazess, R.B., "Photon absorptiometry of soft tissue and fluid content: The method and its precision and accuracy", Phys. Med. Biol., 23:620, 1978.

32. Watt, D.E., "Diameter and scan velocity effects on linear bone measurements by photon attenuation", Phys. Med. Biol., 18:673, 1973.

33. White, D.R., "Tissue substitutes in experimental radiation physics", Med. Phys., 5:6, 467,1978.

34. Hubble, J.H., "Photon CS, attenuation coefficients and energy absorption coefficients from 10 keV to 100 GeV", NSRDS-NBS29, U.S. Dept. of Commerces, 1969.

35. Klein, O., Nishina, Y., Z. Physik, 52:852, 1929.

36. Meitner, L., Hapfeld, H., Naturwiss, 18:534, 1930.

37. Hofstadter, R., McIntyre, J.A., Phys. Rev., 76:1269, 1949.

38. Kahn, H., "Application of Monte Carlo", USAEC report AECU-3259, Rand corporation, 1954.

39. Cavanaugh, G.P., Chilton, A.B., Nucl. Sci. Eng., 53:256, 1974.

40. Cashwell, E.D., Everett, C.J., A practical manual on the Monte Carlo method for random walk problems, Oxford, 1959.

41. Koblinger, L., Nucl. Sci. Eng., 56:218, 1975.

42. Heath, R.L., "Scintillation spectrometry gamma-ray spectrum catalogue", AEC research and development report, Phillips Petroleum Co., 1959.

43. Browne, E., Dairiki, J., Doebler, R., Table of Isotopes, seventh ed., Wiley and Sons, 1978.

44. Attix, F., Radiation Dosimetry, second ed., vol. 1, Academic Press, New York, 1974.

Appendix 1

Dead-time Determination

The dead-time of the electronics system was determined by: (1) measuring the delay time required between two consecutive pulses at the input that would produce one output pulse; and (2) using a short half life radioisotope to induce detector electronics dead-time.

A1.1 Method A

The dead-time of the electronics system (figure 3-1) from the DDL to the SCA was determined using a double pulse, variable width delay circuit. The block diagram of this circuit is shown in figure A1-1. The first set of monostables effectively acts to vary the delay of the pulses while the second stage causes a variation in the pulse width. Variable resistors are used to adjust for the desired width and delay of the two pulses with respect to each other.

To determine the dead-time, the pulse width was kept constant (approximately .3 usec.) while the delay time between the two pulses was varied. The high and low energy channels produced a delay of 1.3 and 1.0 usec respectively. The difference in delay time between the two channels was due to the use of an SCA (Canberra 2037) on the low energy channel and an SCA (Canberra 1437) plus a logic shaper and delay unit (Canberra 2055) on the high energy channel. The added logic shaper and delay unit was probably the cause of

the longer delay time for the high energy channel. However, these values were not the true dead-time because there was a period of instability at the SCA output between the production of one output pulse and two output pulses. Therefore, the dead-time was the delay width just before the signal instability occured at the output. These times were 2.0 and 2.3 usec. for the low and high energy channels respectively.

A1.2 Method B

This method of determining dead-time required the use of a radioactive source with a very short half life and high enough initial activity so that substantial dead-time errors resulted. For this experiment, ammonium iodide containing ^{127}I was irradiated with neutrons in the McMaster nuclear reactor to produce ^{128}I with a half life of 24.99 minutes. To facilitate higher detector efficiency, a 3 by 3 inch diameter NaI detector was used instead of the 1.6 inch diameter detector. Since the dead-time determined by method A was about 2 usec., the minimum source strength that would cause noticeable dead-time was 27 uCi (10^6 dps.). However, this was the required input to the nuclear electronics and not at the NaI crystal. To determine the actual required source strength, the detector efficiency had to be taken into account. Using Heath[42], for a 3 by 3 inch diameter crystal at an energy of 442 keV the detector efficiency ratio was

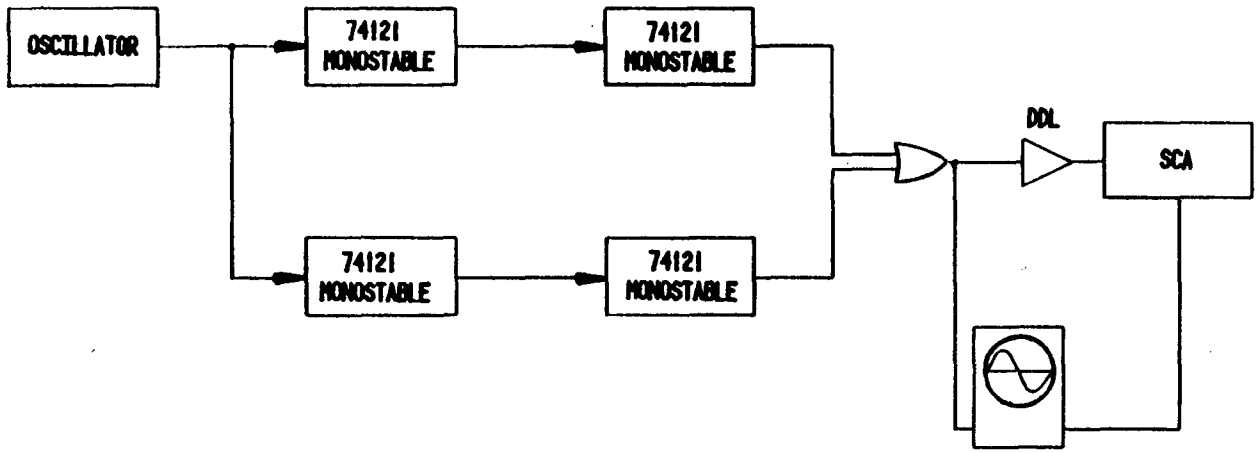

Figure A1-1 Variable pulse width and delay circuit.

.17. This required a source of approximately .2 mCi. in activity. An irradiation time of 10 seconds and sample weight of .1 grams would produce an activity of 2 mCi; an acceptable activity since the .2 mCi quantity stated above would be only a minimum requirement to produce sufficient dead-time errors.

The experimental results are shown in figure A1-2. Time zero was taken as the start of data acquisition and the counts were recorded at the digital counter located in the Nova computer. The level portion of the graph indicates that the system was non-paralyzable. In the interval 0 to 20 minutes, the count rate was approximately 5×10^5 cps and signifies that this was the maximum rate the system could resolve. The dead-time was 2.0 usec. or the inverse of the counts/second at the level portion of the graph. At approximately 60,000 counts/second the decay rate becomes exponential which corresponds to a linear response on a logarithmic plot. If equation 2-15 for a non-paralyzable system is rearranged the observed count rate is:

$$N_o = \frac{N_i}{1 + N_i \tau} \qquad \text{(A1-1)}$$

The fractional error in the counts is:

$$E = \frac{N_i - N_o}{N_i} \qquad \text{(A1-2)}$$

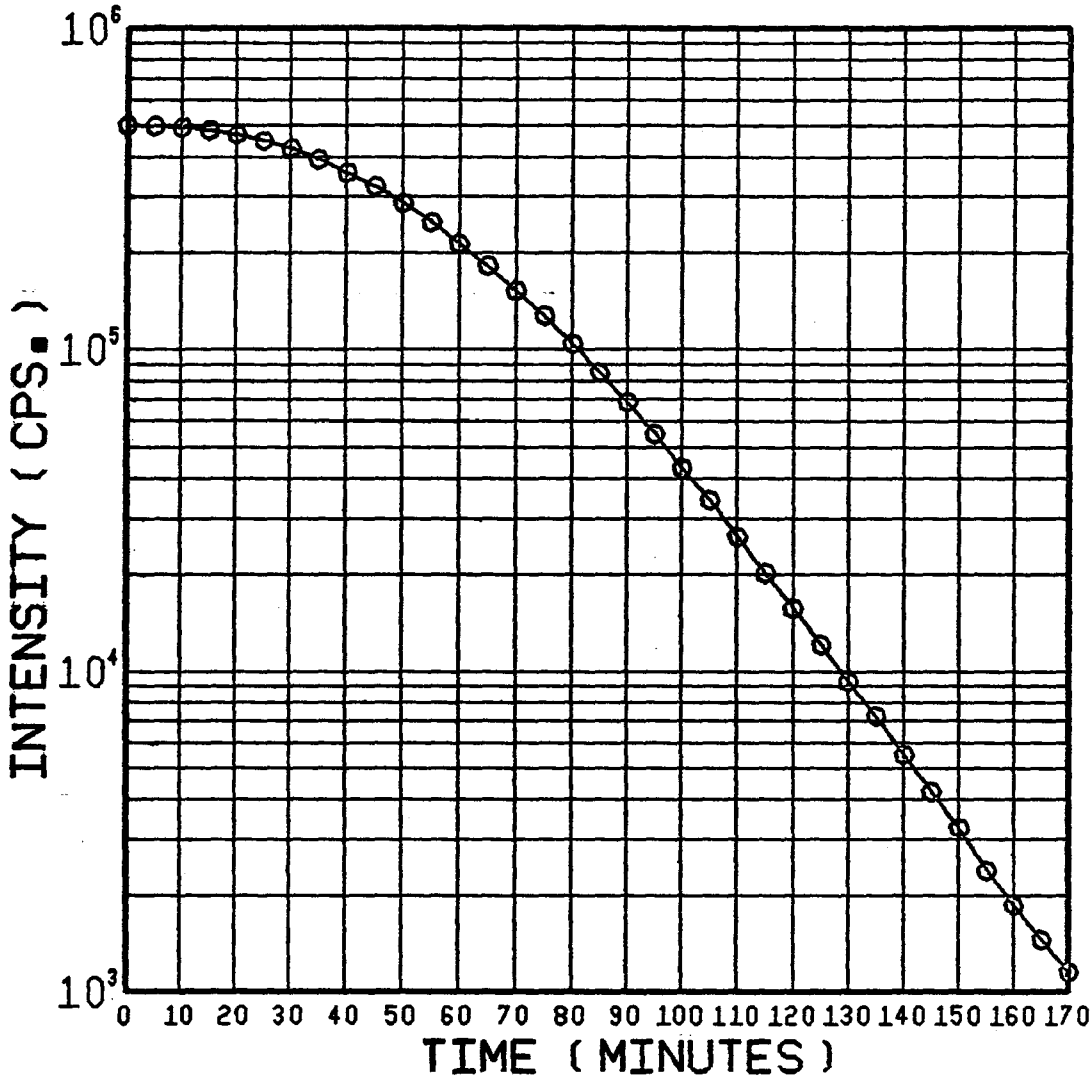

Figure A1-2 Decay curve of ^{128}I for dead-time determination.

Using equations A1-1 and A1-2 the observed counts are:

$$N_o = \frac{E}{\tau} \qquad \text{(A1-3)}$$

Table A1-1 shows the maximum observed count rate versus acquired error.

x	%E	Maximum Observed count rate (cps)
.99	1	5000
.98	2	10000
.97	3	15000
.96	4	20000
.95	5	25000

Table A1-1 Maximum count rate for a non-paralyzable system versus error between observed and true counts.

Appendix 2

Calculation of Minimum Area Density of ^{153}Sm and ^{153}Gd Sources

If exponential decay is considered and self-absorption is of importance, the mathematical representation for the simplified case of a non-distributed source is given by equation 2-1. To determine the minimum area density that will produce a greater intensity for ^{153}Sm than ^{153}Gd for the two photopeaks produced by each source, the condition is:

$$I_{Gd} < I_{SM} \qquad \text{(A2-1)}$$

Rearranging equation 2-1 produces the mass:

$$m > \frac{1}{u_{Gd} - u_{Sm}} \ln\left(\frac{I_{oGd}}{I_{oSm}}\right) \qquad \text{(A2-2)}$$

Equation A2-2 shows the minimum area density such that the two photopeaks have greater intensities for ^{153}Sm than ^{153}Gd. Table 1-2 displays the attenuation coefficients and percent intensities for ^{153}Gd and ^{153}Sm. Using the values in table 1-2 and equation A2-2 the minimum area density of Sm_2O_3 that will produce a greater intensity for both photopeaks than ^{153}Gd is .61 g/cm^2.

Appendix 3

Calibration of SCA Windows

Figure A3-1 shows the block diagram of the equipment used to set the "windows" on the two SCA's. The signals for each stage are shown in figure A3-2(a-d). The DDL doubly differentiates the. incoming pulse from the pre-amplifier (figure A3-2(a)) to create a bipolar signal shown in figure A3-2(b). The cross-over point of this curve was used to trigger the SCA and subsequently generate one output pulse (figure A3-2(c)). Cross-over timing was used since there was a wide amplitude range and the use of leading edge triggering would have produced "walk" resulting in large timing uncertainties. The SCA signal was used by the pulse height analyzer to generate a timing gate so that the PHA could receive pulses at the input (figure A3-2(d)). Because of the inherent delay in the SCA, the DDL signal had to be delayed and therefore, a time delay unit was required. Experimentally, the gate was set so that there was about 1 usec. from the leading edge to the positive peak of the DDL signal as shown in figure A3-3.

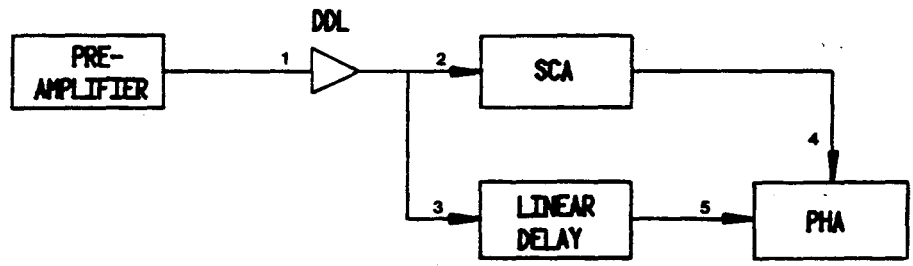

Figure A3-1 Block diagram of the instrumentation for setting SCA "windows".

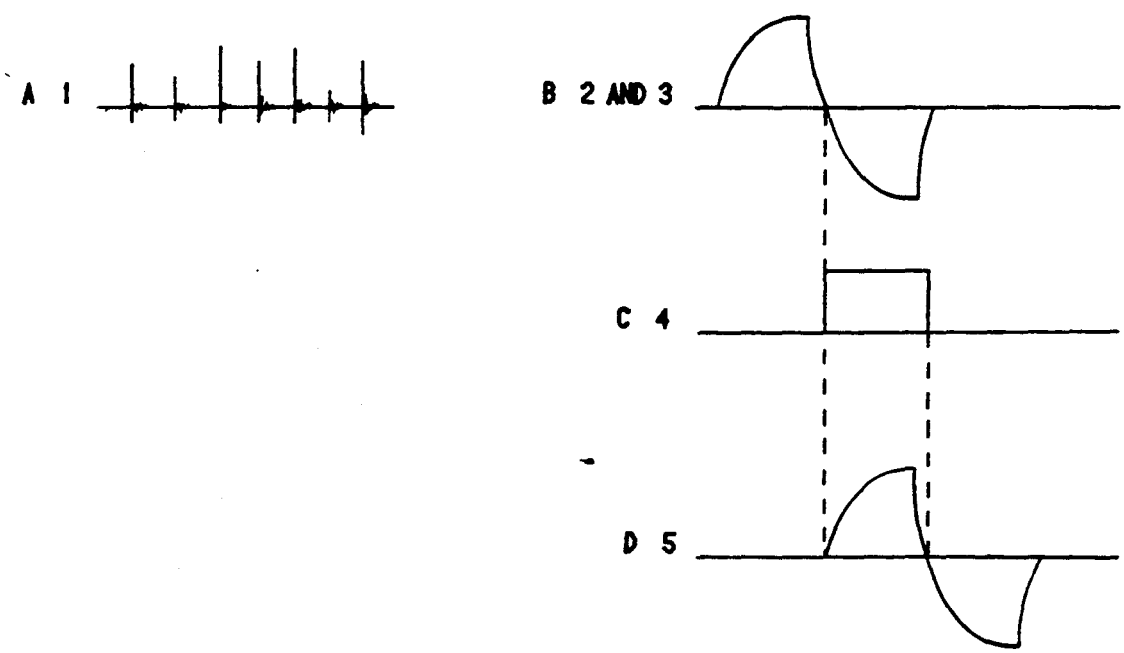

Figure A3-2 Signals generated by the components of figure A3-1. (a) pre-amplifier signal; (b) DDL signal; (c) SCA gating signal; and (d) delayed DDL signal.

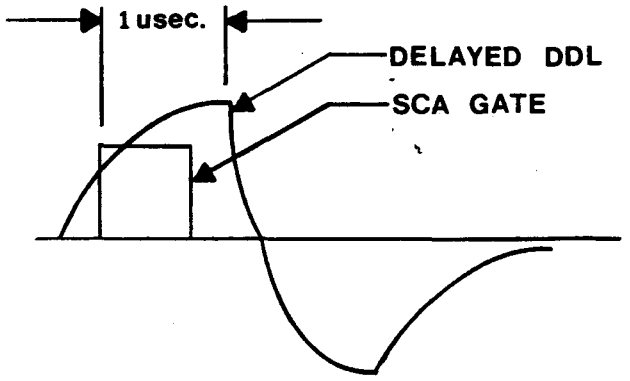

Figure A3-3 Delayed DDL and SCA signals triggered on the DDL signal's cross-over point.

Appendix 4

Calculation of Attenuation Coefficients

The attenuation coefficients at 42.5 and 103 keV were determined by interpolating data from Hubbell[34]. Several non-linear methods were compared including N-th order, geometric, and exponential regression using the correlation coefficient to indicate goodness of fit. The best fit was obtained with the function given by equation A4-1:

$$u=Alpha+Beta(Gamma)^{E} \qquad (A4\text{-}1)$$

where

u- attenuation coefficient (cm^2/g)
E- energy in keV
alpha- constant
beta- constant
gamma- constant

The routine RSMITZ in the IMSL library uses equation A4-1 to model given data. Table A4-1 shows the constants and total mass attenuation coefficents as determined by using RSMITZ. For the Monte Carlo calculations, the mass attenuation coefficients due to photoelectric interaction are given in table A4-2. Note that the constants for equation A4-1 are valid only for the range specified. These calculated interpolation functions are for 100% pure elements. For materials that have trace impurities, a weighted correction in the form of percent composition must be made. Table A4-3 shows the impurity level for each of the experimental aluminum sheets used in phases 1 and 2.

MATERIAL	ENERGY (keV)	ALPHA	BETA	GAMMA	$U_T^{42.5}$ cm^2/g	U_T^{103} cm^2/g	CORR. COEFF.
ALUMINUM	40-100	.1740	6.334	.9329	.505	-	.999
	60-200	.1187	.7762	.9737	-	.169	.996
WATER	40-100	.1693	.7684	.9498	.255	-	.999
	60-200	.1271	.1810	.9860	-	.169	.998
COPPER	40-100	.3484	54.96	.9392	4.17	-	.999
IRON	40-100	.4092	64.07	.9280	3.09	-	.999
POLY-ETHYLENE	40-100	.1625	.2095	.9706	.221	-	.999
	60-200	.0833	.1512	.9950	-	.173	.995
Air	20-50	.1951	6.610	.8835	-	-	.999
	60-150	.1233	.1929	.9818	-	-	.999

Table A4-1 Constants for equation A4-1 and the total attenuation coefficients as determined by routine RSMITZ.

MATERIAL	ENERGY (keV)	ALPHA	BETA	GAMMA	$U_{\tau}^{42.5}$ cm^2/g	U_{τ}^{103} cm^2/g	CORR. COEFF.
ALUMINUM	20-50	.1413	46.80	.8704	.270	-	.999
	60-150	.0060	2.064	.9493	-	.016	.999
WATER	20-50	.0007	.2604	.8704	.0014	-	.999
	60-150	.00003	.0107	.9493	-	.00008	.998

Table A4-2 Constants for equation A4-1 and the mass attenuation coefficients for photoelectric interaction as determined by routine RSMITZ.

Sample Aluminum cm.	Impurity							
	Copper	Iron	Manganese	Zinc	Magnesium (mg/kg)	Chromium	Silicon	Titanium
1/ .314	0	1317	24	47	0	98	286	85.6
2/ .662	2645	912	190	121	6116	760	368	222
3/ .974	1774	3815	227	172	6044	850	352	206
4/1.272	1633	2127	41	28	4492	253	462	189
5/1.908	1605	3051	66	42	4686	428	476	174
6/ .484	157	4055	15	34	0	102	352	137

Table A4-3 Impurity concentrations in the experimental aluminum plates (measured by Guelph Chemical Laboratories Inc.).

Since the impurity levels were in the order of .1% and their attenuation coefficients at 103 keV were, at the maximum, double that of aluminum, the effect of impurities on the 103 keV photons was negligible. However, iron and copper had attenuation coefficients 6 and 8 times that of aluminum at 42.5 keV respectively. Table A4-4 shows the attenuation coefficients of alumimum corrected for the presence of copper and iron.

Sample Aluminum cm.	Attenuation Coeff. (cm^2/g)
1/ .314	.508
2/ .662	.517
3/ .974	.521
4/1.272	.517
5/1.636	.520
6/1.908	.519
7/ .484	.516

Table A4-4 Attenuation coefficients for the experimental aluminum plates corrected for iron and copper impurities.

Appendix 5

Determination of Irradiation Time of ^{152}Sm

The irradiation time can be determined from the interaction model given in figure A5-1. The mathematical equation for this representation is:

$$N_x(t) = \frac{(\lambda_z N_z + \sigma_{c,y} \phi N_y)}{\lambda_x + \sigma_{a,x} \phi} [1 - \exp[-(\lambda_x + \sigma_{a,x} \phi) t]] \quad \text{(A5-1)}$$

where Y is the irradiated material, X is the produced radioactive isotope and Z is an isotope decaying to the produced isotope X. The symbols σ_c, σ_a and λ represent the capture cross—section, the absorption cross-section and the decay constant respectively. For ^{153}Sm, the absorption cross section is negligible and it has no "mother" for this reaction. Therefore equation A5-1 reduces to:

$$N_x(t) = \frac{N_y \sigma_{c,y} \phi}{\lambda_x} [1 - \exp(-\lambda_x t)] \quad \text{(A5-2)}$$

Rearranging for irradiation time:

$$t = -\frac{1}{\lambda_x} \ln \left(1 - \frac{\alpha_x}{N_y \sigma_{c,y} \phi} \right) \quad \text{(A5-3)}$$

For equation A5-3 the variables are calculated as follows:

Sm_2O_3 sample weight = 25 mg.

Molecular weight of Sm_2O_3 = 172

Area of pill(.2cm x .53cm.)= .106 cm^2

σ_c ^{152}Sm(.0254 eV) = 204 x $10^{-24} cm^2$ ([43])

λ (^{153}Sm) = .0214 $Hours^{-1}$ ([43])

ϕ = 10^{13} (n/cm^2-sec.)

The number of ^{152}Sm atoms for a given sample weight is:

$$N_{152Sm} = \frac{wt.Sm_2O_3 \;\Big|\; 1 \text{ mole } Sm_2O_3 \;\Big|\; 2 \text{ moles } ^{152}Sm \;\Big|\; N_a(\text{atoms})}{\text{molecular wt. } Sm_2O_3 \;\Big|\; 1 \text{ mole } Sm_2O_3 \;\Big|\; 1 \text{ mole } ^{152}Sm} \quad \text{(A5-4)}$$

Therefore the number of ^{152}Sm atoms in the irradiated sample is 1.75 x 10^{20} atoms. Substituting the above numbers into equation A5-3 produces the irradition time in hours:

$$t = -46.8 \ln\left(1 - \frac{\alpha_{153Sm}}{357 \times 10^9}\right) \quad \text{(A5-5)}$$

Table A5-1 shows the required theoretical irradiation times for various activities.

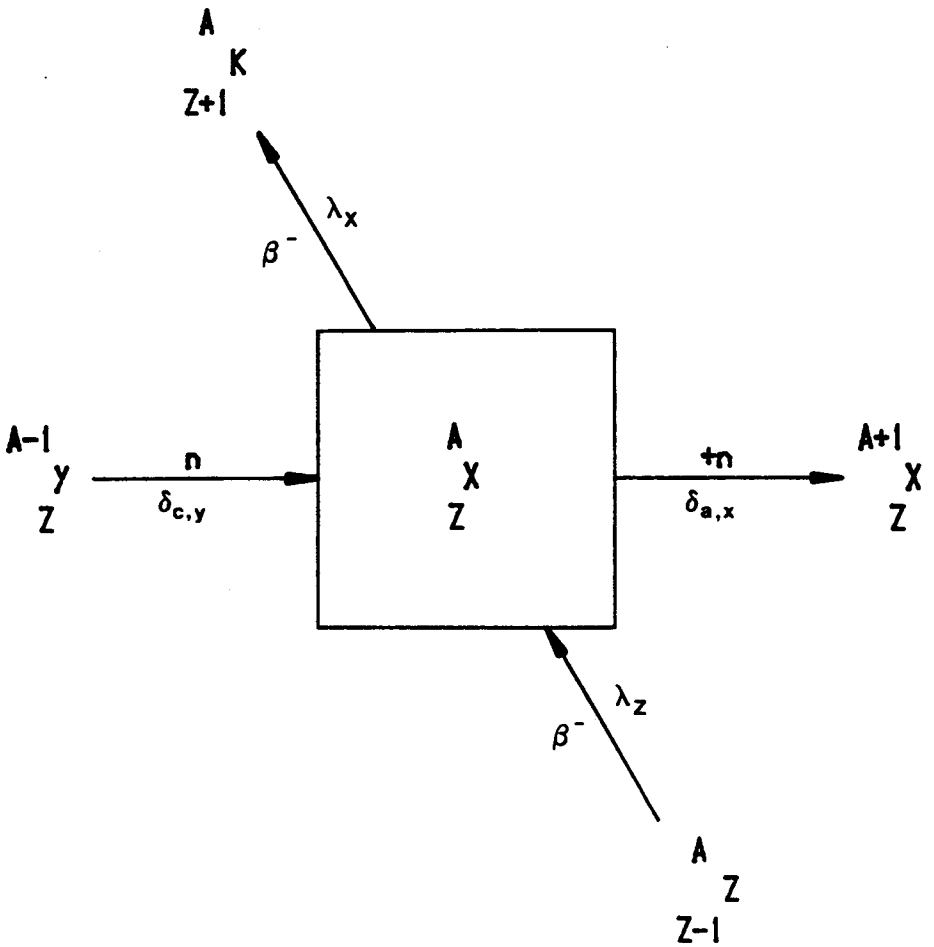

Figure A5-1 Interaction model for neutron irradiation.

Activity (Curies)	Irradiation time (hours)
1	4.6
3	16.9
4	24.2
5	32.8
6	43.5
7	57.0
8	76.9
9	111.4

Table A5-1 Required irradiation times to produce various ^{153}Sm activities.

Appendix 6

Rectilinear Scanner Calibrations

The rectilinear scanner had to be operationally calibrated to ascertain that correct data were obtained. These calibrations included: (1) The determination of the pulses per inch produced by the scanner translator board and to check that the displacement of the scanner matched the displacement as interpreted by the computer; (2) The determination of the relationship between the scan speed dial setting and the transverse speed; and (3) The ascertainment that the low voltage noise created by the scanner motors was not grounded through the detector.

A6.1 Determination of Transverse Pulses per Inch

Since only the pulses per inch in the longitudinal direction (32 p/inch) were documented in the service manual, the transverse pulses per inch had to be determined experimentally. The pulse rate was determined by moving the transverve block 20 feet for a total of five samples. The average number of pulses/inch was $200 \pm .2$. Once this was determined the accuracy of the computer to control the scanner independent of scanner speed was ascertained. Below a dial setting of 100, inaccuracies due to inertia were negligible. The scanner was tested through 30 feet for three samples in both the transverse and longitudinal directions with a scan dial setting of 60. The distance travelled was

exactly 30.00 feet for both directions.

A6.2 Relationship Between the Dial Setting and Scan Speed

The scan speed in the range of 40 to 100 on the scan speed dial was determined by recording the average time to travel 15 inches sampled five times. Figure A6-1 shows the results. The data were fit by linear regression and produced an equation given as:

$$\text{Dial Setting} = 1.35\left(\frac{\text{Transverse}}{\text{speed}}\right)\left[\frac{\text{cm.}}{\text{min.}}\right] + 24.35 \qquad \text{(A6-1)}$$

The correlation coefficient for the fit was .9999.

A6.3 Low Voltage Noise

If the detector window is set to a low enough voltage, low voltage noise caused by the scanner motors grounding through the casing can be detected in the pre-amplifier and subsequently counted as true interactions in the NaI crystal. The motors that were responsible for scanner motion created noise in the casing that distributed in an inverse square fashion. Since the low photon energy window was set at .13 to .31 volts (25.5 to 62.5 keV) any voltages in the scanner casing that were in this range could ground through the pre-amplifier. This caused the thickness estimate (see figure 4-30) to drift upwards as the distance from the motors decreased. To reduce this effect two precautions were

initiated. Firstly, the casing of the scanner was grounded through a large external ground and thus removed the major portion of the noise. Secondly, the detector was electrically isolated from the scanner casing by insulating the detector bracket with plastic bolts and washers. Once this was done the program GRDCHECK (appendix 9) was used to assure that the total counts in the front and rear directions were equal to within 3 percent.

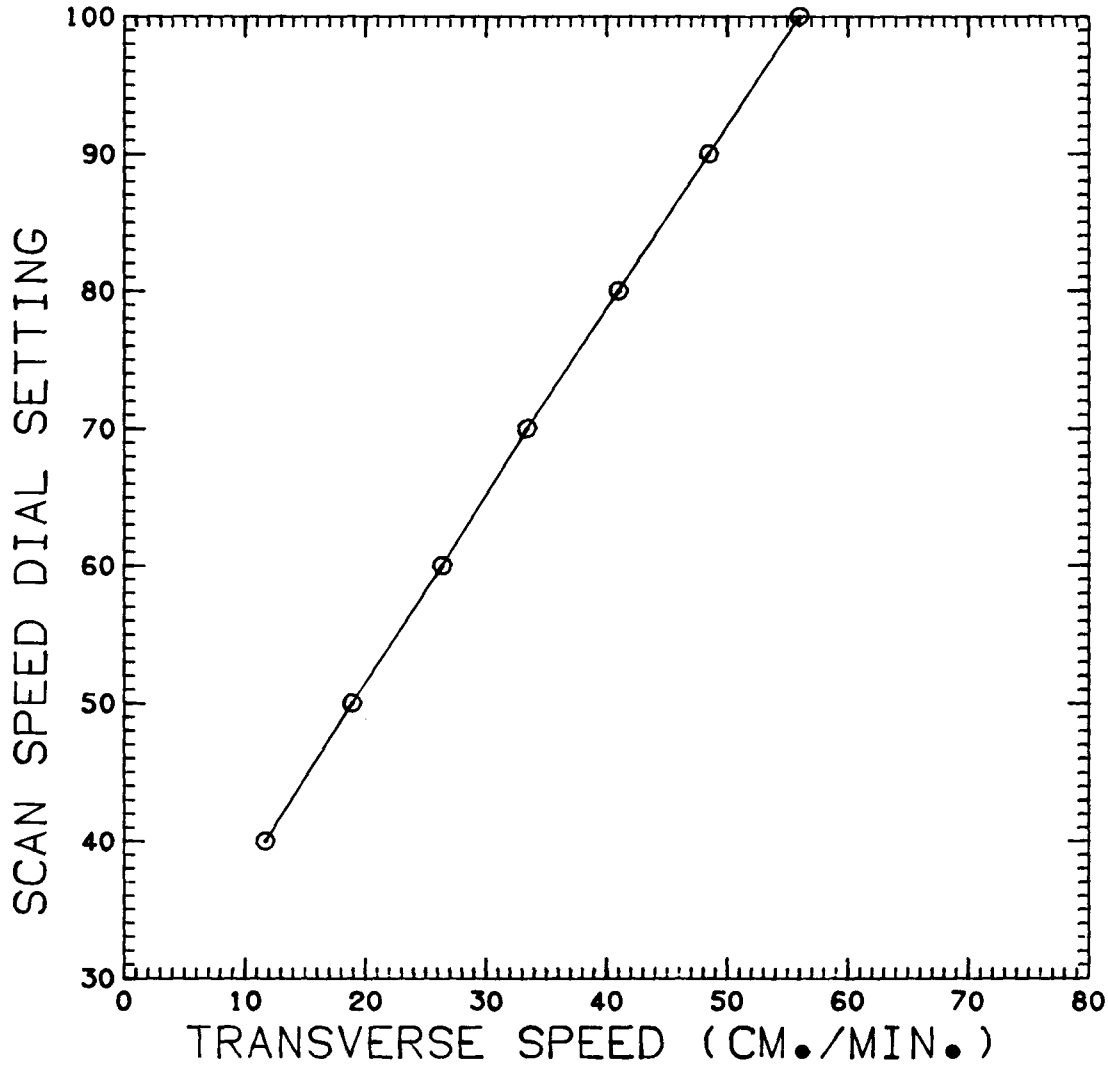

Figure A6-1 Plot of the Ohio Nuclear scanner scan speed dial setting versus transverse speed.

Appendix 7

Mechanical Design

The mechanical designs developed in this or previous projects are: (1) the source container; (2) the detector bracket and collimator; (3) the source holder and collimator; and (4) the standard block.

The source container is shown in figure A7-1 and was developed by Bhaskar[17]. The container is made of graphite and normally holds 25 mg. of Sm_2O_3 mixed with graphite powder. Figure A7-2 displays the detector collimator while the detector bracket is shown in figure A7-3. The collimator and bracket are made of lead and aluminum respectively. The source holder developed by Bhaskar[17] is shown in figure A7-4. Again, for good shielding properties, the body is made of lead and is attached to an adjustable bracket that is affixed to the lower part of the scanner's "C" arm. The standard block is shown in figure A7-5 and is made of low density white polyethylene. The density was determined to be $.930 \pm .005$ g/cm^3 using an "Archimedes" experiment.

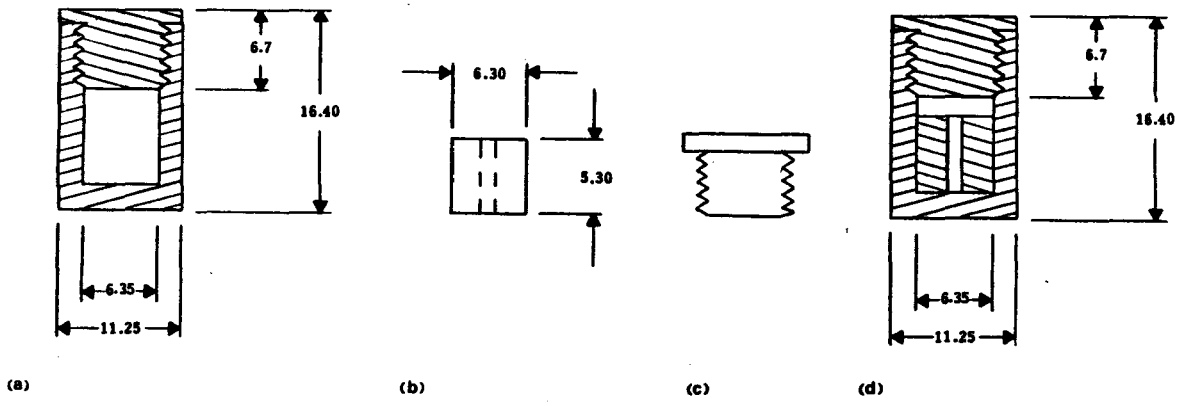

Figure A7-1 The graphite capsule for ^{153}Sm.
(a) graphite capsule; (b) cylindrical graphite insert with central hole; (c) threaded graphite cap; and (d) assembled source capsule.
Dimensions in mm.

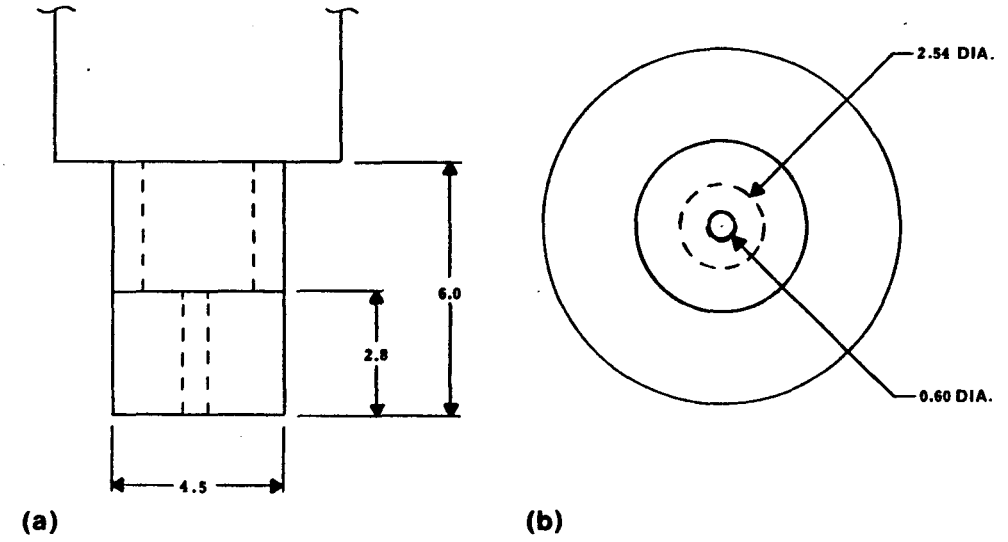

Figure A7-2 The detector collimator.
(a) side view, (b) bottom view.
Dimensions in cm.

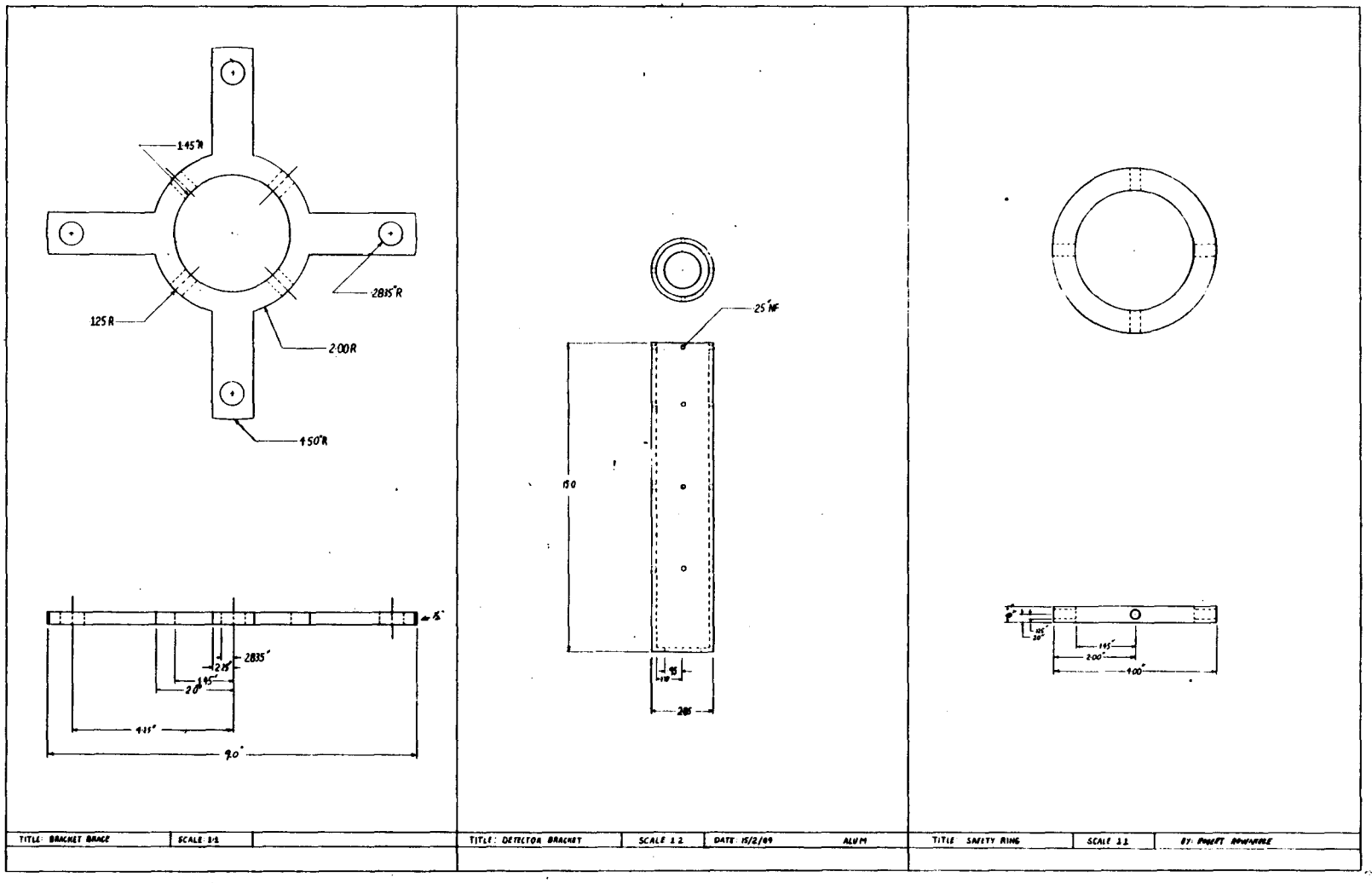

Figure A7-3 The detector bracket.

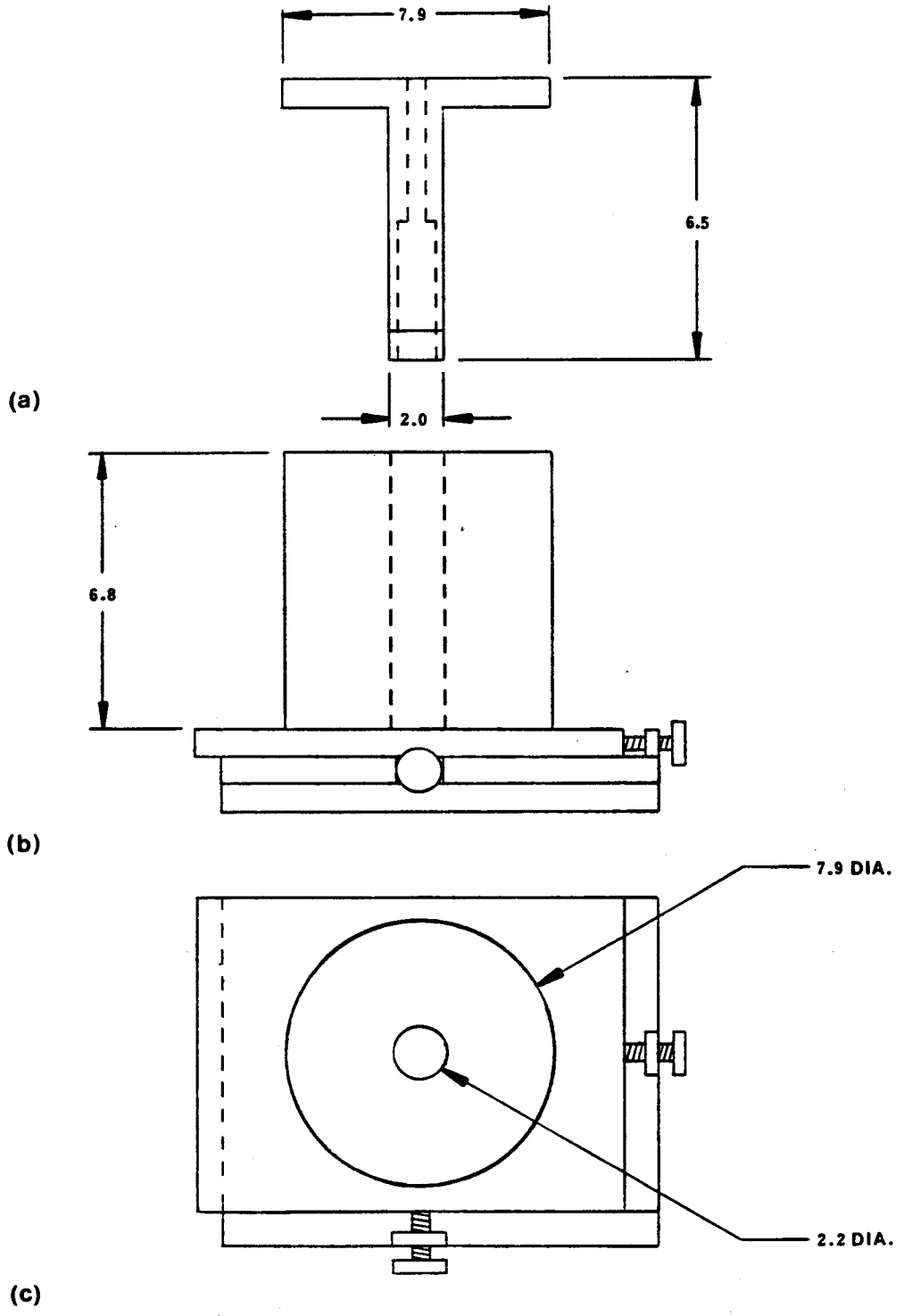

Figure A7-4 The source holder and collimator. (a) source holder; (b) source holder and sliding bracket (side view); and (c) top view. Dimensions in cm.

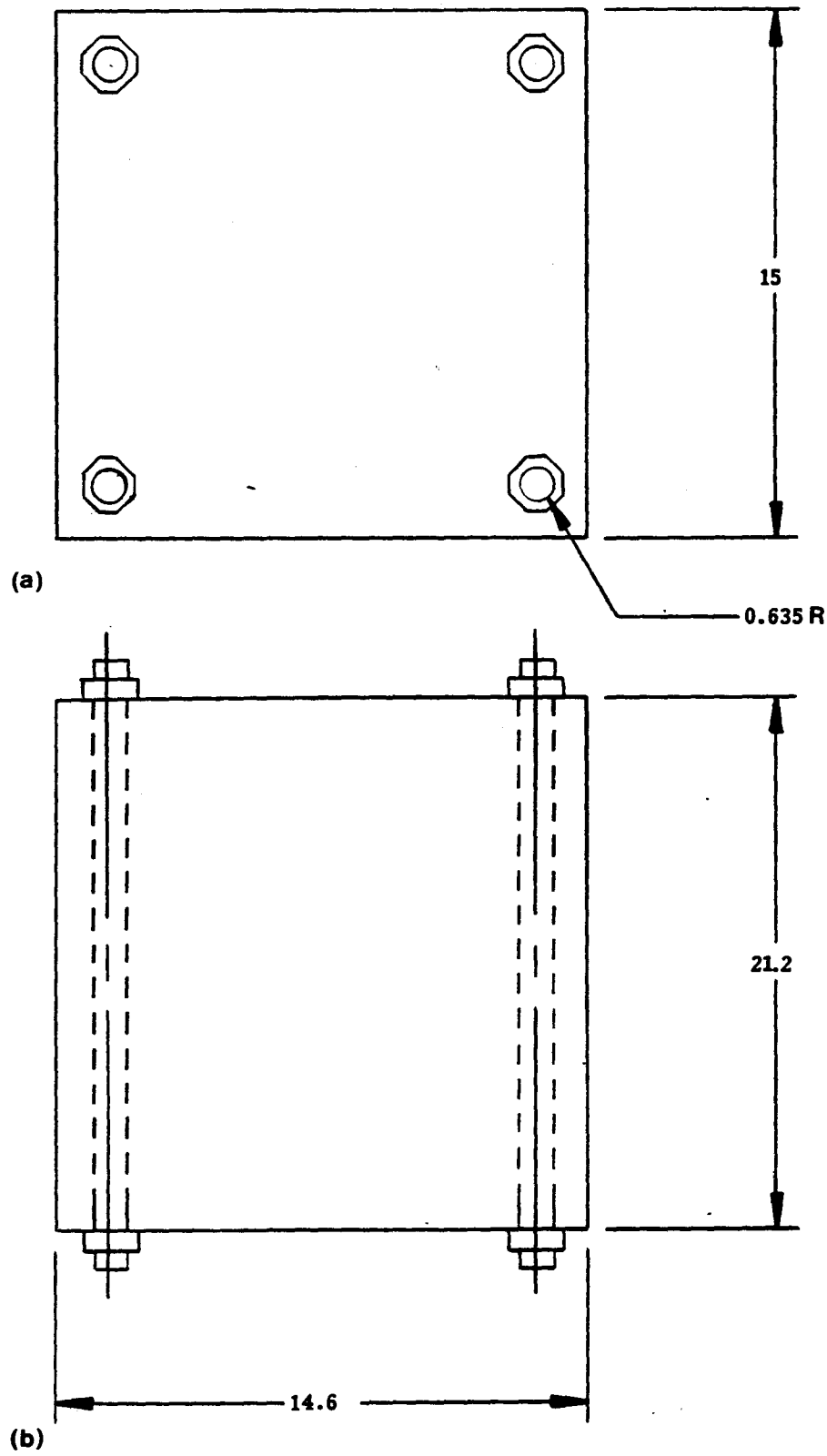

Figure A7-5 The Standard Block.

(a) top view, (b) side view. Dimensions in cm.

Appendix 8

Electronics Design

The electronics design consisted of three major areas: (1) The reception of low and high energy photon counts from the SCAs; (2) The reception of transverse and longitudinal signals from the scanner; and (3) The transmission of scanner control signals.

The low and high energy photon counters were required so that the computer would not have to be continuously polling the data lines coming from the two SCA units. This resulted in a much more efficient use of computer data acquisition time and freed it to perform other tasks such as transverse and longitudinal pulse reception and writing of raw data to a data file. The components labeled U21-U23 plus U29 and U3-U5 plus U27 in figure A8-1 constitute the high and low energy photon counters respectively. With the four components cascaded together, a maximum count cycle of 65,536 (64 k) was possible.

The longitudinal (U13) and transverse (U14,U24) counters are 16 and 256 bit counters respectively. For the transverse counters, the step distant is indicated by the signal "TP STEP" and the directions forward and backward are derived from "TP R". The direction signal is high when the transverse block is moving towards the rear. Both these signal points are obtained from the transverse translator board (drawing 920033 of the model-84 service manual). This

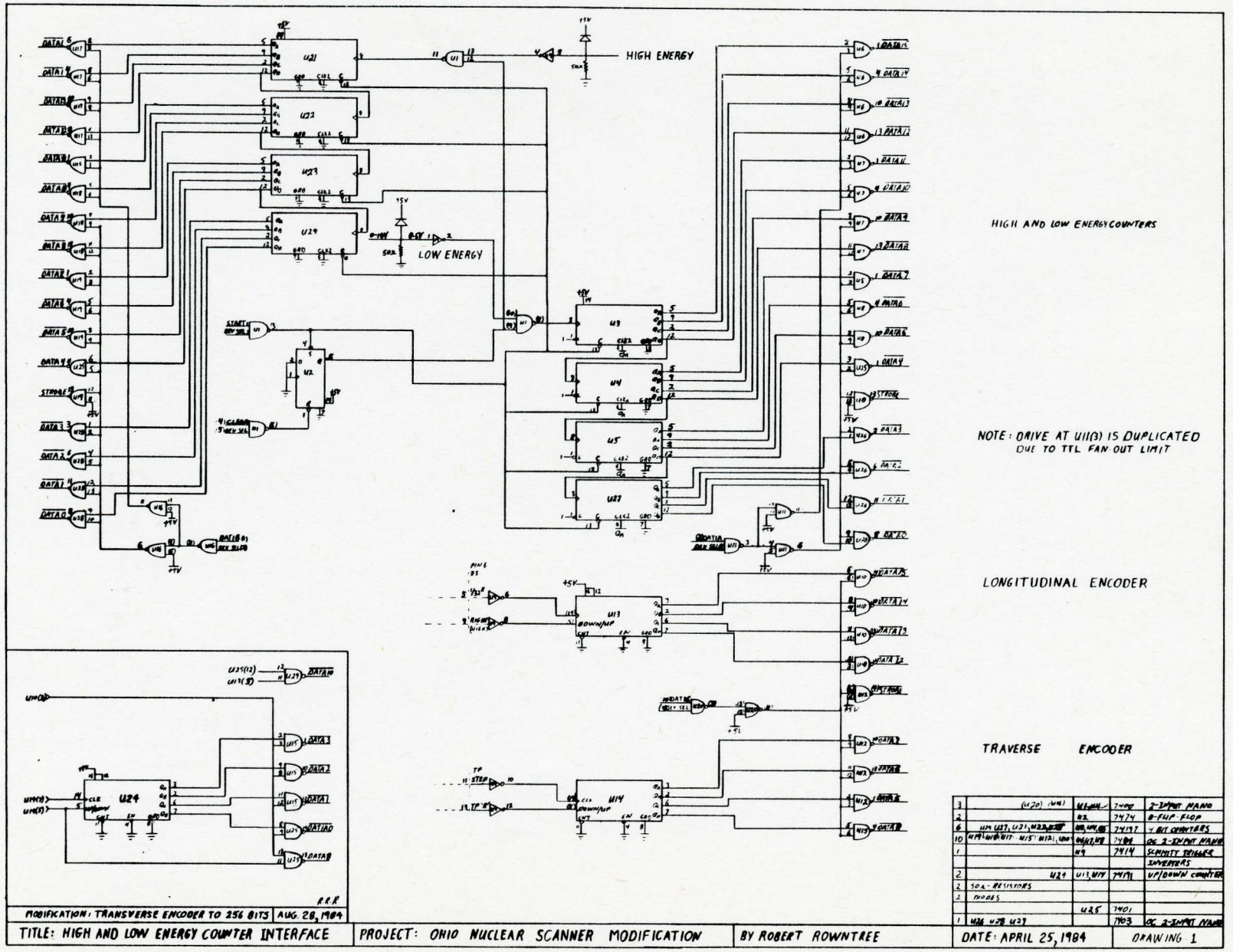

Figure A8-1 Schematic of the high and low energy counter interface.

circuitry was designed by Ohio Nuclear such that approximately 200 pulses per inch would be produced during correct operation. The longitudinal counter receives a count and direction signal from pin 6 of component "Z1" and "RIGHT" respectively (drawing 920029). The direction signal is high when the motion of the transverse block is towards the right (the side opposite the "C frame" is the front). Tables A8-1 and A8-2 show the signals on each of the 14 pin connector/cables and the associated slot numbers on device 21 and 22 respectively. Device 21 constitutes the circuit displayed in figure A8-1. The PC board layout is shown in figure A8-2. Since the signals from the translator boards were originally destined for on-board sites, their current drive capacity was limited (i.e., signal strength). This provided a need for signal boosting by line drivers. The circuitry is shown in figure A8-3. On the left side of this figure is the logic diagram while on the right side the circuit board layout is shown.

The last modification required was to control the transverse and longitudinal motion of the rectilinear scanner. Figure A8-4 shows the logic diagram of the circuit to perform this function. The circuit has device number 22 and interfaces to terminal strip number 5 located on the "C frame" of the scanner. The combination logic performs the control functions while the line drivers U6, U7, and U8 provide a greater current capacity.

Slot	Description	Connector
27	TP STEP transverse	1
26	TP RIGHT transverse	2
25	Pin 6 Z1 longitudinal	3
24	Right longitudinal	4
23	ground	7
21	High energy pulses	Coaxial
20	Low energy pulses	Coaxial cable

Table A8-1 The relationship between the signals on the connector and the interface bin slot numbers for device 21 (base 10).

Slot	Description	Connector
24	+12.6 v	1
20	Front-right(k1)	6
19	Front-left (k2)	5
18	Rear	4
1	Ground	7

Table A8-2 The relationship between the signals on the connector and the interface bin slot numbers for device 22 (base 10).

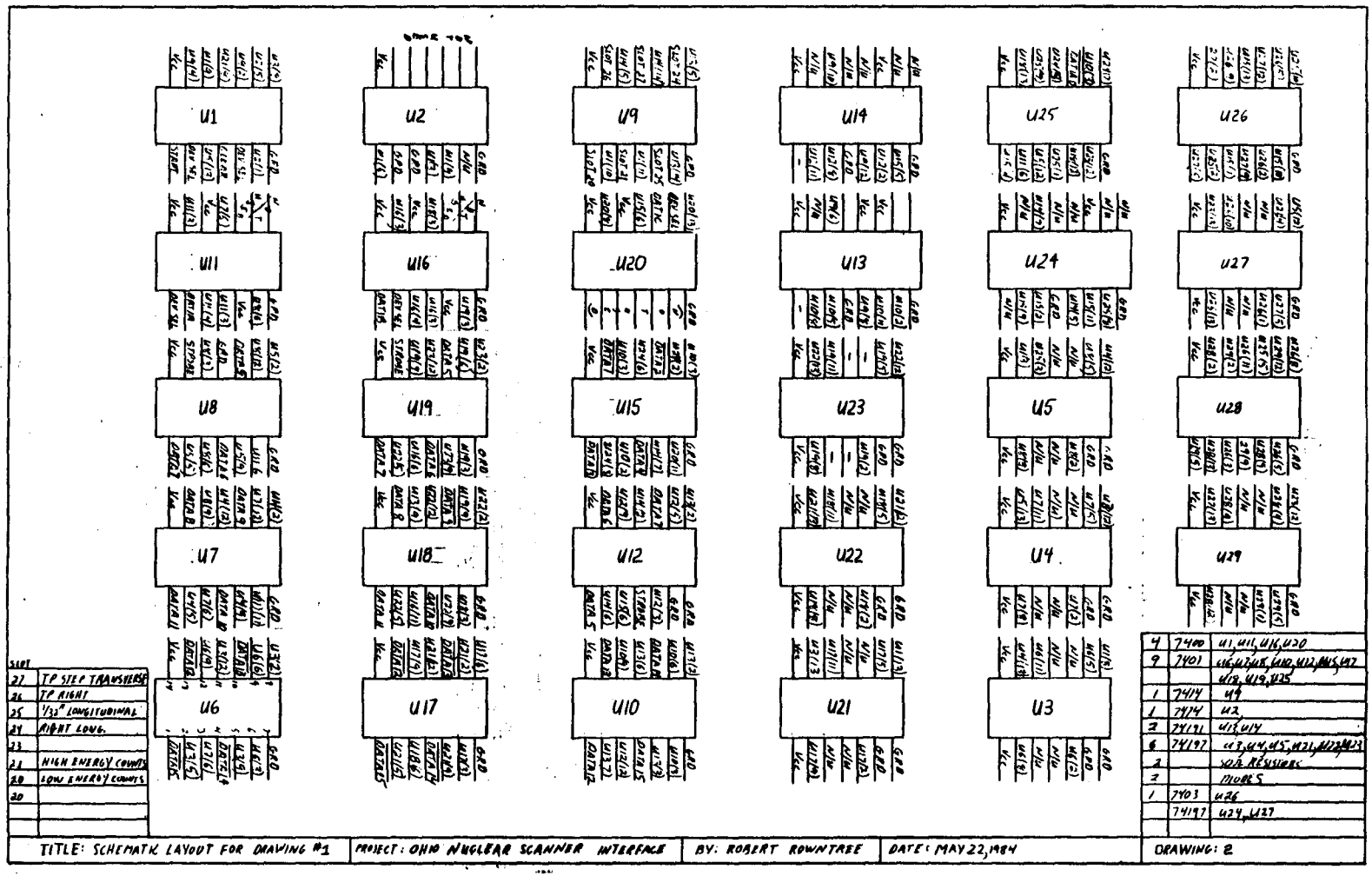

Figure A8-2 The circuit board layout for the design in figure A8-1.

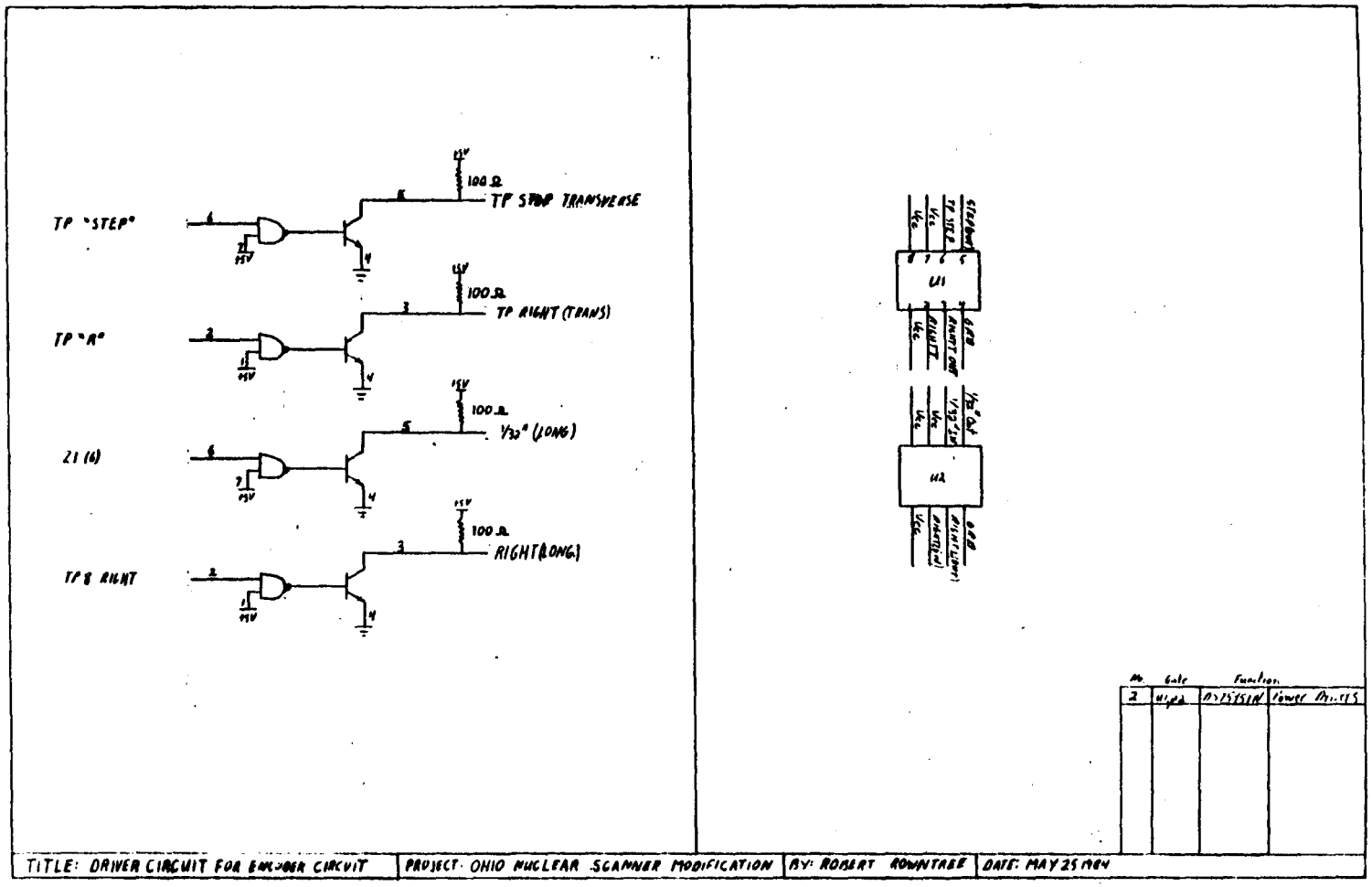

Figure A8-3 The driver circuit for the encoder signals.

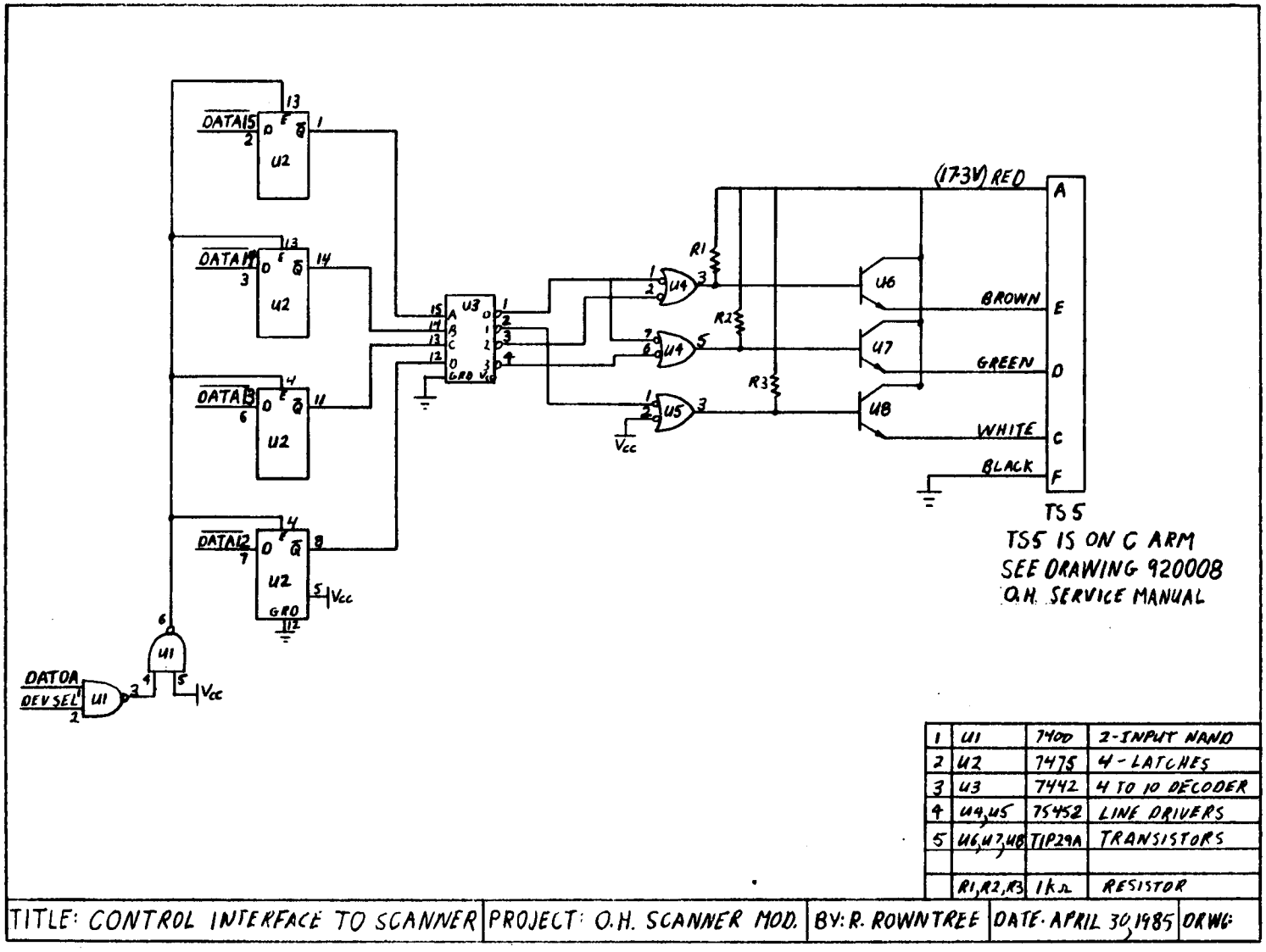

Figure A8-4 Schematic of the scanner control interface from the computer.

Appendix 9

Computer Programs

There are four programs that were important to either the operation of the experimental apparatus or the Monte Carlo simulation. The first three are SCANBONE, ANALYSIS and GRDCHECK and were required for the correct production of experimental results. The last program, SIMDPA, is the computer simulation of the DPA experiment.

The program SCANBONE performs the data collection and analysis. The following steps are performed in SCANBONE:

1/ Receives the scan parameters from the user.
2/ Samples for background counts.
3/ Samples for initial counts.
4/ Performs a RST measurement.
5/ Scans the subject according to user's specifications.
6/ Analyzes the data after the scan and produces a graphical plot of the thickness profile.
7/ Autoresets to the initial starting position.

Files from SCANBONE were transferred to another NOVA computer that was linked to a Tektronix plotter. ANALYSIS was used to produce a hardcopy of the graph on the plotter. To obtain correct plots, several checks of the system were performed. One of the most important checks required the use of

GRDCHECK.

The program GRDCHECK was used to detect a count rate increase due to low voltage noise (see appendix A6.3). The program checks for a consistent count rate in the forward and backward direction. If the difference in count rates at the rear (near the motors) and front are within 3%, then the scanner passes this test.

SIMDPA and the above programs were written in basic and implemented on NOVA (Data General) computers. The program SIMDPA was tested on the NOVA 4X computer with a hardware floating point processor. Random numbers were generated by a software algorithm with a period of 2^{24} or approximately 17 million.

```
0010 REM*****************PROGRAM SCANBONE*******************************
0020 REM AUTHOR: ROBERT R. ROUNTREE
0030 REM DATE :MAY 17,1985
0040 REM FILE NAME: SCANBONE.SR
0050 REM SYSTEM: NOVA BASIC/RDOS
0060 REM PROGRAM:SCANBONE.SR
0070 REM*****************************************************************
0080 REM
0090 REM PROGRAM: MOTIONAL DETERMINATION OF ABSORBER THICKNESS
0100 REM          USING THE **DPA** TECHNIQUE
0110 REM          THE ABSORBERS ARE ALUMINUM AND WATER
0120 REM
0130 REM..*****************************************************************
0140 REM VARIABLES:
0150 REM            D5-COUNTER FOR END OF PASS DETECTION IN FILE DATA
0160 REM            H2-INITIAL COUNT RATE OF THE HIGH ENERGY PHOTONS
0170 REM            H9-HIGH ENERGY PHOTONS COUNT RATE
0180 REM            L2-INITIAL COUNT RATE OF THE LOW ENERGY PHOTONS
0190 REM            L9-LOW ENERGY PHOTONS COUNT RATE
0200 REM            M1- SYSTEM TIME AT WHICH THE LOW AND HIGH ENERGY
0210 REM                COUNTS WERE COLLECTED. USED FOR DECAY CORRECTION
0220 REM            N -NUMBER OF SCANNER CYCLES IN ONE COMPLETE SCAN
0230 REM            P -BACKGROUND COUNT RATE FOR LOW ENERGY PHOTONS
0240 REM            Q -BACKGROUND COUNT RATE FOR HIGH ENERGY PHOTONS
0250 REM            R8-RELATIVE SOFT TISSUE RATIO  (RST)
0260 REM            S9-COUNTER TO DETERMINE THE NUMBER OF DATA POINTS
0270 REM               FOR ONE PASS.
0280 REM            T -STARTING TIME FOR DATA ACQUISITION.
0290 REM            T1- UP-DATED TIME FOR DATA AQUISITION.
0300 REM            T8-DEAD-TIME CONSTANT
0310 REM            U1-MASS ATTENUATION COEFFICIENT FOR 42.5 KEV PHOTONS
0320 REM               IN ALUMINUM
0330 REM            U2-MASS ATTENUATION COEFFICIENT FOR 103 KEV PHOTONS
0340 REM               IN ALUMINUM
0350 REM            U3-MASS ATTENUATION COEFFICIENT FOR 42.5 KEV PHOTONS
0360 REM               IN POLYETHYLENE
0370 REM            U4-MASS ATTENUATION COEFFICIENT FOR 103 KEV PHOTONS
0380 REM               IN POLYETHYLENE
0390 REM            X8-TOTAL DISTANCE IN TRNSVERSE DIRECTION IN PULSES
0400 REM            Y8-TOTAL DISTANCE IN LONGITUDINAL DIRECTION IN
0410 REM               PULSES.
0420 REM            Z -THE TOTAL SAMPLE TIME IN SECONDS
0430 REM-----------------------------------------------------------------
0440 REM ARRAYS:
0450 REM            A1-CONTAINS THE VALUE OF DATA LINES 0-15 WHEN USED
0460 REM               IN CONJUCTION WITH THE "CALL" STATEMENT
0470 REM            B1-USED TO HOLD SCANNER DIRECTION AND DISPLACEMENT
0480 REM               INFORMATION.
0490 REM            D -USED TO SUM THE THICKNESS OF ALUMINUM (BONE)
0500 REM               AT THE X TH POSITION OVER 2*N DATA POINTS IN THE
*
```

```
0510 REM                Y DIRECTION.
0520 REM-----------------------------------------------------------------
0530 REM DESCRIPTION:
0540 REM               THE FUNDAMENTAL EQUATIONS ON WHICH DPA IS
0550 REM      BASED UPON ARE:
0560 REM
0570 REM                 LN(L2/L9)-R8*LN(H2/H9)
0580 REM  THICKNESS = ------------------------
0590 REM                      U1-R8*U2
0600 REM
0610 REM                   LN(L2/L9)
0620 REM           RST =-------------
0630 REM                   LN(H2/H9)
0640 REM
0650 REM*****************************************************************
0660 REM*****************************************************************
0670 DIM A$(10),A1(16),B1(10)
0680 DIM D(100)
0690 PRINT "<26>"
0700 REM-----------------------------------------------------------------
0710 REM               PARAMETER INPUT SECTION
0720 PRINT "CROSS-OVER CORRECTION (X0)"
0730 INPUT F
0740 PRINT "SAMPLE TIME IN SEC. TIMES 10,(DEFAULT=50)"
0750 INPUT B
0760 PRINT "MULTIPLIER,(DEFAULT=60)"
0770 INPUT C
0780 PRINT "THICKNESS FOR LOW AND HIGH PHOTON COUNTS"
0790 INPUT X
0800 REM-----------------------------------------------------------------
0810 REM            ATTENUATION COEFFICIENT INITIALIZATION
0820 REM--- SEE TABLE A4-1 ---
0830 LET U1=.516
0840 LET U2=.169
0850 LET U3=.22*.93
0860 LET U4=.168*.93
0870 LET H9,L9=0
0880 LET T8=.000002
0890 REM-----------------------------------------------------------------
0900 REM               BACKGROUND COUNT SECTION
0910 PRINT "READY FOR BACKGROUND"
0920 INPUT G$
0930 IF G$<>"YES" THEN GOTO 0910
0940 REM---START LOW AND HIGH ENERGY COUNTERS---
0950 CALL 20,A,0,1,21
0960 REM--- TIMER LOOP---
0970 LET T=SYS(17)
0980 LET T1=SYS(17)-T
0990 IF T1<B*C THEN GOTO 0980
1000 REM---BRING IN HIGH(Q) AND LOW(P) ENERGY COUNTS---
*
```

```
1010 CALL 20,P,1,0,21
1020 CALL 20,Q,2,1,21
1030 LET Z=.1*B*C
1040 LET P=P/Z
1050 LET Q=Q/Z
1060 REM---P,Q CONVERTED TO COUNTS/SEC.---
1070 PRINT P,Q
1080 REM-----------------------------------------------------------------
1090 REM           INITIAL COUNTS FOR HIGH AND LOW ENERGY
1100 PRINT "ARE YOU READY TO DO THE INITIAL COUNTS"
1110 INPUT A$
1120 IF A$<>"YES" THEN GOTO 1100
1130 LET L9,H9=0
1140 REM--- START SCANNER, RECORD TIME ---
1150 CALL 20,A,0,1,21
1160 LET T=SYS(17)
1170 PRINT T
1180 FOR I=1 TO C
1190   LET T1=SYS(17)-T
1200   REM--- UNLOAD COUNTERS EVERY "B" SECONDS, OTHERWISE ---
1210   REM--- AN OVERFLOW WILL OCCUR ---
1220   IF T1<B*I THEN GOTO 1190
1230   CALL 20,A,0,2,21
1240   CALL 20,L,1,0,21
1250   CALL 20,H,2,1,21
1260   LET H9=H9+H
1270   LET L9=L9+L
1280   PRINT SYS(17)
1290 NEXT I
1300 LET Z=.1*B*C
1310 REM---CORRECT FOR BACKGROUND---
1320 LET H9=(H9/Z)-Q
1330 REM--- CORRECT FOR DEAD-TIME ---
1340 LET H9=H9/(1-T8*H9)
1350 LET L9=(L9/Z)-P
1360 LET L9=L9/(1-T8*L9)
1370 REM--- CALCULATE THE INITIAL COUNT RATE ---
1380 REM--- AND CORRECT FOR CROSS-OVER ---
1390 LET H2=H9*EXP(U4*X)
1400 LET L2=(L9-F*H9)*EXP(U3*X)
1410 LET L1=L2
1420 LET H1=H2
1430 LET M1=SYS(17)
1440 PRINT "LOW INTIAL COUNTS/SEC",L2
1450 PRINT "HIGH INITIAL COUNTS/SEC",H2
1460 PRINT L9,H9
1470 REM*************************************************************************
1480 REM              RELATIVE SOFT TISSUE (RST) MEASUREMENT
1490 REM                   RST FOR WATER=1.508(1.51)
1500 REM
*
```

```
1510 INPUT "SAMPLE TIME IN SECONDS TIMES 10 (DEFAULT=50)",A
1520 PRINT " "
1530 PRINT "READY TO DO THE SOFT TISSUE MEASUREMENT,(TYPE OK)"
1540 INPUT A$
1550 IF A$<>"OK" THEN GOTO 1530
1560 LET H9,L9=0
1570 REM--- START THE COUNTERS, RECORD TIME ---
1580 CALL 20,B,0,1,21
1590 LET T=SYS(17)
1600 PRINT T
1610 FOR I=1 TO C
1620   REM -- UNLOAD COUNTERS EVERY "A" SECONDS, OTHERWISE ---
1630   REM--- AN OVERFLOW WILL OCCUR.---
1640   LET T1=SYS(17)-T
1650   IF T1<A*I THEN GOTO 1640
1660   REM--- UNLOAD LOW AND HIGH ENERGY COUNTERS AND ADD TO L9, H9 ---
1670   CALL 20,B,0,2,21
1680   CALL 20,L,1,0,21
1690   CALL 20,H,2,1,21
1700   PRINT SYS(17)
1710   LET H9=H9+H
1720   LET L9=L9+L
1730 NEXT I
1740 PRINT L9,H9
1750 LET Z=.1*A*C
1760 REM--- CORRECT FOR CROSS-OVER AND BACKGROUND ---
1770 LET L9=((L9-F*H9)/Z)-P
1780 LET H9=(H9/Z)-Q
1790 LET H9=H9/(1-T8*H9)
1800 REM--- CALCULATE RST (R8) ---
1810 LET R6=LOG(H2/H9)
1820 LET R7=LOG(L2/L9)
1830 LET R8=R7/R6
1840 PRINT L9,H9
1850 PRINT R8
1860 PRINT "DO YOU WANT ANOTHER SOFT TISSUE MEASUREMENT ,Y "
1870 INPUT P$
1880 IF P$="Y" THEN GOTO 1510
1890 REM..*****************************************************************
1900 REM                  DATA COLLECTION
1910 REM  DATA IS WRITTEN TO A FILE SPECIFIED BY THE USER
1920 REM-------------------------------------------------------------------
1930 INPUT "DIAL SETTING (DEFAULT=60), SET CONSOLE NOW!",S3
1940 INPUT "SAMPLE LENGTH IN CM. (DEFAULT=.5)",S4
1950 LET A=200/2.54*S4
1960 REM--- S5 CONVERTS "A"(PULSES/SAMPLE FOR TRNS. DIRECTION) ---
1970 REM--- TO TIME FOR 1 SAMPLE (TYPICALLY 1.5 SEC.)---
1980 REM--- SEE APPENDIX 6 FOR DETAILS---
1990 LET S5=((S3-24.35)/1.35)*1.31
2000 LET S6=A/S5
*
```

```
2010 PRINT "SAMPLE TIME IN SECONDS=",S6
2020 INPUT "TYPE OK IF SAMPLE TIME OK",A$
2030 IF A$<>"OK" THEN GOTO 1930
2040 INPUT "FILENAME",F$
2050 REM--- 1 CYCLE CONSTITUTES TWO PASSES ---
2060 REM--- FOR DETAILS SEE FIGURE 4-18 ---
2070 PRINT "NO. OF CYCLES"
2080 INPUT N
2090 REM--- FORWARD= 1 TRANSVERSE PASS, ACROSS= 1 LONGITUDINAL PASS---
2100 REM--- FOR DETAILS SEE FIGURE 4-18---
2110 PRINT "DISTANCE (FORWARD,ACROSS) INCHES"
2120 PRINT "DEFAULT=9,.0625"
2130 INPUT X9,Y9
2140 LET X8=X9*200
2150 LET Y8=Y9*32
2160 REM---SET UP THE SCAN PATTERN---
2170 REM--- VALUES FOR ARRAY B1 ARE ---
2180 REM---DIRECTION FRONT=0
2190 REM             REAR =1
2200 REM             RIGHT=2
2210 REM             LEFT =3
2220 REM--- CORRECT FOR SOURCE DECAY---
2230 LET T=SYS(17)
2240 LET J1=EXP((M1-T)/(46.8*3600*10))
2250 LET L2=L1*J1
2260 LET H2=H1*J1
2270 REM---X8=TRANSVERSE DISTANCE, Y8=LONGITUDINAL DISTANCE---
2280 LET B1(1)=0
2290 LET B1(2)=2
2300 LET B1(3)=1
2310 LET B1(4)=2
2320 LET B1(5)=X8
2330 LET B1(6)=Y8
2340 LET B1(7)=X8
2350 LET B1(8)=Y8
2360 LET B1(9)=3
2370 LET O1,T1,T3=0
2380 LET G3=U1-R8*U2
2390 CLOSE
2400 OPEN FILE (1,1),F$
2410 REM--- SAVE IMPORTANT PARAMETERS ---
2420 WRITE FILE (1),G3,R8,L2,H2,F,P,Q,T8
2430 FOR K=1 TO N
2440   FOR I=1 TO 4
2450     LET T9,F1=0
2460     LET M=1
2470     LET G=256
2480     REM--- F1=FLAG, SET IF SCANNER DIRECTION IS FRONT OR RIGHT---
2490     IF B1(I)=0 THEN LET F1=1
2500     IF B1(I)=2 THEN LET F1=1
*
```

```
2510 REM--- IF MOVING RIGHT REQUIRED, MOVE WITH NO DATA COLLECTION---
2520 IF B1(I)<>2 THEN GOTO 2600
2530 REM--- WRITE END OF DATA IN THIS DIRECTION ---
2540 WRITE FILE (1),-1,-1,-1
2550 REM--- MOVE THE SCANNER RIGHT ---
2560 GOSUB 4170
2570 REM--- NEXT DIRECTION ---
2580 GOTO 2980
2590 REM--- START SCANNER AND GET INITIAL POSITION COUNT ---
2600 CALL 21,B1(I),1,0,22
2610 CALL 23,A1(1),3,0,21
2620 REM---CHECK THAT DIRECTION SIGNAL A1(9) HAS---
2630 REM---CHANGED TO AGREE WITH F1---
2640 IF F1=A1(9) THEN GOTO 2610
2650 REM--- CONVERT BINARY TO DECIMAL ---
2660 GOSUB 4050
2670 LET D1=C1
2680 REM--- TURN PHOTON COUNTERS ON ---
2690 CALL 20,B,0,1,21
2700 LET T=SYS(17)
2710 REM---DELAY TO ALLOW SCANNER TO REACH CONSTANT SPEED---
2720 FOR J=1 TO 500
2730 NEXT J
2740 PRINT "GOSUB",A1(9)
2750 REM--- COLLECT DATA OVER ONE SAMPLE SPACE :::
2760 GOSUB 4420
2770 REM---STOP PHOTON COUNTERS AND GET COUNTS---
2780 CALL 20,B,0,2,21
2790 CALL 20,L,1,2,21
2800 CALL 20,H,2,1,21
2810 REM---GET SAMPLE TIME---
2820 LET T1=SYS(17)-T
2830 REM---RESET TIMER---
2840 LET T=SYS(17)
2850 PRINT T1
2860 LET T1=T1/10
2870 REM--- SAVE PHOTON COUNTS AND SAMPLE TIME ---
2880 WRITE FILE (1),L,H,T1
2890 PRINT T9,D1,D1,N1,K
2900 LET N=N+1
2910 IF T9<B1(I+4) THEN GOTO 2760
2920 REM--- FINISHED IN THIS DIRECTION, STOP SCANNER MOTION ---
2930 LET B=5
2940 CALL 21,B,1,0,22
2950 REM---DELAY SO SCANNER RELAYS HAVE TIME TO STABLIZE---
2960 FOR J=1 TO 1000
2970 NEXT J
2980 NEXT I
2990 NEXT K
3000 CLOSE FILE (1)
*
```

```
3010 REM--- MOVE SCANNER BACK TO START POSITION ---
3020 LET F1,T9=0
3030 LET A=2*Y8*N
3040 LET M=1
3050 LET G=16
3060 LET I=9
3070 CALL 21,3,1,0,22
3080 CALL 23,A1(1),3,0,21
3090 IF F1=A1(11) THEN GOTO 3080
3100 GOSUB 4100
3110 LET D1=C1
3120 GOSUB 4420
3130 REM--- STOP SCANNER ---
3140 CALL 21,5,1,0,22
3150 REM*************************************************************************
3160 REM            DATA ANALYSIS SECTION
3170 REM
3180 REM--- DETERMINE SIZE OF FILE ---
3190 OPEN FILE (1,3),F$
3200 READ FILE (1),G3,R8,L2,H2,F,P,Q,T8
3210 PRINT P,Q
3220 LET S9=0
3230 READ FILE (1),L9,H9,T1
3240 IF L9=-1 THEN GOTO 3270
3250 LET S9=S9+1
3260 GOTO 3230
3270 CLOSE FILE (1)
3280 REM*************************************************************************
3290 LET F5,D5,C1=0
3300 REM--- CLEAR THE SUMMING ARRAY ---
3310 FOR I=1 TO 100
3320   LET D(I)=0
3330 NEXT I
3340 OPEN FILE (1,3),F$
3350 READ FILE (1),G3,R8,L2,H2,F,P,Q,T8
3360 REM---READ TILL END OF DATA---
3370 IF EOF(1) THEN GOTO 3650
3380 READ FILE (1),L9,H9,T1
3390 LET C1=C1+1
3400 REM--- CHECK FOR END OF DATA IN PRESENT DIRECTION ---
3410 IF L9<>-1 THEN GOTO 3510
3420 REM--- EVEN NUMBERED PASS FLAG=1, ODD NUMBERED PASS FLAG=0 ---
3430 LET D5=D5+1
3440 LET X5=D5/2-INT(D5/2)
3450 IF X5>0 THEN LET F5=1
3460 IF X5=0 THEN LET F5=0
3470 LET C1=0
3480 GOTO 3370
3490 REM--- GET COUNT RATE AND CORRECT FOR BACKGROUND ---
3500 REM--- CROSS-OVER AND SOURCE DECAY ---
*
```

```
3510 LET L8=L9/T1
3520 LET H8=H9/T1
3530 LET L8=L8-F*H8
3540 LET L9=(L8-P)/(1-T8*L8)
3550 LET H9=(H8-Q)/(1-T8*H8)
3560 REM-- CALCULATE THICKNESS ---
3570 LET G1=LOG(L2/L9)
3580 LET G2=LOG(H2/H9)*R8
3590 LET G4=((G1-G2)/G3/2.698)
3600 REM--- SUM OF THE XTH POSITION IN THE Y DIRECTION---
3610 REM--- SEE FIGURE 4-18---
3620 IF F5=0 THEN LET D(C1)=D(C1)+G4
3630 IF F5=1 THEN LET D(S9-C1+1)=D(S9-C1+1)+G4
3640 GOTO 3370
3650 CLOSE FILE (1)
3660 REM-----------------------------------------------------------------
3670 REM              GRAPHICS DISPLAY SECTION
3680 INPUT "TRUE PLATE THICKNESS",P1
3690 INPUT "SCREEN MAXIMUM IN CM.",M2
3700 REM--- SET PARAMETERS FOR **VDT** GRAPHICS DISPLAY---
3710 LET B9=250/M2
3720 LET B0=25
3730 LET B8=1.05*P1*B9+B0
3740 LET B7=P1*B9+B0
3750 LET B6=.95*P1*B9+B0
3760 CALL 17
3770 REM---DRAW THE GRAPHICS---
3780 CALL 14,0,250,1
3790 CALL 14,0,0,1
3800 CALL 14,250,0,1
3810 CALL 14,250,250,1
3820 CALL 14,0,250,1
3830 CALL 14,0,B8,1
3840 CALL 14,250,B8,1
3850 CALL 14,250,B7,1
3860 CALL 14,0,B7,1
3870 CALL 14,0,B6,1
3880 CALL 14,250,B6,1
3890 CALL 14,250,B0,1
3900 CALL 14,0,B0,1
3910 CALL 16
3920 REM---PLOT THE DATA---
3930 FOR I=1 TO S9
3940   LET D(I)=D(I)/(D5-1)*B9+B0
3950   LET X3=(I-1)/(S9-1)*250
3960   CALL 14,X3,D(I),1
3970 NEXT I
3980 INPUT "ANOTHER SCAN(OK)",A$
3990 IF A$="OK" THEN GOTO 1930
4000 STOP
*
```

```
4010 REM*****************************************************************
4020 REM              SUBROUTINE SECTION
4030 REM-----------------------------------------------------------------
4040 REM              SUBROUTINE BINARY TO DECIMAL (8 BITS)
4050 LET Z=8*A1(4)+16*A1(3)+32*A1(2)+64*A1(1)
4060 LET C1=A1(8)+2*(A1(7)+2*A1(6)+4*A1(5)+Z)
4070 RETURN
4080 REM-----------------------------------------------------------------
4090 REM              SUBROUTINE BINARY TO DECIMAL (4 BITS)
4100 LET C1=A1(16)+2*(A1(15)+2*A1(14)+4*A1(13))
4110 RETURN
4120 REM-------------------------------------------------------------
4130 REM              SUBROUTINE SCAN ADVANCE
4140 REM   SCAN ADVANCE MOVES THE SCANNER RIGHT FOR THE NEXT
4150 REM   DATA ACQUISITION PASS
4160 REM
4170 CALL 21,B1(I),1,0,22
4180 CALL 23,A1(1),3,0,21
4190 IF F1=A1(11) THEN GOTO 4180
4200 GOSUB 4100
4210 LET O1=C1
4220 LET G=16
4230 CALL 23,A1(1),3,0,21
4240 GOSUB 4100
4250 LET N1=C1
4260 IF N1=O1 THEN GOTO 4300
4270 IF N1>O1 THEN LET D1=N1-O1
4280 IF N1<O1 THEN LET D1=G-O1+N1
4290 LET T9=D1+T9
4300 LET O1=N1
4310 PRINT T9,D1,1,N1
4320 IF T9<Y8 THEN GOTO 4230
4330 LET B=5
4340 CALL 21,B,1,0,22
4350 FOR J=1 TO 1000
4360 NEXT J
4370 RETURN
4380 REM-----------------------------------------------------------
4390 REM              SUBROUTINE 1 SAMPLE
4400 REM  THIS SUBROUTINE DETERMINES WHEN THE SCANNER HAS
4410 REM  MOVED ONE SAMPLE LENGTH
4420 IF F1=0 THEN GOTO 4560
4430 CALL 23,A1(1),3,0,21
4440 ON (B1(I)+1) THEN GOSUB 4050, 4050
4450 IF B1(I)=3 THEN GOSUB 4100
4460 LET N1=C1
4470 IF N1=O1 THEN GOTO 4540
4480 LET D1=N1-O1
4490 IF N1<O1 THEN LET D1=G-O1+N1
4500 LET T9=D1+T9
*
```

```
4510 LET O1=N1
4520 FOR J=1 TO 20
4530 NEXT J
4540 IF T9<A*M THEN GOTO 4430
4550 GOTO 4680
4560 CALL 23,A1(1),3,0,21
4570 ON (B1(I)+1) THEN GOSUB 4050, 4050
4580 IF B1(I)=3 THEN GOSUB 4100
4590 LET N1=C1
4600 IF N1=O1 THEN GOTO 4670
4610 LET D1=O1-N1
4620 IF N1>O1 THEN LET D1=G-N1+O1
4630 LET T9=D1+T9
4640 LET O1=N1
4650 FOR J=1 TO 20
4660 NEXT J
4670 IF T9<A*M THEN GOTO 4560
4680 RETURN
4690 FOR I=1 TO 30
4700   PRINT I,D(I)
4710 NEXT I
4720 RETURN
4730 REM**********END**********
*
```

```
0010 REM*****************PROGRAM ANALYSIS*******************************
0020 REM AUTHOR: ROBERT R. ROWNTREE
0030 REM DATE: MAY 28,1985
0040 REM FILE NAME:ANALYSIS.SR (UNDOCUMENTED)
0045 REM           ANALYSIS.DC (DOCUMENTED)
0050 REM SYSTEM: NOVA BASIC/RDOS AND TEKTRONIX PLOTTER(4662)
0060 REM*****************************************************************
0070 REM
0080 REM  PROGRAM: TO PLOT THE THICKNESS (BMC) PROFILE USING
0090 REM           DATA ACQUIRED BY PROGRAM SCANBONE.
0100 REM..
0110 REM..*****************************************************************
0120 REM VARIABLES AND ARRAYS:
0130 REM           ALL DATA VARIABLES ARE THE SAME AS IN SCANBONE EXCEPT
0140 REM           C1-D ARRAY POINTER FOR SORTING DATA INTO BINS
0150 REM           E2-COUNTER FOR END OF FILE DETECTION.
0160 REM
0170 REM*****************************************************************
0180 REM            INITIALIZE THE VARIABLES AND ARRAYS
0190 DIM A$[10],A1[16],B1[10]
0200 DIM D$[30],G$[30]
0210 DIM D[300]
0220 LET K5=0
0230 LET C1=0
0240 LET E1=0
0250 INPUT "FILEMANE",F$
0260 REM*****************************************************************
0270 REM            GET THE NUMBER OF SAMPLES IN ONE PASS
0280 OPEN FILE[1,3],F$
0290 INPUT FILE[1],G3,R8,L2,H2,F,P,Q,T8
0300 PRINT G3,R8,L2,H2
0310 PRINT F,P,Q,T8
0320 LET S9=0
0330 INPUT FILE[1],L9,H9,T1
0340 IF L9<0 THEN GOTO 0370
0350 LET S9=S9+1
0360 GOTO 0330
0370 CLOSE FILE[1]
0380 REM*****************************************************************
0390 FOR I=1 TO 100
0400   LET D[I]=0
0410 NEXT I
0420 OPEN FILE[1,3],F$
0430 INPUT FILE[1],G3,R8,L2,H2,F,P,Q,T8
0440 REM---END OF FILE HAS 2 (-1)---
0450 IF E1=2 THEN GOTO 0740
0460 REM---GET LOW AND HIGH COUNTS,SAMPLE TIME---
0470 INPUT FILE[1],L9,H9,T1
0480 LET C1=C1+1
0490 REM---IF END OF PASS L9=H9=-1 IN FILE---
0500 IF L9>0 THEN GOTO 0600

*
```

```
0510 LET E1=E1+1
0520 LET D5=D5+1
0525 REM---IF THE NUMBER OF PASSES IS EVEN F5=0---
0530 REM---                              ODD  F5=1---
0540 LET X5=D5/2-INT(D5/2)
0550 IF X5>0 THEN LET F5=1
0560 IF X5=0 THEN LET F5=0
0570 LET C1=0
0580 GOTO 0450
0590 REM---CALCULATE THE THICKNESS (BMC) AND SUM IN THE Y-DIRECTION---
0600 LET L8=L9/T1
0610 LET E1=0
0620 LET H8=H9/T1
0630 LET L8=L8-F*H8
0640 LET L9=(L8-P)/(1-T8*L8)
0650 LET H9=(H8-Q)/(1-T8*H8)
0660 LET G1=LOG(L2/L9)
0670 LET G2=LOG(H2/H9)*R8
0680 LET G4=((G1-G2)/G3/2.698)
0690 REM---UNRAVEL---
0700 REM---EVERY SECOND PASS IS STORED BACKWARDS---
0710 IF F5=0 THEN LET D[C1]=D[C1]+G4
0720 IF F5=1 THEN LET D[S9-C1+1]=D[S9-C1+1]+G4
0730 GOTO 0450
0740 REM
0750 CLOSE FILE[1]
0760 IF K5=1 THEN CALL 9,2
0770 IF K5=1 THEN GOTO 1370
0780 REM---INITIALIZE THE PLOT PARAMETERS---
0790 INPUT "TRUE PLATE THICKNESS IN CM.",P1
0800 INPUT "TYPE BOARDER OFFSET(DEFAULT=100,100)=",X1,Y1
0810 INPUT "SIZE OF AXIS TICK(DEFAULT=20)",S1
0820 INPUT "FULL SCALE(DEFAULT=3200,2400)=",F7,F8
0830 LET F8=F8+.1
0840 REM---INITIALIZE THE PLOTTER---
0850 CALL 9,2
0860 CALL 12,40,80,0
0870 CALL 10,X1,Y1,0
0880 REM--- CONVERT FULL SCALE TO SCAN DISTANCE IN CM.---
0890 LET S5=(3400+X1)/F7
0900 REM---DRAW THE X-AXIS,TICKS AND NUMBERS---
0910 FOR I=X1 TO 3650+X1 STEP S5
0920   LET K=(I-X1)/S5
0930   LET A$=STR$(INT(K+.5))
0940   CALL 10,I,Y1,1
0950   CALL 10,I,Y1+S1,1
0960   CALL 10,I-50,Y1-100,0
0970   CALL 11,A$
0980   CALL 10,I,Y1,0
0990 NEXT I
1000 CALL 10,X1,Y1,0

*
```

```
1010 REM---CONVERT FULL SCALE TO THICKNESS IN CM.---
1020 LET S6=(2400+Y1)/(F8*10+1)
1030 REM---DRAW Y-AXIS , TICKS AND NUMBERS---
1040 FOR J=Y1 TO 2400+Y1 STEP S6
1050   LET K=(J-Y1)/(S6*10)-.1
1060   LET A$=STR$(K)
1070   CALL 10,X1,J,1
1080   CALL 10,X1+S1,J,1
1090   CALL 10,X1-125,J,0
1100   CALL 11,A$
1110   CALL 10,X1,J,0
1120 NEXT J
1130 CALL 10,X1+F7*S5,J,1
1140 CALL 10,X1+F7*S5,Y1,1
1150 REM---LABEL THE AXIS---
1160 LET D$="TRANSVERSE DISTANCE (CM.)"
1170 LET G$="ALUMINUM THICKNESS (CM.)"
1180 CALL 10,1200+X1,0,0
1190 CALL 11,D$
1200 CALL 12,40,80,90
1210 CALL 10,100,900+Y1,0
1220 CALL 11,G$
1230 REM---DRAW THE 0,-5% AND +5% VALUE OF THE---
1240 REM---TRUE ALUMINUM THICKNESS---
1250 LET C1=X1+F7*S5
1260 LET B7=S6*(P1*10+1)+Y1
1270 LET B8=1.05*B7
1280 LET B6=.95*B7
1290 CALL 10,X1,B6,0
1300 CALL 10,C1,B6,1
1310 CALL 10,C1,B7,0
1320 CALL 10,X1,B7,1
1330 CALL 10,X1,B8,0
1340 CALL 10,C1,B8,1
1350 CALL 10,C1,S6+Y1,0
1360 CALL 10,X1,S6+Y1,1
1370 LET D5=D5-1
1380 REM---PLOT THE DATA---
1390 FOR I=1 TO S9
1400   LET D[I]=S6*((D[I]*10)/D5+1)+Y1
1410   LET X3=(I-1)/(S9-1)*F7*S5
1420   CALL 10,X3+X1,D[I],1
1430 NEXT I
1440 CALL 9,0
1450 INPUT "ANOTHER FILE ON THIS PLOT",A$
1460 IF A$<>"OK" THEN GOTO 1490
1470 LET K5=1
1480 GOTO 0250
1490 STOP
1500 REM*****************END OF PROGRAM*************************************
```

*

```
0010 REM**********   PROGRAM GROUND-CHECK  ****************************
0020 REM AUTHOR: ROBERT R. ROWNTREE
0030 REM DATE:MAY 22,1985
0040 REM FILE NAME:GRDCHECK.SR
0050 REM SYSTEM: NOVA BASIC/RDOS
0052 REM-------------------------------------------------------------------
0060 REM PROGRAM: MOTIONAL CHECK OF STRAY VOLTAGE EFFECTING
0070 REM          THE LOW ENERGY CHANNEL
0080 REM          ONCE A GOOD GROUND HAS BEEN FOUND THE PROGRAM
0090 REM          ACKNOWLEDGES WITH "GOOD GROUND"
0100 REM          THE CONDITION THAT MUST BE MET IS THAT
0110 REM          THE DIFFERENCE OF THE TOTAL LOW ENERGY COUNTS
0120 REM          IN THE FORWARD AND REAR DIRECTION MUST BE LESS
0130 REM          THEN 3%.
0140 REM..*****************************************************************
0150 DIM A$(10),A1(16),B1(10)
0160 DIM D(300)
0170 REM-------------------------------------------------------------------
0180 REM                  INPUT DATA SECTION
0190 INPUT "DIAL SETTING (NORMALLY 60)",S3
0200 INPUT "SAMPLE LENGTH IN CM.(NORMALLY 1)",S4
0210 LET A=200/2.54*S4
0220 LET S5=((S3-24.35)/1.35)*1.31
0230 LET S6=A/S5
0240 PRINT "SAMPLE TIME IN SECONDS=",S6
0250 INPUT "TYPE OK IF SAMPLE TIME OK",A$
0260 IF A$<>"OK" THEN GOTO 0190
0270 INPUT "FILENAME",F$
0280 LET N=1
0290 INPUT "DISTANCE(TRANSVERSE,LONG.),NORMALLY 11,.5,INCHES",X9,Y9
0300 REM-------------------------------------------------------------------
0310 REM                  INITIAL VARIABLES
0320 LET X8=X9*200
0330 LET Y8=Y9*32
0340 LET B1(1)=1
0350 LET B1(2)=2
0360 LET B1(3)=0
0370 LET B1(4)=2
0380 LET B1(5)=X8
0390 LET B1(6)=Y8
0400 LET B1(7)=X8
0410 LET B1(8)=Y8
0420 LET O1,T1,T3=0
0430 CLOSE
0440 REM-------------------------------------------------------------------
0450 REM                  DATA ACQUISITION SECTION
0460 OPEN FILE (1,1),F$
0470 FOR K=1 TO N
0480   FOR I=1 TO 4
0490     LET T9,F1=0
0500     LET M=1
*
```

```
0510 LET G=256
0520 IF B1(I)=0 THEN LET F1=1
0530 IF B1(I)=2 THEN LET F1=1
0540 IF B1(I)<>2 THEN GOTO 0580
0550 GOSUB 1550
0560 GOTO 1040
0570 REM-----START SCANNER AND GET INITIAL TRANSVERSE COUNT------
0580 CALL 21,B1(I),1,0,22
0590 CALL 23,A1(1),3,0,21
0600 IF F1=A1(9) THEN GOTO 0590
0610 GOSUB 1480
0620 LET O1=C1
0630 REM-----CLEAR AND START HIGH AND LOW ENERGY COUNTERS--------
0640 CALL 20,B,0,1,21
0650 LET T=SYS(17)
0660 REM-----F1=0 (COUNT DOWN) F1=1 (COUNT UP)-------------------
0670 IF F1=0 THEN GOTO 0780
0680 CALL 23,A1(1),3,0,21
0690 GOSUB 1480
0700 LET N1=C1
0710 IF N1=O1 THEN GOTO 0760
0720 LET D1=N1-O1
0730 IF N1<O1 THEN LET D1=G-O1+N1
0740 LET T9=D1+T9
0750 LET O1=N1
0760 IF T9<A*M THEN GOTO 0680
0770 GOTO 0870
0780 CALL 23,A1(1),3,0,21
0790 GOSUB 1480
0800 LET N1=C1
0810 IF N1=O1 THEN GOTO 0860
0820 LET D1=O1-N1
0830 IF N1>O1 THEN LET D1=G-N1+O1
0840 LET T9=D1+T9
0850 LET O1=N1
0860 IF T9<A*M THEN GOTO 0780
0870 CALL 20,B,0,2,21
0880 CALL 20,L,1,2,21
0890 CALL 20,H,2,1,21
0900 LET T1=SYS(17)-T
0910 LET T=SYS(17)
0920 PRINT T1
0930 LET T1=T1/10
0940 WRITE FILE (1),L,H,T1
0950 PRINT T9,D1,O1,N1
0960 LET M=M+1
0970 IF T9<B1(I+4) THEN GOTO 0670
0980 REM ------DIRECTION CHANGE - STOP SCANNER-----
0990 LET B=5
1000 CALL 21,B,1,0,22
*
```

```
1010 REM -----WASTE SOME TIME-------
1020 FOR J=1 TO 1000
1030 NEXT J
1040 NEXT I
1050 NEXT K
1060 CLOSE FILE (1)
1070 REM*************************************************************************
1080 REM                  DATA ANALYSIS
1090 REM---DETERMINE THE NO. OF SAMPLES IN ONE DIRECTION-------
1100 OPEN FILE (1,3),F$
1110 LET S9=0
1120 READ FILE (1),L9,H9,T1
1130 IF L9=-1 THEN GOTO 1160
1140 LET S9=S9+1
1150 GOTO 1120
1160 CLOSE FILE (1)
1170 REM-------------------------------------------------------------------
1180 REM                   INITIALIZE THE VARIABLES
1190 LET C1=0
1200 FOR I=1 TO 100
1210   LET D(I)=0
1220 NEXT I
1230 LET S1,S2=0
1240 REM-------------------------------------------------------------------
1250 OPEN FILE (1,3),F$
1260 IF EOF(1) THEN GOTO 1370
1270 READ FILE (1),L9,H9,T1
1280 LET S2=S2+L9/T1
1290 REM----- IF -1 THEN END OF ONE DIRECTION IN DATA FILE-----
1300 IF L9<>-1 THEN GOTO 1260
1310 PRINT S2
1320 LET C1=C1+1
1330 IF C1=2 THEN LET S3=S2
1340 IF C1=1 THEN LET S1=S2
1350 LET S2=0
1360 GOTO 1260
1370 CLOSE FILE (1)
1380 LET S4=ABS((S3-S1)/S1)
1390 IF S4<.03 THEN GOTO 1420
1400 PRINT "GROUND NOT GOOD ENOUGH,TRY AGAIN!"
1410 GOTO 0190
1420 PRINT "GROUND IS OK"
1430 STOP
1440 REM*****************THE END*****************************
1450 REM                SUBROUTINE SECTION
1460 REM-------------------------------------------------------------------
1470 REM             SUBROUTINE CONVERT BINARY TO DECIMAL
1480 LET Z=8*A1(4)+16*A1(3)+32*A1(2)+64*A1(1)
1490 LET C1=A1(8)+2*(A1(7)+2*A1(6)+4*A1(5)+Z)
1500 RETURN
*
```

```
1510 LET C1=A1(16)+2*(A1(15)+2*A1(14)+4*A1(13))
1520 RETURN
1530 REM-------------------------------------------------------------------
1540 REM            SUBROUTINE MOVE LONGITUDINAL
1550 CALL 21,B1(I),1,0,22
1560 CALL 23,A1(1),3,0,21
1570 GOSUB 1510
1580 LET O1=C1
1590 LET G=16
1600 WRITE FILE (1),-1,-1,-1
1610 CALL 23,A1(1),3,0,21
1620 GOSUB 1510
1630 LET N1=C1
1640 IF N1=O1 THEN GOTO 1680
1650 IF N1>O1 THEN LET D1=N1-O1
1660 IF N1<O1 THEN LET D1=G-O1+N1
1670 LET T9=D1+T9
1680 PRINT T9,D1,O1,N1
1690 LET O1=N1
1700 FOR S=1 TO 500
1710 NEXT S
1720 IF T9<Y8 THEN GOTO 1610
1730 LET B=5
1740 CALL 21,B,1,0,22
1750 FOR J=1 TO 1000
1760 NEXT J
1770 RETURN
*
```

```
0010 REM**********PROGRAM SIMDPA**************************************
0020 REM
0030 REM AUTHOR: ROBERT R. ROWNTREE
0040 REM DATE: AUGUST 8,1985
0050 REM FILE NAME:MANYTH.SR(DOCUMENTED),MULTIPLE.SR(UNDOCUMENTED)
0060 REM SYSTEM: NOVA BASIC/RDOS
0070 REM
0080 REM*****************************************************************
0090 REM
0100 REM PROGRAM:  A MONTE CARLO SIMULATION OF DUAL PHOTON ABSORPTIOMETRY
0110 REM           TO DETERMINE THE OPTIMAL DETECTOR GEOMETRY.
0120 REM
0130 REM*****************************************************************
0140 REM
0150 REM VARIABLES:
0160 REM           A1-COS(THETA),COMPTON SCATTER ANGLE W.R.T. THE Z-AXIS
0170 REM           A2-SIN(THETA)
0180 REM           A3-SIN(PHI),
0190 REM           A4-COS(PHI)
0200 REM           C1-MINIMUM INITIAL PHOTON COUNTS AT THE LOW ENERGY
0210 REM           C5-NUMBER OF THICKNESS DETERMINATIONS AT THE SAME
0220 REM              SIMULATION PARAMETERS.
0230 REM           C6-COPY OF C5
0240 REM           D1-DEPTH OF SOURCE IN COLLIMATOR IN CM.
0250 REM           D2-DETECTOR ENTRANCE HEIGHT IN CM.
0260 REM           D3-DEPTH OF DETECTOR COLLIMATOR IN CM.
0270 REM           D4-DETECTOR ENTRANCE WIDTH IN CM.
0280 REM           E0-OLD PHOTON ENERGY DIVIDED BY THE REST MASS(511 KEV)
0290 REM           E1-NEW PHOTON ENERGY DIVIDED BY THE REST MASS(511 KEV)
0300 REM           E2-COPY OF THE PHOTON ENERGY USED AT SOURCE(.I.E 42.5
0310 REM              OR 103 KEV DIVIDED BY THE REST MASS 511KEV
0320 REM           F -VDT SCREEN VERTICAL OFFSET MAX.=256,DEFAULT=128
0330 REM           H1-THICKNESS OF ALUMINUM IN CM.
0340 REM           H2-THICKNESS OF WATER IN CM.
0350 REM           K1-PHOTON COUNTER FOR 42.5 LOOP
0360 REM           P -COPY OF S
0370 REM           P1-COPY OF X
0380 REM           S -SOURCE EXIT COLLIMATOR WIDTH IN CM.
0390 REM           S1-PHOTON COLLISION COUNTER - RESET EACH HISTORY
0400 REM           S5-VARIABLE FOR THE CARLESON EQUATION
0410 REM           S6-COUNT OF NUMBER OF PHOTONS WITH MORE THAN 3 SCATTERS
0420 REM           X -DISTANCE FROM SOURCE COLLIMATOR EXIT TO DETECTOR
0430 REM              COLLIMATOR ENTRANCE IN CM.
0440 REM           X0,Y0,Z0-IS THE INITIAL STARTING POINT
0450 REM           V1-REPRESENTS THE RANDOM NUMBER
0460 REM
0470 REM-----------------------------------------------------------------
*
```

```
0480 REM
0490 REM ARRAYS:   I0-CONTAINS THE ATTENUATED AND UNATTENUATED COUNTS FOR
0500 REM             SEVERAL COLLIMATOR DIMENSIONS.
0510 REM           I1-UNATTENUATED PHOTON COUNTS AT 103 KEV
0520 REM           I2-COPY OF I1
0530 REM           I4-UNATTENUATED PHOTON COUNTS AT 42.5 KEV
0540 REM           I5-COPY OF I4
0550 REM           I7-ATTENUATED PHOTON COUNTS AT 42.5 KEV
0560 REM           I8-ATTENUATED PHOTON COUNTS AT 103 KEV
0570 REM           K9-OLD COORDINATES OF THE PHOTON
0580 REM           S9-NEW COORDINATES OF THE PHOTON
0590 REM           T9-THE INVERSE TRANSFORMATION MATRIX
0600 REM           U9-PRODUCT OF THE PATH LENGTH ARRAY  X9  AND THE
0610 REM             INVERSE TRANSFORMATION MATRIX T9
0620 REM           X9-POSITION MAGNITUDE ARRAY
0630 REM
0640 REM*************************************************************
0650 REM
0660 REM DESCRIPTION:
0670 REM               THE FUNDAMENTAL EQUATION ON WHICH DPA
0680 REM               IS BASED IS:
0690 REM
0700 REM                         LN(L4/L7)-R5*LN(L1/L8)
0710 REM               THICKNESS=-----------------------
0720 REM                              U1-R5*U2
0730 REM
0740 REM               THE COORDINATE SYSTEM IS SHOWN IN FIGURE 5-1.
0750 REM               FOR MATRIX K9 AND S9 THE Z-AXIS IS HORIZONTAL
0760 REM               (LEFT TO RIGHT), THE X-AXIS IS VERTICAL (BOTTOM
0770 REM               TO TOP) AND THE Y-AXIS IS POINTING OUT OF THE
0780 REM               VDT SCREEN.
0790 REM
0800 REM               THE COMPTON SCATTERING EQUATION IS GIVEN BY:
0810 REM
0820 REM                               E0-E1
0830 REM               COS(THETA)= 1 - --------
0840 REM                               E0*E1
0850 REM
0860 REM               THE PROBABILITY DENSITY FUNCTION THAT APPROXIMATES
0870 REM               THE COMPTON EQUATION IS CALLED THE CARLESON
0880 REM               EQUATION AND IS GIVEN BY:
0890 REM
0900 REM                           E0
0910 REM               E1=----------------------
0920 REM                  1+S5*V1+(2*E0-S5)*V1^3
0930 REM
0940 REM               WHERE
0950 REM
0960 REM                     E0
0970 REM               S5=-----------
0980 REM                   1+.5625*E0
0990 REM
1000 REM*************************************************************
*
```

```
1010 REM---------------MAIN PROGRAM-----------------------------------
1020 DIM T9(3,3),X9(3),S9(3),F9(3,3),U9(3),K9(3),M9(3)
1030 DIM I0(10),I7(10),I8(10)
1040 REM---------------------------------------------------------------
1050 REM
1060 REM---ATTENUATION COEFFICIENTS AS A FUNCTION OF ENERGY---
1070 REM---FUNCTIONS A,C,E,G,J ARE VALID IN THE ENERGY RANGE 20-60 KEV---
1080 REM---FUNCTIONS B,D,F,H,I ARE VALID IN THE ENERGY RANGE 60-150 KEV-
1090 REM---ALL FUNCTIONS ARE CREATED FROM HUBBLE(34) FOR 153-SM---
1100 DEF FNA(X)=(.341+47.2*(.8723)^(X*511))*2.7/10
1110 DEF FNB(X)=(.119+.7762*(.9737)^(X*511))*2.7/10
1120 DEF FNC(X)=(.214+6.66*(.883)^(X*511))/10
1130 DEF FND(X)=(.127+.181*(.986)^(X*511))/10
1140 DEF FNE(X)=(.1951+6.61*(.8835)^(511*X))*.001205/10
1150 DEF FNF(X)=(.1233+.1929*(.9818)^(X*511))*.001205/10
1160 DEF FNG(X)=(.141+46.8*(.87)^(X*511))*2.7/10
1170 DEF FNH(X)=(.00598+2.064*(.9493)^(X*511))*2.7/10
1180 DEF FNI(X)=(8.738E-04+.3217*(.9493)^(X*511))/10
1190 DEF FNJ(X)=(.02059+7.775*(.8704)^(511*X))/10
1200 LET U1=FNA(42.5/511)
1210 LET U2=FNC(42.5/511)
1220 LET U3=.00003
1230 LET U4=FNB(103/511)
1240 LET U7=FND(103/511)
1250 LET R5=U2/U7
1260 LET B1=U1-R5*U4
1270 REM
1280 REM---------------------------------------------------------------
1290 CLOSE
1300 REM---INPUT THE VARIABLES---
1310 INPUT "THICKNESS OF ALUMINUM IN CM.",H1
1320 LET H1=H1*10
1330 LET H2=H1+10
1340 LET F=128
1350 CALL 17
1360 PRINT "<26>"
1370 INPUT "NO. OF RUNS AT EACH DIMENSION",C5
1380 LET C6=C5
1390 PRINT "ENTER SOURCE EXIT WIDTH IN CM."
1400 INPUT S
1410 LET S=S*10
1420 LET P=S
1430 PRINT "ENTER DETECTOR ENTRANCE HEIGHT IN CM. "
1440 INPUT D2
1450 LET D2=D2*10
1460 LET N=D2/S
1470 INPUT "ENTER DETECTOR ENTRANCE WIDTH IN CM.",D4
1480 LET D4=D4*10
1490 PRINT "<26>"
1500 PRINT "TOTAL COUNTS REQUIRED"
1510 INPUT C1
*
```

```
1520 PRINT "SOURCE TO COLLIMATOR DISTANCE IN CM."
1530 INPUT X
1540 LET X=X*10
1550 LET P1=X
1560 PRINT "DEPTH OF SOURCE IN COLLIMATOR IN CM."
1570 INPUT D1
1580 LET D1=D1*10
1590 PRINT "DEPTH OF DETECTOR COLLIMATOR"
1600 INPUT D3
1610 LET D3=D3*10
1620 INPUT "FILENAME",F$
1630 REM--WRITE IMPORTANT DATA TO FILE---
1640 OPEN FILE (1,1),F$
1650 WRITE FILE (1),H1,C5,P,D2,C1,P1,D1,D3
1660 LET E2=42.5/511
1670 CALL 17
1680 PRINT "<26>"
1690 FOR J=1 TO 2
1700   REM.. DRAW THE EXPERIMENTAL APPARATUS
1710   GOSUB 4460
1720   REM
1730   REM*************************************************************************
1740   REM                    DO INITIAL COUNTS
1750   REM
1760   REM INITIALIZE VARIABLES
1770   LET U0=U3
1780   LET S=P
1790   LET T1=0
1800   FOR L=1 TO 6
1810     LET I0(L)=0
1820   NEXT L
1830   REM..INITIALIZE STARTING POINT
1840   GOSUB 5370
1850   MAT K9=S9
1860   REM-------------------------------------------------------------------
1870   REM      GET  ANGLE AND PATH
1880   REM
1890   REM---GET A PATH LENGTH---
1900   GOSUB 4790
1910   LET X9(1)=0
1920   LET X9(2)=0
1930   LET X9(3)=R
1940   CALL 5,V1,1,.5
1950   IF S1<>0 THEN GOTO 2040
1960   REM.. GAMMA AT SOURCE..SIMULATE COLLIMATOR
1970   LET A1=ATN((S*V1-(X0-(F-S/2)))/D1)
1980   LET A1=COS(A1)
1990   REM---CALCULATE THE TRANSFORMATION MATRIX
2000   GOSUB 4890
2010   GOTO 2050
2020   REM GET NEW ENERGY AND INVERSE MATRIX
*
```

```
2030 REM.. GAMMA BETWEEN SOURCE AND DETECTOR
2040 GOSUB 4840
2050 IF S1>0 THEN LET E0=E1
2060 MAT U9=T9*X9
2070 MAT S9=S9+U9
2080 LET S1=S1+1
2090 REM..-----------------------------------------------------------
2100 REM--GRAPHICS BOUNDARY CHECK..S9(3) CHECKS Z AXIS(HORIZONTAL)--
2110 REM                           S9(1) CHECKS X AXIS(VERTICAL)--
2120 IF S9(2)>3*D4 THEN GOTO 2440
2130 IF S9(3)<0 THEN GOTO 2440
2140 IF S9(1)<F/8 THEN GOTO 2190
2150 IF S9(1)>1.85*F THEN GOTO 2190
2160 IF S9(3)>255 THEN CALL 14,255,S9(1),1
2170 IF S9(3)<=255 THEN CALL 14,S9(3),S9(1),1
2180 IF S9(3)<X THEN GOTO 1850
2190 IF S9(3)=K9(3) THEN GOTO 2440
2200 REM--CALCULATE THE SLOPE AND LINE EQUATION--
2210 REM--IN THE (Z,X) M1 AND X8,X7--
2220 REM--IN THE (Z,Y) M2 AND Y8,Y7---
2230 REM--8 IS AT THE DETECTOR COLLIMATOR FACE,7 IS AT THE DETECTOR---
2240 LET M1=(S9(1)-K9(1))/(S9(3)-K9(3))
2250 LET M2=(S9(2)-K9(2))/(S9(3)-K9(3))
2260 LET X8=M1*(X-K9(3))+K9(1)
2270 LET X7=M1*(X+D3-K9(3))+K9(1)
2280 LET Y8=M2*(X-K9(3))+K9(2)
2290 LET Y7=M2*(X+D3-K9(3))+K9(2)
2300 REM-DETERMINE IF THE PHOTON IS IN DETECTOR AT SEVERAL COLLIMATIONS-
2310 FOR L=1 TO 6
2320   LET D8=D3-2*(L-1)
2330   LET D7=D4-2*(L-1)
2340   IF X8>F+D8/2 THEN GOTO 2430
2350   IF X8<F-D8/2 THEN GOTO 2430
2360   IF X7>F+D8/2 THEN GOTO 2430
2370   IF X7<F-D8/2 THEN GOTO 2430
2380   IF Y8>D7/2 THEN GOTO 2430
2390   IF Y8<-D7/2 THEN GOTO 2430
2400   IF Y7>D7/2 THEN GOTO 2430
2410   IF Y7<-D7/2 THEN GOTO 2430
2420   LET I0(L)=I0(L)+1
2430 NEXT L
2440 IF T1=C1 THEN GOTO 2480
2450 LET T1=T1+1
2460 GOTO 1830
2470 REM--STORE THE INITIAL COUNTS GENERATED FOR SEVERAL COLLIMATIONS---
2480 FOR L=1 TO 6
2490   IF J=1 THEN LET I4(L)=I0(L)
2500   IF J=2 THEN LET I1(L)=I0(L)
2510 NEXT L
2520 LET E2=103/511
2530 NEXT J
2540 REM
2550 REM*************************************************************
*
```

```
2560 REM*************************************************************************
2570 REM                GET THE ATTENUATED COUNTS **I**
2580 REM
2590 REM---MAKE A COPY OF ARRAY I1,I4---
2600 FOR L=1 TO 6
2610   PRINT I4(L),I1(L)
2620   LET I5(L)=I4(L)
2630   LET I2(L)=I1(L)
2640 NEXT L
2650 PRINT "I4","I1","I7","I8","AL","H"
2660 CALL 17
2670 PRINT "<26>"
2680 LET E2=42.5/511
2690 LET K1=1
2700 FOR J=1 TO 2
2710   REM.. SET UP EXPERIMENT USING GRAPHICS
2720   GOSUB 4460
2730   REM..DRAW THE ALUMINUM AND WATER BOUNDARIES
2740   GOSUB 5090
2750   REM..INITIALIZE THE VARIABLES
2760   LET S=P
2770   LET S1,T1,I=0
2780   FOR L=1 TO 6
2790     LET I0(L)=0
2800   NEXT L
2810   REM.. INITIALIZE A STARTING POINT
2820   GOSUB 5370
2830   MAT K9=S9
2840   REM-----------------------------------------------------------------
2850   REM             GET ANGLE AND PATH
2860   REM
2870   IF J=2 THEN GOTO 3010
2880   REM--DETERMINE THE ATTENUATION COEFFICIENT AS A FUNCTION---
2890   REM--OF ENERGY AND PHOTON POSITION---
2900   REM--30 AND 60 ARE THE LOWER PHOTON ENERGY WINDOW MARKERS---
2910   IF E0*511<40 THEN GOTO 3930
2920   IF S9(3)<=H1 THEN LET U0=FNA(E0)
2930   IF S9(3)>H1 THEN LET U0=FNC(E0)
2940   IF H1=0 THEN LET U0=FNC(E0)
2950   IF S9(3)>H2 THEN LET U0=FNE(E0)
2960   IF S9(3)<=H1 THEN LET U8=FNG(E0)
2970   IF S9(3)>H1 THEN LET U8=FNJ(E0)
2980   IF H1=0 THEN LET U8=FNJ(E0)
2990   IF S9(3)>H2 THEN LET U8=FNE(E0)/10
3000   GOTO 3110
3010   IF E0*511<=60 THEN GOTO 3930
3020   IF S9(3)<=H1 THEN LET U0=FNB(E0)
3030   IF S9(3)>H1 THEN LET U0=FND(E0)
3040   IF H1=0 THEN LET U0=FND(E0)
3050   IF S9(3)>H2 THEN LET U0=FNF(E0)
3060   IF S9(3)<=H1 THEN LET U8=FNH(E0)
3070   IF S9(3)>H1 THEN LET U8=FNI(E0)
3080   IF H1=0 THEN LET U8=FNI(E0)
3090   IF S9(3)>H2 THEN LET U8=FNF(E0)/10
*
```

```
3100 REM--GET A PATH LENGTH---
3110 GOSUB 4790
3120 LET X9(1)=0
3130 LET X9(2)=0
3140 LET X9(3)=R
3150 LET R1=R*U0
3160 CALL 5,V1,1,.5
3170 IF S1<>0 THEN GOTO 3260
3180 REM.. GAMMA AT SOURCE-SIMULATE COLLIMATOR
3190 LET A1=ATN((S*V1-(X0-(F-S/2)))/D1)
3200 LET A1=COS(A1)
3210 REM---CALCULATE THE TRANSFORMATION MATRIX---
3220 GOSUB 4890
3230 GOTO 3270
3240 REM.. GET NEW ENERGY AND INVERSE MATRIX
3250 REM.. GAMMA BETWEEN SOURCE AND DETECTOR
3260 GOSUB 4840
3270 MAT U9=T9*X9
3280 MAT S9=U9+S9
3290 LET S1=S1+1
3300 IF S1>2 THEN LET S6=S6+1
3310 REM..-------------------------------------------------------
3320 REM..BOUNDARY CORRECTION FOR PHOTONS TRAVELLING THROUGH
3330 REM..2 OR 3 MATERIALS
3340 IF K9(3)>H1 THEN GOTO 3450
3350 IF S9(3)<=H1 THEN GOTO 3570
3360 IF S9(3)>H2 THEN GOTO 3530
3370 LET H5=H1
3380 IF J=1 THEN LET U6=FNC(E0)
3390 IF J=2 THEN LET U6=FND(E0)
3400 IF J=1 THEN LET U5=FNA(E0)
3410 IF J=2 THEN LET U5=FNB(E0)
3420 GOSUB 5210
3430 IF S9(3)>H2 THEN GOSUB 5540
3440 GOTO 3570
3450 IF K9(3)>H2 THEN GOTO 3570
3460 IF S9(3)<=H2 THEN GOTO 3570
3470 LET H5=H2
3480 LET U6=U3
3490 IF J=1 THEN LET U5=FNC(E0)
3500 IF J=2 THEN LET U5=FND(E0)
3510 GOSUB 5210
3520 GOTO 3570
3530 GOSUB 5540
3540 REM-------------------------------------------------------------
3550 REM..GRAPHICS BOUNDARY CHECK S9(3) CHECKS Z AXIS(HORIZONTAL)
3560 REM                         S9(1) X AXIS(VERTICAL)
3570 LET E0=E1
3580 CALL 5,V2,1,.5
3590 REM---TEST FOR A PHOTOELECTRIC INTERACTION---
3600 IF V2>U8/U0 THEN GOTO 3630
*
```

```
3600 IF V2>U8/U0 THEN GOTO 3630
3610 IF S9(3)<X+D3 THEN GOTO 3930
3620 GOTO 3710
3630 IF S9(3)<0 THEN GOTO 3930
3640 IF ABS(S9(2))>1.85*F THEN GOTO 3710
3650 IF S9(1)<F/8 THEN GOTO 3710
3660 IF S9(1)>1.85*F THEN GOTO 3710
3670 GOTO 3700
3680 IF S9(3)>255 THEN GOSUB 5480
3690 IF S9(3)<=255 THEN CALL 14,S9(3),S9(1),1
3700 IF S9(3)<X+D3 THEN GOTO 2830
3710 IF S9(3)=K9(3) THEN GOTO 3930
3720 REM---CALCULATE THE SLOPE AND LINE EQUATION--
3730 LET M1=(S9(1)-K9(1))/(S9(3)-K9(3))
3740 LET M2=(S9(2)-K9(2))/(S9(3)-K9(3))
3750 LET X8=M1*(X-K9(3))+K9(1)
3760 LET X7=M1*(X+D3-K9(3))+K9(1)
3770 LET Y8=M2*(X-K9(3))+K9(2)
3780 LET Y7=M2*(X+D3-K9(3))+K9(2)
3790 REM--CHECK FOR PHOTON IN COLLIMATOR AND DETECTOR--
3800 FOR L=1 TO 6
3810   LET D8=D3-2*(L-1)
3820   LET D7=D4-2*(L-1)
3830   IF X8>F+D8/2 THEN GOTO 3920
3840   IF X8<F-D8/2 THEN GOTO 3920
3850   IF X7>F+D8/2 THEN GOTO 3920
3860   IF X7<F-D8/2 THEN GOTO 3920
3870   IF Y8>D7/2 THEN GOTO 3920
3880   IF Y8<-D7/2 THEN GOTO 3920
3890   IF Y7<-D7/2 THEN GOTO 3920
3900   IF Y7>D7/2 THEN GOTO 3920
3910   LET I0(L)=I0(L)+1
3920 NEXT L
3930 IF J=2 THEN GOTO 3970
3940 IF I0(1)>=5000 THEN GOTO 4010
3950 LET K1=K1+1
3960 GOTO 2810
3970 LET T1=T1+1
3980 IF T1=K1 THEN GOTO 4010
3990 GOTO 2810
4000 REM--SAVE THE ATTENUATED PHOTON COUNTS FOR 6 COLLIMATOR SIZES---
4010 FOR L=1 TO 6
4020   IF J=1 THEN LET I7(L)=I0(L)
4030   IF J=2 THEN LET I8(L)=I0(L)
4040 NEXT L
4050 LET E2=103/511
4060 NEXT J
4070 REM
*
```

```
4080 REM*****************************************************************
4090 REM              CALCULATED THICKNESS
4100 REM
4110 PRINT "K1,C1",K1,C1
4120 REM---CALCULATE THE THICKNESS OF ALUMINUM FOR 6 COLLIMATIONS---
4130 FOR L=1 TO 6
4140   LET I4=I5(L)*K1/C1
4150   LET I1=I2(L)*K1/C1
4160   LET A1=LOG(I4/I7(L))-R5*LOG(I1/I8(L))
4170   LET A2=A1/(10*B1)
4180   PRINT I4,I1,I7(L),I8(L),A2,(H2-H1)/10
4190   WRITE FILE (1),A2,H2,I4,I1,I7(L),I8(L),K1
4200 NEXT L
4210 LET C5=C5-1
4220 IF C5>0 THEN GOTO 2660
4230 LET C5=C6
4240 LET H2=H2+10
4250 IF H2<100 THEN GOTO 2660
4260 CLOSE FILE (1)
4270 REM
4280 REM*****************************************************************
4290 REM         ROUTINE TO LIST DATA FILE CONTENTS
4300 REM
4310 OPEN FILE (1,3),F$
4320 READ FILE (1),H1,C5,P,D2,C1,P1,D1,D3
4330 PRINT H1/10,C5,P/10,D2/10,C1
4340 PRINT P1/10,D1/10,D3/10
4350 PRINT "THICKNESS";"   ";"WATER THICKNESS"
4360 IF EOF(1) THEN GOTO 4400
4370 READ FILE (1),A2,H2,I4,I1,I7,I8,K1
4380 PRINT "   ";A2;"      ";(H2-H1)/10
4390 GOTO 4360
4400 CLOSE FILE (1)
4410 STOP
4420 REM*****************************************************************
4430 REM*****************************************************************
4440 REM        SUBROUTINE DRAW EQUIPMENT
4450 REM
4460 CALL 17
4470 REM.. DRAW THE SOURCE-----------
4480 LET X=0
4490 LET S=P
4500 GOSUB 4630
4510 REM.. DRAW THE DETECTOR----------
4520 LET X=P1
4530 LET S=D2
4540 GOSUB 4630
4550 CALL 14,X,F-D2/2,0
4560 CALL 14,X+D3,F-D2/2,1
4570 CALL 14,X+D3,F+D2/2,1
4580 CALL 14,X,F+D2/2,1
4590 RETURN
*
```

```
4600 REM-------------------------------------------------------------
4610 REM          SUBROUTINE DRAW
4620 REM
4630 LET Y1=F-(60+S/2)
4640 LET Y2=F-(S/2)
4650 LET Y3=F+S/2
4660 LET Y4=F+S/2+60
4670 IF X>0 THEN LET P5=255
4680 IF X=0 THEN LET P5=0
4690 CALL 14,X,Y1,0
4700 CALL 14,P5,Y1,1
4710 CALL 14,X,Y1,0
4720 CALL 14,X,Y2,1
4730 CALL 14,X,Y3,0
4740 CALL 14,X,Y4,1
4750 CALL 14,P5,Y4,1
4760 RETURN
4770 REM-------------------------------------------------------------------
4780 REM               SUBROUTINE PATH LENGTH SAMPLE
4790 CALL 5,V1,1,.5
4800 LET R=-LOG(V1)/U0
4810 IF R>300 THEN LET R=255
4820 RETURN
4830 REM-----------------------------------------------------------------------
4840 REM             SUBROUTINE INVERSE MATRIX
4850 LET S5=E0/(1+.5625*E0)
4860 LET E1=E0/(1+S5*V1+(2*E0-S5)*V1^3)
4870 LET A1=1-(E0-E1)/(E1*E0)
4880 REM---EMISSION FROM SOURCE-NO COMPTON SCATTERING ANGLE CALCULATION--
4890 LET A2=SQR(1-A1^2)
4900 CALL 5,V1,1,.5
4910 IF V1<.5 THEN LET A2=-A2
4920 CALL 5,V3,1,.5
4930 LET A3=SIN(V3*2*SYS(15))
4940 LET A4=COS(V3*2*SYS(15))
4950 REM---FOR THE INVERSE TRANSFORMATION MATRIX SEE EQUATION 5-11
4960 LET F9(1,1)=A1*A4
4970 LET F9(1,2)=-A3
4980 LET F9(1,3)=A2*A4
4990 LET F9(2,1)=A1*A3
5000 LET F9(2,2)=A4
5010 LET F9(2,3)=A2*A3
5020 LET F9(3,1)=-A2
5030 LET F9(3,2)=0
5040 LET F9(3,3)=A1
5050 MAT T9=F9
5060 RETURN
5070 REM..-----------------------------------------------------------------
*
```

```
5080 REM              DRAW THE MATERIALS
5090 CALL 14,1,50,0
5100 CALL 14,H1,50,1
5110 CALL 14,H1,205,1
5120 CALL 14,1,205,1
5130 CALL 14,1,50,1
5140 CALL 14,H2,50,1
5150 CALL 14,H2,205,1
5160 CALL 14,1,205,1
5170 RETURN
5180 REM..-----------------------------------------------------------------
5190 REM..                    SUBROUTINE BOUNDARY CORRECTION
5200 REM THIS SUBROUTINE CORRECTS FOR A PHOTON CROSSING 1 BOUNDARY
5210 LET Q1=S9(3)-K9(3)
5220 LET Q2=SQR((S9(3)-K9(3))^2+(S9(2)-K9(2))^2+(S9(1)-K9(1))^2)
5230 LET Q3=Q1/Q2
5240 IF Q3=1 THEN LET A5=1
5250 IF Q3=1 THEN GOTO 5280
5260 LET A5=-ATN(Q3/SQR(1-Q3*Q3))+SYS(15)/2
5270 LET A5=COS(A5)
5280 LET X9(3)=R1/U6+(1-U5/U6)*(H5-K9(3))/A5
5290 LET X9(2)=0
5300 LET X9(1)=0
5310 MAT U9=T9*X9
5320 MAT S9=U9+K9
5330 RETURN
5340 REM-----------------------------------------------------------------
5350 REM                    SUBROUTINE START POINT
5360 REM THIS SUBROUTINE STARTS THE PHOTON AT Z0,X0,Y0
5370 LET Z0,S1=0
5380 LET E0=E2
5390 LET E1=E2
5400 REM.. SET UP STARTING POINT
5410 CALL 5,V1,S,S/2
5420 LET X0=(F-S/2)+V1
5430 LET S9(1)=X0
5440 LET S9(2)=0
5450 LET S9(3)=0
5460 CALL 14,Z0,X0,1
5470 RETURN
5480 LET M1=(S9(1)-K9(1))/(S9(3)-K9(3))
5490 LET X3=M1*(255-K9(3))+K9(1)
5500 CALL 14,255,X3,1
5510 RETURN
5520 REM-----------------------------------------------------------------
5530 REM     SUBROUTINE BOUNDARY CORRECTION FOR 3 MATERIALS
5540 LET Q1=S9(3)-K9(3)
5550 LET Q2=SQR((S9(3)-K9(3))^2+(S9(2)-K9(2))^2+(S9(1)-K9(1))^2)
5560 LET Q3=Q1/Q2
5570 IF Q3=1 THEN GOTO 5610
5580 LET A5=-ATN(Q3/SQR(1-Q3*Q3))+SYS(15)/2
5590 LET A5=COS(A5)
*
```

```
5600 REM   PARTICLE MEDIUM 1 TO MEDIUM 3
5610 IF J=1 THEN GOTO 5660
5620 LET U1=FNB(E0)
5630 LET U2=FND(E0)
5640 LET U3=FNF(E0)
5650 GOTO 5710
5660 LET U1=FNA(E0)
5670 LET U2=FNC(E0)
5680 LET U3=FNE(E0)
5690 REM---FOR 3 MATERIALS THE CORRECTED PATH LENGTH ---
5700 REM---IS GIVEN BY EQUATION 5-29---
5710 LET X9(3)=R1/U3+((1-U2/U3)*(H2-H1)+(1-U1/U3)*(H1-K9(3)))/A5
5720 LET X9(2)=0
5730 LET X9(1)=0
5740 MAT U9=T9*X9
5750 MAT S9=K9+U9
5760 RETURN
*
```

Appendix 10

Calculation of Dose to Tissue and Bone

The dose to a human subject was determined by theoretical calculations and compared to values measured using $Li_2B_4O_7$:Cu thermoluminescent dosimeters (TLDs). This type of TLD exhibits a near tissue equivalent dose response for gamma ray energies in the range 40 keV to 70 MeV and has a sensitivity 2 to 3 times greater than the more widely used LiF TLDs. To calculate the dose for DPA the first step was to determine the quantity that was directly measured in a photon field; namely, the exposure rate. The exposure is given by:

$$X = \frac{\Gamma(\lambda N)}{r^2} \qquad \text{(A10-1)}$$

where Γ is given by Attix[44]:

$$\Gamma = .0193 \sum n_i (hv)_i \left(\frac{u_{en}}{\rho}\right)_i \qquad \text{(A10-2)}$$

and

λN = the activity in disintegrations/sec.

r = the distance from the source to point of measurement in cm.

n_i = the ratio of photon output at $(hv)_i$ to the total output of the isotope.

hv = the energy of the photons (keV).

$\frac{u_{en}}{\rho}$ = Mass-energy absorption coefficient (cm^2/g).

The parameter r is valid for r much greater than the photon beam diameter. For the experimental geometry r>>.2 mm. where r can be considered the distance from the source to the middle of the lumbar vertebrae with the patient lying face up on the scan table. Figures A7-1 and A7-4 show that the distance from the top of the source container to the exit slit surface of the lead source collimator is 5 $\pm$ .5 cm. About 3 cm. above this, or a total of 8 cm. from the source, the mid-lumbar region would normally be located. Therefore, r was taken as approximately 8 cm. Table A10-1 shows the tabulation of n_i, the mass-energy absorption coefficients, and partial gamma ray values for each energy using equation A10-2. The n_i values were taken from Browne et al.[43] and the energy attenuation coefficents were interpolated using a linear fit on data contained in Attix[44]. The gamma ray constant for ^{153}Sm was calculated to be .0928 R/hour per Curie at 1 meter. The source was typically irradiated for 44 hours with a "cool-down" period of 49 hours. The activity is given by:

$$\alpha = \alpha_o e^{-t} \qquad \text{(A10-3)}$$

where

λ = the decay constant (.0149 hours^{-1}).

t = time in hours (49).

α_o = the activity at the end of irradiation.
6 curies for 44 hours of irradiation (see appendix 5).

Using equation A10-3, the activity for a 44 hour irradiation and 49 hour "cool-down" period would be 2.9 Curies. But this activity was for the full surface area of the source. Since the source was collimated with a 2 mm. exit slit, the collimated activity would be much less. Therefore, a geometrical factor must be included to compensate for only partial use of the source activity. The dimensions of the source container and insert are shown in figure A7-1. The source volume was cylindrical with a radius of 1 mm. and a height of 5.3 mm. A reasonable estimate of the activity at the exit slit would be the ratio of the exit slit area to the surface area of the source cavity. This is given by:

$$\frac{\text{Area of exit slit}}{\text{Surface area of the cavity}} = \frac{r^2}{2\,r^2 + 2\,rh} \qquad \text{(A10-4)}$$

The above dimensions produced a correction value of .079 and a source exit slit activity of .23 Ci. Using equation A10-1 the exposure rate becomes .92 mR/s (3.4 R/hr.) at 8 cm. above the source top surface. However, in terms of

Photon Energy (keV)	n_i (Curie)	u_{en} (cm^2/g)	R/h/Ci. at 1 meter
40.9	.284	.0644	.0144
44.0	.514	.0563	.0246
47.3	.156	.0485	.0069
48.3	.049	.0451	.0021
69.7	.16	.0275	.0059
103.0	.84	.0233	.0039
			.0928

Table 10-1 Tabulation of the gamma ray constant for ^{153}Sm.

biological damage, the exposure has little significance. To determine the damage caused by the radiation, the dose was calculated because it is dependent not only on the radiation field but also on the material being irradiated. The relationship between dose rate and exposure rate is:

$$\dot{D}_M\left(\frac{\text{mRad}}{\text{sec.}}\right) = .87\,\frac{\left(\frac{u_{en}}{\rho}\right)_m}{\left(\frac{u_{en}}{\rho}\right)_{air}}\,\dot{X}\left(\frac{\text{mR}}{\text{sec.}}\right) \qquad \text{(A10-5)}$$

The ratio of the energy attenuation coefficent of material m to air is a function of energy and, therefore, the exposure and dose would have to be determined for a particular energy in question. However, if the maximum dose is required for worst-case analysis than the energy representing the maximum dose can be used. From Attix[44] the ratio in equation A10-5 for muscle in the energy range of 30 to 103 keV was relatively constant at $1.07\pm.03$. However, in the same energy range the ratio for bone varies from 1.65 at 100 keV to 4.86 at 30 keV. Therefore, the worst-case conversion factors from exposure rate to dose rate were .96 and 4.23 for muscle and bone respectively. This would give an absorbed dose rate of 3.9 mrad/s for bone and .88 mrad/s for muscle. Since the overlying tissue would attenuate the beam, the dose rate for bone <u>in vivo</u> would be less than the above values based on calculated results.

To determine the dose to a particular area of the body, the beam size, scan speed and scan sample time must be known. At a speed of 4.4 mm./s (dial setting of 60), any body area would be exposed to part of the photon beam for a maximum of 1.6 seconds. At 49 hours after irradiation, the first clinical scan could be performed and concurrently produce the maximum expected dose for the week. The dose to bone and muscle will be 6.2 and 1.4 mrad/scan respectively. These values were calculated and must be compared to measured values.

The measured high energy photon count rate at 49 hours after irradiation was 1.1×10^5 c/s (see figure 4-32). This produced a dose rate to bone and muscle at 5 cm. of 6.3 and 1.4 mRads/s respectively. At 8 cm. the dose rate is given by:

$$D_{8cm.} = D_{5cm.}\left(\frac{.05}{.08}\right)^2 \left[\frac{R}{hr.}\right] \qquad \text{(A10-6)}$$

Using equation A10-6, the dose rate at 8 cm. from the source to mid-lumbar for bone and muscle would be 2.5 and .55 mRads/second respectively. The skin dose based on TLD measurements for a scan sample time of 1.6 seconds were 4.0 mrads for bone and .88 mRad for muscle. Table A10-2 compares the calculated and measured dose to muscle and bone. The measured dose rate could be substantially underestimated because of misalignment of the photon beam and the TLD. The calculated values are maximum worst-case estimates and probably overestimate the dose.

Component	Dose (mRads)		Difference %
	Calculated	Measured	
Bone	6.2	4.0	35
Muscle	1.4	.88	37

Table A10-2 Comparison of the calculated and measured dose at the optimal sample rate for bone and muscle.